1-1-2014

Insights From Pretzel Syndrome: The Role of STRADA in Neuronal Migration and Cortical Development

Whitney Erin Parker
University of Pennsylvania, wparkermed@gmail.com

Insights From Pretzel Syndrome: The Role of STRADA in Neuronal Migration and Cortical Development

Abstract
Pretzel Syndrome (also Polyhydramnios, Megalencephaly, and Symptomatic Epilepsy syndrome; PMSE) is a recently described rare neurodevelopmental disorder occurring in the Old Order Mennonite pediatric population, and characterized by intractable infantile-onset epilepsy, neurocognitive delay, craniofacial dysmorphism, and histopathological evidence of heterotopic neurons in subcortical white matter, suggestive of failed neuronal migration. PMSE is caused by a homozygous deletion of exons 9-13 of LYK5/STRADA, which encodes the pseudokinase STRADA, an upstream inhibitor of mammalian target of rapamycin (mTOR). Therefore, we hypothesize that STRADA plays a critical role in neuronal migration through modulating mTOR (specifically mTOR complex 1, mTORC1) signaling, and that therapeutic mTORC1 inhibition can ameliorate features of the PMSE disease phenotype. To test this hypothesis, we model PMSE in vitro using stable shRNA knockdown of STRADA (STRADA KD) in mouse neural progenitor cells (mNPCs). In vivo, we use in utero electroporation to create focal STRADA KD in the developing mouse brain. We show that STRADA depletion disrupts pathfinding and polarization in migrating mNPCs in vitro, and this effect can be rescued by inhibition of mTORC1 with rapamycin or of its downstream effector p70S6kinase (p70S6K) with PF-4708671 (p70S6Ki), indicating an mTORC1-specific dependence. We then define a pathway for this effect downstream of mTORC1, through insulin receptor substrate 1 (IRS1) signaling to cofilin, and finally modulating actin dynamics. In vivo, we demonstrate that STRADA KD causes a cortical lamination defect in the mouse, which can be rescued with rapamycin treatment, confirming the dependence of STRADA's effect on mTORC1 signaling and suggesting an important target for patient therapy. To correlate our mouse model with PMSE, we demonstrate congruent mTORC1 and downstream signaling and rescue of migration deficit with rapamycin and p70S6Ki in PMSE patient fibroblasts. Finally, we report reduction of seizure frequency with rapamycin treatment in previously intractable PMSE patients. Our findings define a novel role for STRADA in neuronal migration, demonstrate a mechanistic link between STRADA loss and mTORC1 hyperactivity in PMSE, and suggest that mTORC1 inhibition can serve as an effective therapeutic bio-target in PMSE as well as other devastating mTOR-associated neurodevelopmental disorders.

Degree Type
Dissertation

Degree Name
Doctor of Philosophy (PhD)

Graduate Group
Neuroscience

First Advisor
Peter B. Crino

INSIGHTS FROM PRETZEL SYNDROME: THE ROLE OF STRADA IN NEURONAL MIGRATION AND CORTICAL DEVELOPMENT

Whitney Erin Parker

A DISSERTATION

in

Neuroscience

Presented to the Faculties of the University of Pennsylvania

in

Partial Fulfillment of the Requirements for the

Degree of Doctor of Philosophy

2014

Supervisor of Dissertation

_____

Peter B. Crino, M.D., Ph.D., Professor of Neurology, Temple University School of Medicine

Graduate Group Chairperson

_____

Joshua I. Gold, Ph.D., Professor of Neuroscience

Dissertation Committee

Steven S. Scherer, M.D., Ph.D. (Chair), Professor of Neurology
Marc A. Dichter, M.D., Ph.D., Professor of Neurology
Thomas N. Ferraro, Ph.D., Research Associate Professor of Psychiatry
Dennis L. Kolson, M.D., Ph.D., Professor of Neurology

DEDICATION

To my father, William H. Parker V, who thinks this still doesn't make me a "real" doctor.

To my mother, Mary Ellen Parker, who thinks it does.

And to my brother, William H. Parker VI. I couldn't have done it without you, dork.

ACKNOWLEDGMENT

I would like to thank, first and foremost, my advisor Pete Crino. He has been the best mentor a young scientist could ask for, and I am inspired every day by his brilliance, insight, and dedication to our training. I would like to thank also the members of my Thesis Committee, Steve Scherer, Marc Dichter, Tom Ferraro, and Dennis Kolson, for all of their helpful advice, and for having the patience to teach me so much and share this experience with me. I also have to thank the Neuroscience Graduate Group, particularly Josh Gold and Jane Hoshi, as well as our former leaders Mikey Nusbaum, Rita Balice-Gordon and Angela Gilmore, for all of their support and encouragement.

I would also like to thank our lab manager and my dear friend Marianna Baybis, for everything she has taught me, and all the support she has given me throughout this process. I have to thank all the members of our lab, past and present, Ksenia Orlova, Greg Heuer, Victoria Tsai, Julie Chen, William Parker, Leah Marcotte, Jackie Birnbaum, Kei Okochi, Ben Berg, TK, Lori Atkinson, Jackie Estevez, and Jason Yoon. They are a family to me, and I am so thankful to have been able to share this experience with all of them. I would like to thank the members of the Kolson and Soldan labs as well. They have been the most wonderful "lab neighbors," and I can't thank them enough for all the advice they've given me through the years.

I would like to thank all of our collaborators, including Vera Krymskaya, Tom Ferraro, John Seykora, Jeff Field, and Doug Coulter, as well as members of their labs. I also want to thank Kevin Strauss and colleagues at the Clinic for Special Children, as well as all of the brave patients and families.

I have to thank my incredible mentors from my undergraduate training, Russell Epstein and Sharon Thompson-Schill, for their inspiration, without which I would never have pursued research in the first place. I also have to thank Dorothy Cheney and Robert Seyfarth, exceptional scientists with whom I consider myself extremely fortunate to have a friendship.

I have to thank all my wonderful friends at school, including Harveen, Henry, Carol Yan, Joy, Tanya, Kevan, Eric, Cindy, Rohan, Tripti, Alice, Omar, Greg, Jiyeon, Jared and everybody else who has been kind enough to listen to my lab and life stories and offer support and advice. I also have to thank my wonderful friends in other places, specifically, Sasha, Jason, Josh, Carolyn, Doug, Nora, and Mike.

I especially have to thank my family. My parents have given me a lifetime of love and support, and without them, I would never have been able to get where I am. My mother stays proud of me no matter what, and always inspires me with her never-give-up attitude. My father is always there for me, and gives me the best advice. My brother William, my best friend of 21 years, has played a huge part in helping me with the experiments for my thesis. He's the smartest kid I know and will be an amazing scientist and/or doctor someday. I would like to thank my extended family, particularly my grandparents for everything they've taught me, and my godfamily. Also family, Ksenia and Carol Li are effectively my sisters, and always the ones I can call for advice about anything. I am so thankful to have them in my life, and I don't know what I would have done without them.

Last, I have to thank Brad Wells, the love of my life, for his encouragement and support. He inspires me to be better, and I look forward to sharing the rest of this adventure with him.

I thankfully acknowledge the grant support I have received during my training, including grants from: Alpha Omega Alpha, American Association of Neurological Surgeons, Hearst Foundation, NIH (T32 Genetics Training Grant), and NINDS/NIH (NRSA F31 NS078845).

ABSTRACT

INSIGHTS FROM PRETZEL SYNDROME: THE ROLE OF STRADA IN NEURONAL MIGRATION AND CORTICAL DEVELOPMENT

Whitney E. Parker

Peter B. Crino, M.D., Ph.D.

Pretzel Syndrome (also Polyhydramnios, Megalencephaly, and Symptomatic Epilepsy syndrome; PMSE) is a recently described rare neurodevelopmental disorder occurring in the Old Order Mennonite pediatric population, and characterized by intractable infantile-onset epilepsy, neurocognitive delay, craniofacial dysmorphism, and histopathological evidence of heterotopic neurons in subcortical white matter, suggestive of failed neuronal migration. PMSE is caused by a homozygous deletion of exons 9-13 of *LYK5/STRADA*, which encodes the pseudokinase STRADA, an upstream inhibitor of mammalian target of rapamycin (mTOR). Therefore, we hypothesize that STRADA plays a critical role in neuronal migration through modulating mTOR (specifically mTOR complex 1, mTORC1) signaling, and that therapeutic mTORC1 inhibition can ameliorate features of the PMSE disease phenotype. To test this hypothesis, we model PMSE *in vitro* using stable shRNA knockdown of STRADA (STRADA KD) in mouse neural progenitor cells (mNPCs). *In vivo*, we use *in utero* electroporation to create focal STRADA KD in the developing mouse brain. We show that STRADA depletion disrupts pathfinding and polarization in migrating mNPCs *in vitro*, and this effect can be rescued by inhibition of mTORC1 with rapamycin or of its downstream effector p70S6kinase (p70S6K) with PF-4708671 (p70S6Ki), indicating an mTORC1-specific dependence. We then define a

pathway for this effect downstream of mTORC1, through insulin receptor substrate 1 (IRS1) signaling to cofilin, and finally modulating actin dynamics. *In vivo*, we demonstrate that STRADA KD causes a cortical lamination defect in the mouse, which can be rescued with rapamycin treatment, confirming the dependence of STRADA's effect on mTORC1 signaling and suggesting an important target for patient therapy. To correlate our mouse model with PMSE, we demonstrate congruent mTORC1 and downstream signaling and rescue of migration deficit with rapamycin and p70S6Ki in PMSE patient fibroblasts. Finally, we report reduction of seizure frequency with rapamycin treatment in previously intractable PMSE patients. Our findings define a novel role for STRADA in neuronal migration, demonstrate a mechanistic link between STRADA loss and mTORC1 hyperactivity in PMSE, and suggest that mTORC1 inhibition can serve as an effective therapeutic bio-target in PMSE as well as other devastating mTOR-associated neurodevelopmental disorders.

TABLE OF CONTENTS

LIST OF TABLES

LIST OF FIGURES

CHAPTER 1

INTRODUCTION[1]

[1] Figures in this chapter are adapted from images originally published in *The Journal of Clinical Investigation*, Vol. 120, No. 5, May 2010. Orlova, K.A., Parker, W.E., Heuer, G.G., Tsai, V., Yoon, J., Baybis, M., Fenning, R.S., Strauss, K., and Crino, P.B. STRADalpha deficiency results in aberrant mTORC1 signaling during corticogenesis in humans in mice.

STRAD Structure and Classification

STe20-Related ADaptor (STRAD) was first identified in a yeast 2 hybrid screen of a fetal brain library, as a binding partner of the tumor suppressor protein serine/threonine kinase 11 (STK11, also known as liver kinase B1, LKB1) (1). Its sequence most closely resembles the STE20 homologues SPAK and ILPIP or PAP kinase (1-4). Unlike these homologous kinases, however, STRAD lacks residues indispensable for intrinsic catalysis (phosphoryl transfer), and is thus categorized as a pseudokinase. Specifically, it lacks the DFG motif for magnesium interaction in the ATP-binding cleft and harbors a serine replacement of the aspartic acid residue critical for mediating proton transfer in the catalytic site (1, 5). As a consequence, STRAD remains unable to autophosphorylate or to phosphorylate any of a number of substrates tested in *in vitro* kinase assays (1). Interestingly, much like a kinase, STRAD can adopt an "active" closed conformation, stabilized through association with ATP or binding partner mouse protein 25 (MO25) (5). This has led to speculation that STRAD may have evolved from a kinase capable of catalysis (6).

Cellular Role of STRAD as a Pseudokinase

Prompted by STRAD's discovery as an LKB1-binding partner, Baas et al. chose to investigate this interaction. Co-immunoprecipitation experiments with mutant strains of LKB1 revealed that the entire kinase domain as well as C-terminal amino acid residues 319-343 are essential for LKB1 to bind the pseudokinase domain of STRAD (1). This interaction results in activating autophosphorylation of LKB1 at at least four sites including Thr336, Thr363, Thr185, and Thr402, as well as phosphorylation of STRAD at

Thr329 and Thr419 by LKB1 (1). Kinase assays measuring the phosphorylation of myelin basic protein (MBP), a non-specific LKB1 substrate, as an indicator of LKB1 catalysis revealed that STRAD binding enhances LKB1 activity approximately 4-fold (7). Additionally, STRAD translocates LKB1 from nucleus to cytoplasm (1). Dorfman et al. have shown that STRAD accomplishes LKB1 cytoplasmic localization by serving as an adapter between LKB1 and nuclear export proteins chromosomal region maintenance 1 (CRM1) and exportin7 and by serving as a competitive inhibitor to importin-α binding LKB1 (8). Localization in the cytoplasm is crucial for several of LKB1's functions, including growth arrest (9), G1 cell cycle arrest (1), neuronal axon specification (10, 11), and modulation of mTORC1 signaling (12). This was confirmed through a study demonstrating that an exclusively cytoplasmic LKB1 mutant (lacking the nuclear localization signal) remained able to induce cell growth arrest, while its exclusively nuclear mutant counterpart did not (9).

The STRAD/LKB1/MO25 Complex

STRAD and LKB1 form a heterotrimeric complex with the scaffolding protein MO25 in a 1:1:1 ratio. MO25 interacts directly with STRAD by binding to STRAD's last three C-terminal amino acid residues. MO25 binding enhances formation of the STRAD-LKB1 complex, and formation of the trimer enhances LKB1's catalytic activity approximately 10-fold (7, 13). STRAD and MO25 each exist in alpha and beta isoforms, with large sequence homology and considerable phenotypic overlap. STRADα/β and MO25α/β can each participate in the formation of the heterotrimeric complex to activate LKB1 (7, 13-15).

AMPK Regulation of Cell Energy

LKB1 functions as a master kinase, phosphorylating several downstream kinases, including 13 of the AMP-activated protein kinase (AMPK) subfamily (16). AMPK is an evolutionarily-conserved cellular energy sensor that serves to inhibit energy-consuming metabolic pathways in the setting of increased cellular AMP/ATP ratio, by promoting catabolic and antagonizing anabolic processes (17, 18). LKB1 activated through complexation with STRAD and MO25 phosphorylates AMPK at Thr172, a modification essential to AMPK function (14, 16, 19). In fact, LKB1-deficient murine embryonic fibroblasts (MEFs) exhibit negligible AMPK (Thr172) phosphorylation and consequent lack of AMPK downstream signaling (19). The drug 5-aminoimidazole-4-carboxamide riboside (AICAR) is immediately converted in cells to an AMP mimetic, which activates AMPK by simulating low cellular energy levels (20). AICAR, as well as two additional AMPK-stimulating drugs, metformin and phenformin, failed to activate AMPK in LKB1-null MEFs or LKB1-deficient HeLa cervical cancer cells (14, 21-23). Expression of LKB1 in either of these cell lines, however, restores AMPK sensitivity to pharmacological activation, indicating an essential role for LKB1 in the response of AMPK to cellular energy levels (14, 19).

mTOR Signaling

AMPK plays a key role in modulating activity of the energy-demanding mammalian target of rapamycin (mTOR) cascade. Complexed with and activated by STRAD and MO25, LKB1 activates AMPK. Activated AMPK phosphorylates Tuberous Sclerosis Complex 2 (TSC2) (Thr1227, Ser1345), activating the TSC1:TSC2 complex

(23-26). The TSC1:TSC2 heterodimer inactivates Ras-homolog expressed in brain (Rheb), stimulating the conversion of Rheb-GTP to Rheb-GDP, and thereby inhibiting mTOR kinase activity (25-30). mTOR forms two distinct complexes, mTORC1 (with raptor) and mTORC2 (with rictor) (31) (reviewed in (32)). Additionally, AMPK phosphorylates raptor, modifying the mTORC1 complex and inhibiting mTORC1 through a second mechanism (33). Notably, the macrolide antibiotic rapamycin powerfully inhibits mTORC1 almost exclusively, with minimal effects on mTORC2 signaling after prolonged treatment (34, 35). mTORC1 regulates several key cellular processes including cell growth, transcription, translation, ribosome biogenesis, differentiation, autophagy, and metabolism (26). Perhaps most notably, activated mTORC1 directly phosphorylates ribosomal protein p70S6kinase1 (p70S6K), important for cell growth, and eukaryotic translation initiation factor 4E binding protein 1 (4E-BP1), critical for initiation of cap-dependent mRNA translation (36-39). Phosphorylation of p70S6K1 and its substrate ribosomal S6 protein (S6) serves as an important clinical biomarker for mTORC1 activation in neurons (40, 41). Recent phosphoproteomic analyses have identified several hundred mTOR-associated substrates, suggesting broad relevance in the pathogenesis of several diseases as well as numerous therapeutic targets (42, 43).

mTOR Dysregulation and Cortical Malformation

Enhanced mTOR activity has been shown to be associated with focal cortical malformation (FCM) characterized by altered cortical cytoarchitecture and epilepsy in human disease, and a similar phenotype in murine models with mutation or knockdown

of an mTOR inhibitor. Four FCM subtypes, Tuberous sclerosis complex (TSC), hemimegalencephaly (HME), ganglioglioma (GG), and focal cortical dysplasia type IIB (FCDIIB) all express evidence of aberrant mTORC1 activation in cortex, associated with epilepsy, suggesting a causative link (40, 44-49).

mTOR is expressed in the proliferative zones of the murine brain during early development, and likely plays a critical role in corticogenesis (50), and its dysregulation disrupts this process. Astrocyte-specific conditional knockout of mTOR inhibitor Tsc1 in mice ($Tsc1^{GFAP}$ cKO) results in abnormal hippocampal neuronal organization, astrocytosis, seizures, and early death (51). Similarly, conditional KO of Tsc1 in neurons results in structural abnormality of hippocampus and cortex, associated with cytomegaly and enhanced phosphorylated S6 (P-S6) immunohistochemical staining, as well as seizures and early death (52). Selective KO of Tsc2 in radial glial progenitor cells results in cortical and hippocampal lamination defects, cytomegalic dysplastic neurons and glia, enhanced mTORC1 signaling, and early death (53). Conditional astrocytic KO of Tsc2 results in a more drastic phenotype than astrocytic KO of Tsc1, with astrogliosis, progressive megalencephaly, more severe epilepsy, and earlier premature mortality, associated with higher levels mTORC1 activity (54). Interestingly, treatment with rapamycin ameliorates disease phenotype associated with either Tsc1 or Tsc2 depletion, implicating a causative role for enhanced mTORC1 signaling in pathogenesis (54, 55).

Phosphatase and tensin homolog detected on chromosome ten (PTEN) serves as an upstream inhibitor of mTOR through antagonizing PI3kinase and thus, mTOR's response to extracellular growth signals (reviewed in (56)). Conditional neuronal Pten

KO in mice results in neuronal cytomegaly and macrocephaly, with enhanced mTORC1 activity and spontaneous seizures (57, 58). Importantly, as with TSC models, rapamycin can suppress disease phenotype in Pten-deficient mice, further implicating loss of mTORC1 inhibition as a key step in neuropathogenesis of cortical malformation and epileptogenesis (59, 60).

PMSE, a Rare Disorder From STRADA Mutation

In 2004, researchers and physicians at the Clinic for Special Children in Lancaster County, Pennsylvania identified a cohort of seven previously undiagnosed pediatric patients in the Old Order Mennonite community who shared a constellation of symptoms including macrocephaly, craniofacial dysmorphism, skeletal muscle hypoplasia, hypotonia, and infantile-onset medically-intractable complex partial epilepsy (61). All patients exhibited severe neurodevelopmental deficits, with projected adult mental ages between 6 and 12 months across four developmental domains assessed with the Denver Developmental Screening Test II. All patients were distantly related, and all parents were asymptomatic, suggestive of a recessive inheritance pattern. Single nucleotide polymorphism (SNP) analysis of patients produced "no calls" for the marker rs721575 located within chromosome 17. DNA sequencing and amplification within that region revealed that all patients shared a homozygous 7304 bp deletion of exons 9-13 of *LYK5/STRADA* (61). This was the first time that a *STRADA* mutation had been described in a human disease. The disorder was designated Polyhydramnios, Megalencephaly, and Symptomatic Epilepsy syndrome (PMSE), and referred to colloquially as Pretzel Syndrome, to describe the common posturing assumed by the patients. To date, only 25

patients have been diagnosed with PMSE. Genotyping of healthy individuals in the Old Order Mennonite community of Lancaster County reveals the carrier frequency of the mutated allele to be approximately 4% within that community.

Cranial magnetic resonance imaging (MRI) studies from PMSE patients reveal ventriculomegaly, multiple areas of high water diffusion within the white matter thought to correspond to astrogliosis and white matter vacuolization seen on histopathological analysis, and evidence of subependymal dysplasia (61). Analysis of a postmortem 7-month old PMSE patient brain revealed enlarged neurons and areas of vacuolization within the cerebellum, hippocampal dentate gyrus, trochlear nerve nuclei, substantia nigra, anterior pituitary, and anterior horn of the spinal cord. Large dysmorphic cells, reminiscent of balloon cells found in focal cortical dysplasia, were seen in frontal cortex (61). Importantly, dysmorphic cells in both putamen and cortex were highly reactive for P-S6, indicating enhanced mTORC1 activation (12, 61). Immunohistochemical staining for the protein product of *LYK5/STRADA*, STRADA (also referred to as STRADα), revealed a lack of protein expression in PMSE, relative to control cortex, indicating the likelihood that the pathogenic mutation produces an unstable variant of the protein (12). Indeed, attempted expression in 293 cells of the truncated STRADA protein (truncation at residue 251) that serves as the product of the PMSE mutation results in negligible protein levels. Additionally, this variant does not bind or activate LKB1 (5). Importantly, PMSE brain exhibits blurring of the grey-white matter junction, due to the presence of neurons heterotopically in the subcortical white matter (**Figure 1.1**) (12). This pathological characteristic is highly suggestive of failed neuronal migration, and

primes consideration of this as a mechanism contributing to neurodevelopmental abnormalities in PMSE and possibly other mTOR-associated disorders.

Mouse Models of PMSE

Earlier work from our lab has demonstrated that experimental models of PMSE largely replicate disease pathology through depletion of STRADA. Stable or transient knockdown (KD) of STRADA in mouse neural progenitor cells (mNPCs) using targeted short-hairpin RNA (shRNA) *in vitro* results in cytomegaly associated with enhanced mTORC1 signaling (**Figure 1.2**) (12). Importantly, treatment with rapamycin is able to prevent these effects. Knockdown of STRADA in the embryonic day 14 (E14) mouse brain using *in utero* electroporation (IUE) results in an abnormal retention of STRADA-deplete cells in the germinal center ventricular/subventricular zone (VZ/SVZ) at E17 and E19, and failure to reach the cortical plate (CP), their appropriate destination by E19 (**Figure 1.3**) (12). We show that this phenotype is associated with enhanced P-S6, indicative of aberrant mTORC1 signaling (**Figure 1.4**). Interestingly, we report that depletion of STRADA *in vitro* and *in vivo* is associated with almost exclusively nuclear localization of LKB1, consistent with a failure of LKB1 translocation from nucleus to cytoplasm in the absence of STRADA (**Figures 1.4, 1.5**) (8, 12). This effect is replicated in PMSE patient cortex, suggesting that absence of LKB1 in the cytoplasm may contribute to disease pathogenesis (**Figure 1.6**) (12).

STRADA, mTOR, and Cell Migration

Our PMSE modeling studies contribute to a growing body of evidence that mTORC1 signaling is important for proper cortical lamination and neuronal migration

during brain development. Similar to STRADA *in vivo* knockdown experiments, knockdown or knockout of Tsc1 or Tsc2 in murine models of cortical development results in a failure of Tsc-deficient neurons to reach their intended destination of CP layers II/III, adjacent to pia (62, 63). Importantly, treatment with rapamycin results in significant histological rescue (63, 64). LKB1 knockdown through RNA interference (RNAi) *in vivo* at E14 results in a predominance of LKB1-deficient neurons abnormally in the intermediate zone (IZ) at E16, E17, and E18, suggestive of migratory arrest (65). Recent studies *in vitro* have indicated a role for mTOR signaling in fibroblast migration, through the Rho GTPases Rac1 and Cdc42. Tsc2-null rat embryonic fibroblasts demonstrate impaired migration and polarity in a wound-healing scratch migration assay, associated with reduced activation of Rac1 and Cdc42 (66). Consistent with an established link between mTORC1 and Rho GTPase signaling, through p70S6K phosphorylation of the insulin receptor substrate 1 protein (IRS1), the migration phenotype in Tsc2-deficient cells was significantly rescued through expression of constitutively-active PI3kinase or treatment with rapamycin (66, 67). Previously, Rac1 and Cdc42 have been implicated as playing an essential role in the radial migration of cortical neurons, possibly through establishment of appropriate cell polarity (68, 69).

STRAD-associated signaling mechanisms are intimately linked to cell polarity. LKB1 was originally identified in a genetic screen for mutations that disrupt the zygotic anterior-posterior axis determination (70). Downregulation of STRAD or LKB1 *in vivo* in the developing murine brain results in disruption of neuronal polarization, seen as a failure of axonal formation (10, 11). Conversely, overexpression of STRAD or LKB1 resulted in the formation of supernumerary axons. Correlatively, neurons reaching the

CP (representing a minority of cells) in LKB1 knockdown IUE experiments exhibited inverted apical-basal orientation, with axon-like neurites oriented toward the pia instead of the ventricle. This effect was significantly prevented by co-transfection with an RNAi-resistant LKB1 mutant, indicating an essential role for LKB1 in neuronal polarization (65). These studies are reminiscent of a very compelling set of experiments demonstrating that induced expression of STRAD in intestinal epithelial cells is sufficient to cause cells to remodel their actin cytoskeleton to polarize and form an apical brush border, in an LKB1-dependent manner, and independently of cell-cell contacts (71).

Given the severity of neurological disease phenotype in PMSE, the strong association of STRADA loss with aberrant mTOR activity, and the relationship of STRAD/LKB1 and mTOR signaling to cell polarization, we hypothesize that *STRADA plays a critical role in neuronal migration and polarity through regulating actin dynamics*. Work in our lab shows that depletion of STRADA *in vitro* in mNPCs results in migration impairment in a wound-healing migration assay, in an mTORC1-/p70S6K-dependent manner. Analysis of this phenomenon on an individual-cell level, using time-lapse video microscopy, reveals that STRADA knockdown causes a loss of neuronal pathfinding capacity, without deficit in total distance translocated. This corresponds to a disruption of mNPC polarity, which is prevented by inhibition of mTORC1 with rapamycin or p70S6K with a novel inhibitor PF-4708671 (72). We propose that STRADA loss in PMSE leads to aberrant corticogenesis through impairing neuronal polarity and pathfinding in an mTORC1- and p70S6K-dependent manner. In support of this mechanism, rapamycin treatment rescues the cortical lamination defect associated with STRADA KD in the developing mouse brain. Polymerized or filamentous (F) actin

plays a critical role in establishing polarity of migrating cells (73). We demonstrate that STRADA knockdown in mNPCs results in enhanced mTORC1 activity, inhibiting IRS1 signaling, reducing PAK1 and LIMK activation, and consequently disinhibiting cofilin, which serves to depolymerize actin. We confirm this mechanism in STRADA-deficient PMSE patient fibroblasts extracted from human skin-punch biopsy samples, and show that signaling abnormalities can be rescued through inhibition of mTORC1 or p70S6K. Immunohistochemical analysis reveals enhanced IRS1 phopshorylation in PMSE cortex, linking STRADA/mTOR activation to downstream cofilin signaling in this disease process in the human brain. Finally, we demonstrate that dysregulated mTORC1/IRS1 signaling associated with STRADA loss results in the functional consequence of diminished actin polymerization, seen as an increase in the ratio of depolymerized globular (G) to polymerized F actin, in both STRADA-deplete mNPCs and PMSE patient fibroblasts. We propose that disruption of actin dynamics as a consequence of STRADA loss impairs neuronal polarity and pathfinding, resulting in aberrant corticogenesis. Thus, we add STRADA to the list of mTOR-regulatory proteins that play a critical role in neuronal polarization and pathfinding, and submit that PMSE serves as a novel model disorder for investigation of mechanisms responsible for the pathogenesis of focal cortical dysplasia.

The following chapters address our investigation of the role of STRADA as well as mTOR signaling in cortical development:

- Chapter 2 provides a descriptive account of the expression of several growth factors and receptors that modulate mTOR signaling, in a related canonical

mTOR-associated neurodevelopmental disorder, TSC. This provides an initiation to the study of mTOR dysregulation and neurological disease.

- Chapter 3 defines the role of STRADA in cortical development as a director of neuronal pathfinding and migration, through regulating actin dynamics.
- Chapter 4 describes our progress in generating a STRADA knockout mouse to model PMSE and STRADA's role in cortical development *in vivo*.
- Chapter 5 provides an overall summary of dissertation studies and their implications for future work and clinical treatments.

Significance

mTOR cascade signaling regulates several key processes in cortical development. Loss of any of several modulators of this signaling pathway results in aberrant corticogenesis, and a common spectrum of clinical symptoms including epilepsy and autism-like features. While much work has been done to define the effects of TSC1/2 or PTEN depletion, associated with the clinical syndromes TSC and autism-macrocephaly syndrome, respectively, relatively little is known about the newly-identified mTOR regulator STRADA and its rare but dramatic associated clinical syndrome PMSE. We believe that STRADA serves as an ideal model mTOR regulatory protein, and PMSE an ideal model disorder for several reasons. First, PMSE is the only known human disorder resulting from a homozygous mutation in an mTOR inhibitor. Second, STRADA homozygous mutation is associated with 100% penetrance of the disease, with a severe epileptic and neurocognitive phenotype common to all patients. Finally, all patients with PMSE share the same STRADA deletion (61).

It is an especially exciting time for the development of biologically-targeted therapies, with the mTORC1 inhibitor rapamycin already showing promising results in several clinical trials for related mTOR-associated disorders, and with the development of other inhibitors to target nodes on the mTOR pathway, such as the p70S6kinase inhibitor PF-4708671 and the dual mTORC1/mTORC2 inhibitor Torin1 (72, 74, 75). In our studies, we define a novel role for the mTOR inhibitory protein STRADA in directing migrating neurons, a function we propose to be critical in cortical development, and the disruption of which can account for several neuropathological features of PMSE. Importantly, we develop STRADA-depletion PMSE models as a mechanism for defining the role of mTOR signaling in cortical development and for identifying molecular targets for the development of novel therapeutics for mTOR-associated neurodevelopmental disorders.

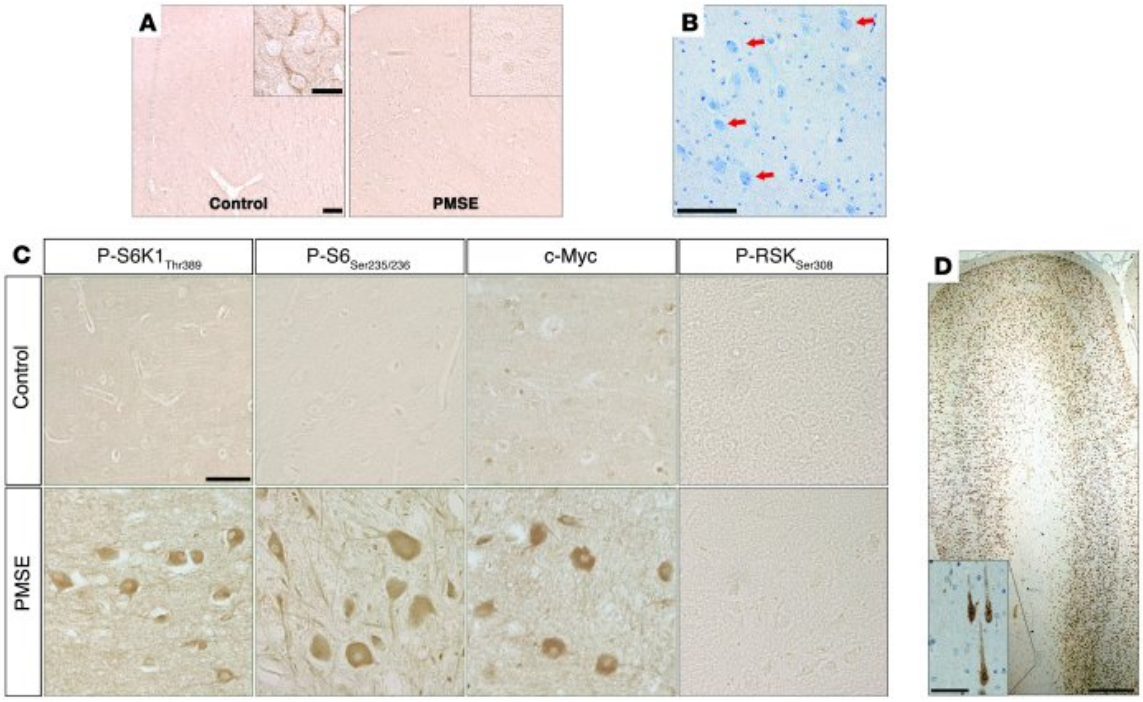

Figure 1.1. PMSE patient brain exhibits lack of STRADA, cytomegaly, enhanced mTORC1 activity, and neuronal heterotopia. ***A,*** Immunohistochemical analysis reveals a lack of STRADA expression in PMSE versus control cortex. ***B,*** Luxol Fast Blue-Cresyl Violet (LFB-CV) staining reveals numerous cytomegalic cells present in basal ganglia (indicated by red arrows). ***C,*** Enhanced P-S6K1, P-S6, and c-Myc, in the absence of enhanced P-RSK, in PMSE cortex indicates hyperactive mTORC1. ***D,*** PMSE cortex exhibits heterotopic neurons present in the subcortical white matter, highly suggestive of a neuronal migratory defect. Scale bars: ***A,*** 100 μm, 20 μm inset; ***B,*** 50 μm; ***C,*** 50 μm; ***D,*** 1 mm, 50 μm inset.

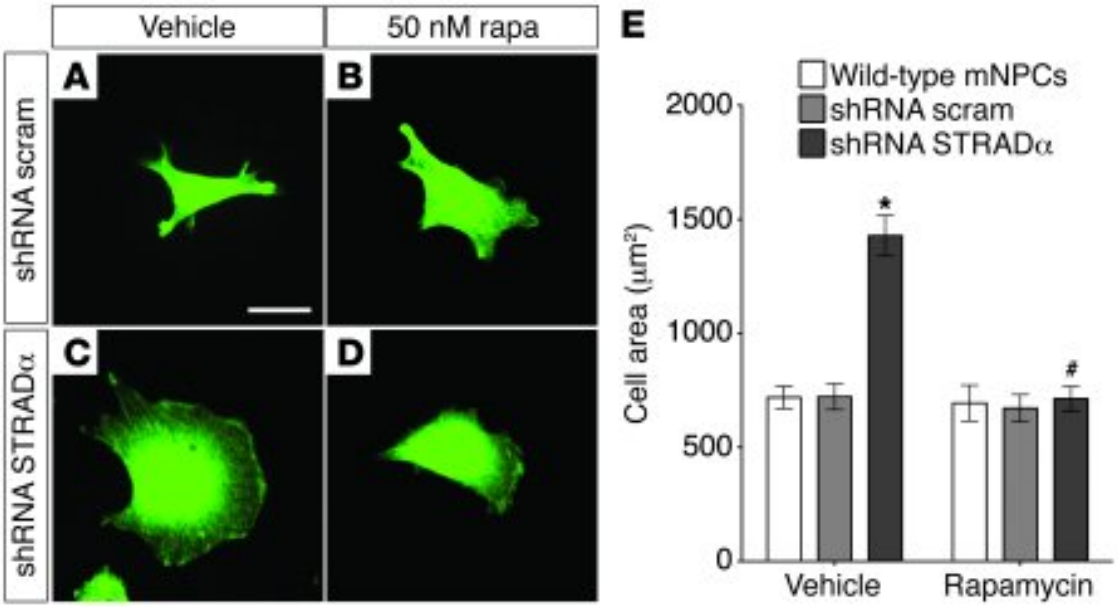

Figure 1.2. Knockdown of STRADA (STRADα) *in vitro* in mNPCs results in mTORC1-dependent cytomegaly. ***A,C,*** GFP-tagged STRADA KD mNPCs have significantly greater surface area than Scrambled shRNA transfected GFP-tagged control mNPCs. ***B,D,E,*** This effect is fully prevented with 50 nM rapamycin treatment, indicating that STRADA's effects on cell size are mTORC1-dependent. The experiment was conducted 2 independent times; data are from n=30 cells per transfection and treatment condition. *$P < 0.01$ versus other vehicle-treated control groups; $^{\#}P < 0.01$ versus vehicle-treated STRADA KD cells. Scale bar, 20 μm.

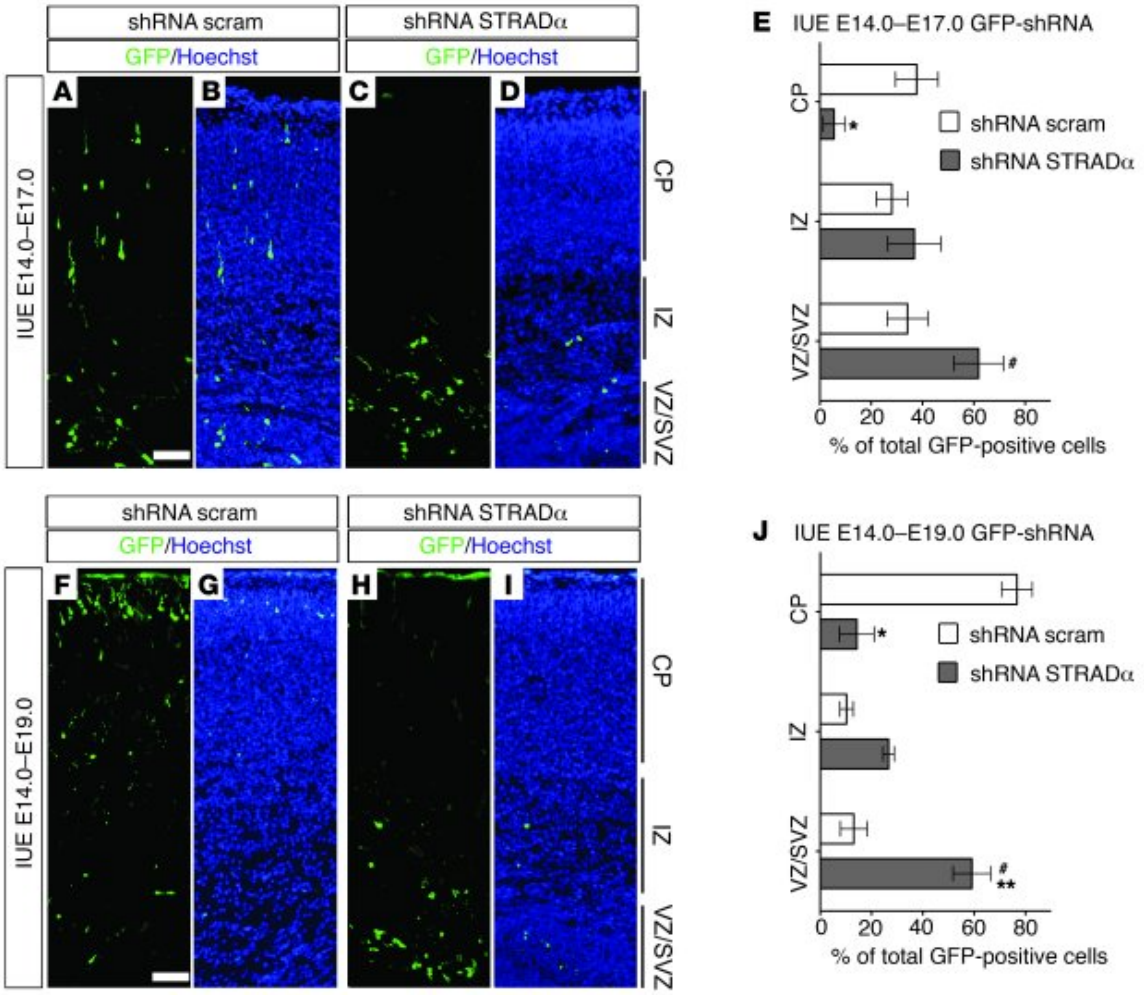

Figure 1.3. Knockdown of STRADA (STRADα) *in vitro* results in aberrant cortical lamination. ***A,B,*** Transfection of neural progenitor cells in the ventricular/subventricular zone (VZ/SVZ) via IUE with control GFP-tagged scrambled shRNA (Scram) at embryonic day 14.0 (E14.0) results in a pattern of transfected cells migrating from the VZ/SVZ through the intermediate zone (IZ) at E17.0. ***F,G,*** By E19.0, Scram transfected cells have predominantly reached their destination of Layer II/III of the cortical plate (CP). ***C,D,*** In contrast, transfection of neural progenitor cells with GFP-tagged STRADA shRNA (STRADA KD) at E14.0 results in an abnormal retention of GFP^+ cells in the VZ/SVZ at E17.0, persisting at E19.0 (***H,I***). ***E,J,*** Statistical analysis indicates a failure of STRADA KD neural progenitor cells to reach the CP at both E17.0 and E19.0, compared with Scram control cells. n = 5 animals per condition at each time point. $^*P < 0.05$ versus CP Scram; $^{**}P < 0.05$ versus VZ/SVZ Scram; $^{\#}P < 0.05$ versus CP STRADA KD. Scale bars, 50 μm.

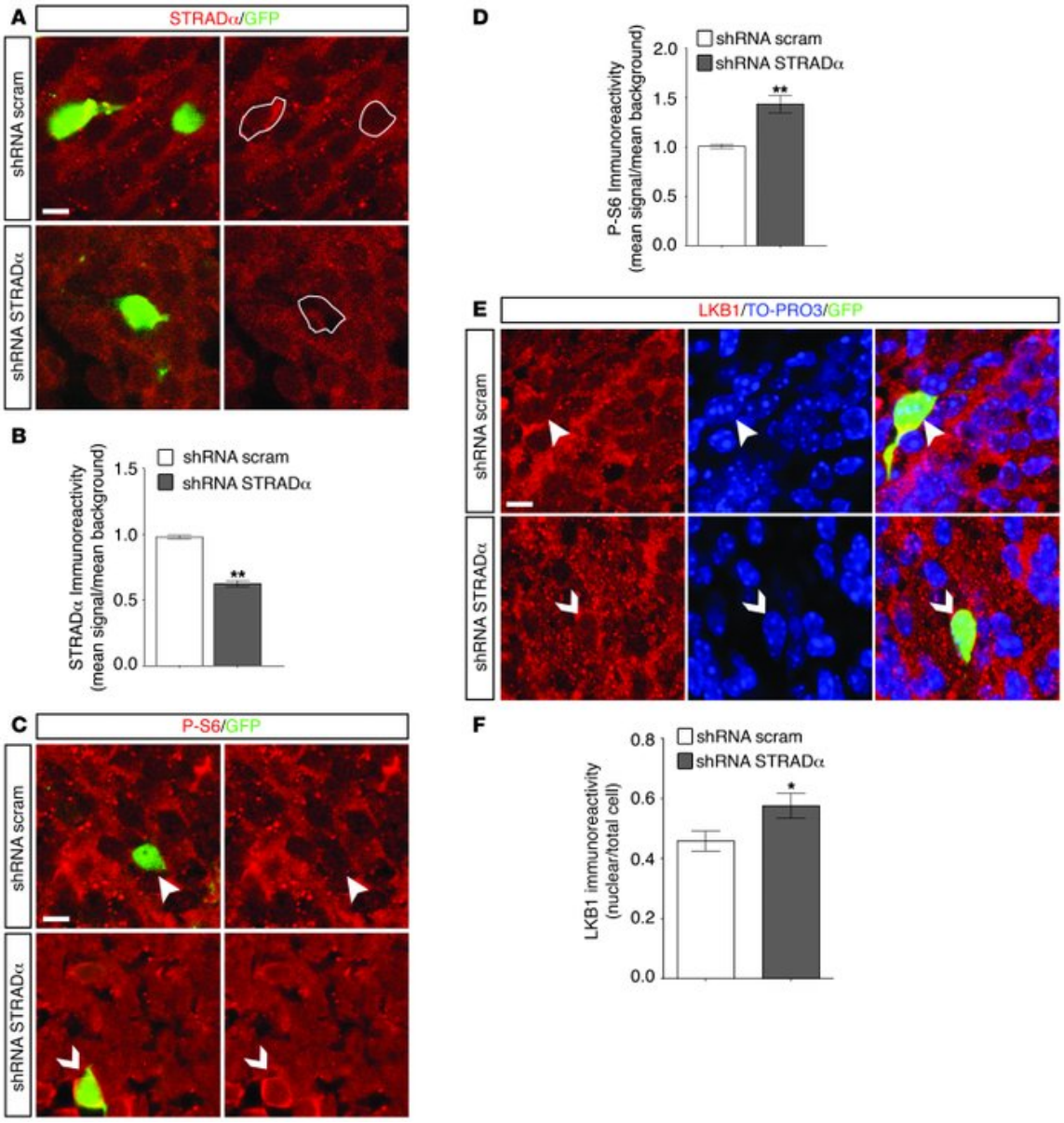

Figure 1.4. STRADA (STRADα) knockdown *in vivo* through IUE results in depletion of STRADA, enhanced mTORC1 activity, and a shift toward nuclear localization of LKB1. ***A,B,*** Immunofluorescent staining reveals a significant decrease in STRADA expression in cells transfected with GFP-tagged STRADA shRNA (STRADA KD) versus control cells transfected with GFP-tagged scrambled shRNA (Scram). ***C,D,*** GFP^{+} STRADA KD cells exhibit enhanced P-S6, indicative of aberrant mTORC1 activation. ***E,F,*** Knockdown of STRADA results in a significant increase in the percentage of LKB1 localized to the nucleus. Data are mean signal/background (***B,D***) or mean nuclear/total LKB1 (***F***). n = 10 cells per condition. $*P < 0.05$; $**P < 0.01$. Scale bars, 6.08 μm.

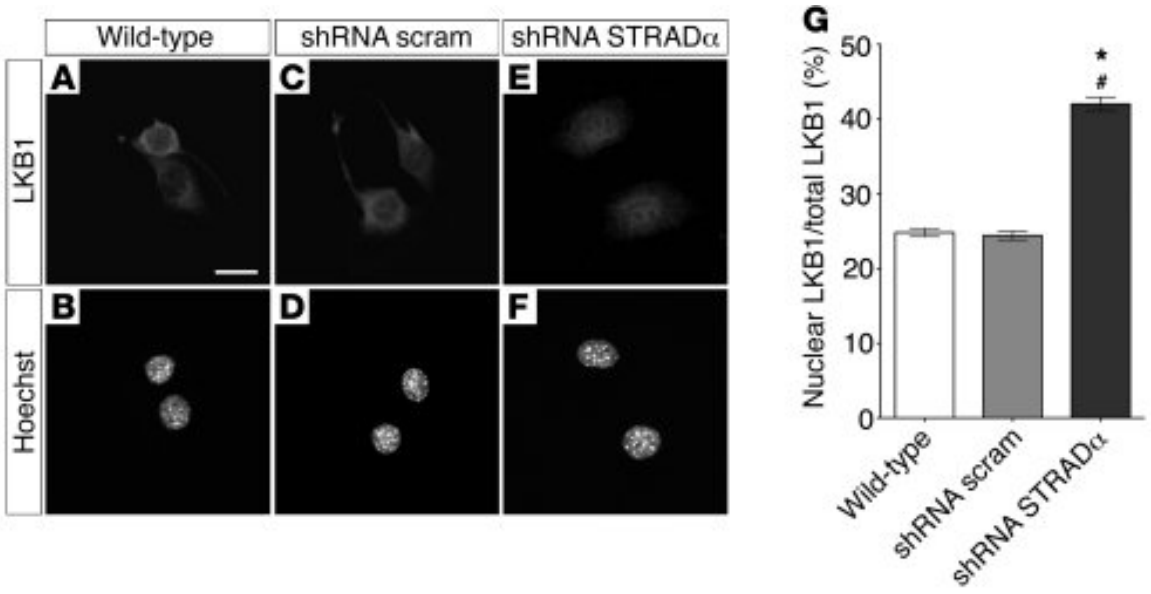

Figure 1.5. Knockdown of STRADA (STRADα) *in vitro* in mNPCs results in increased nuclear localization of LKB1. ***A,B,*** Wild-type and ***C,D,*** stably-transfected control scrambled shRNA (Scram) mNPCs exhibit predominantly cytoplasmic LKB1. Nuclear area is defined by Hoechst nuclear staining (in ***B,D,F***). ***E,F,G,*** Stably-transfected STRADA shRNA (STRADA KD) mNPCs exhibit a significant increase in the percentage of total LKB1 localized in the nucleus. n = 132 wild-type cells, 143 Scram cells, 149 STRADA KD cells. **P* < 0.01 versus wild-type; $^{\#}P$ < 0.01 versus Scram. Scale bar, 20 μm.

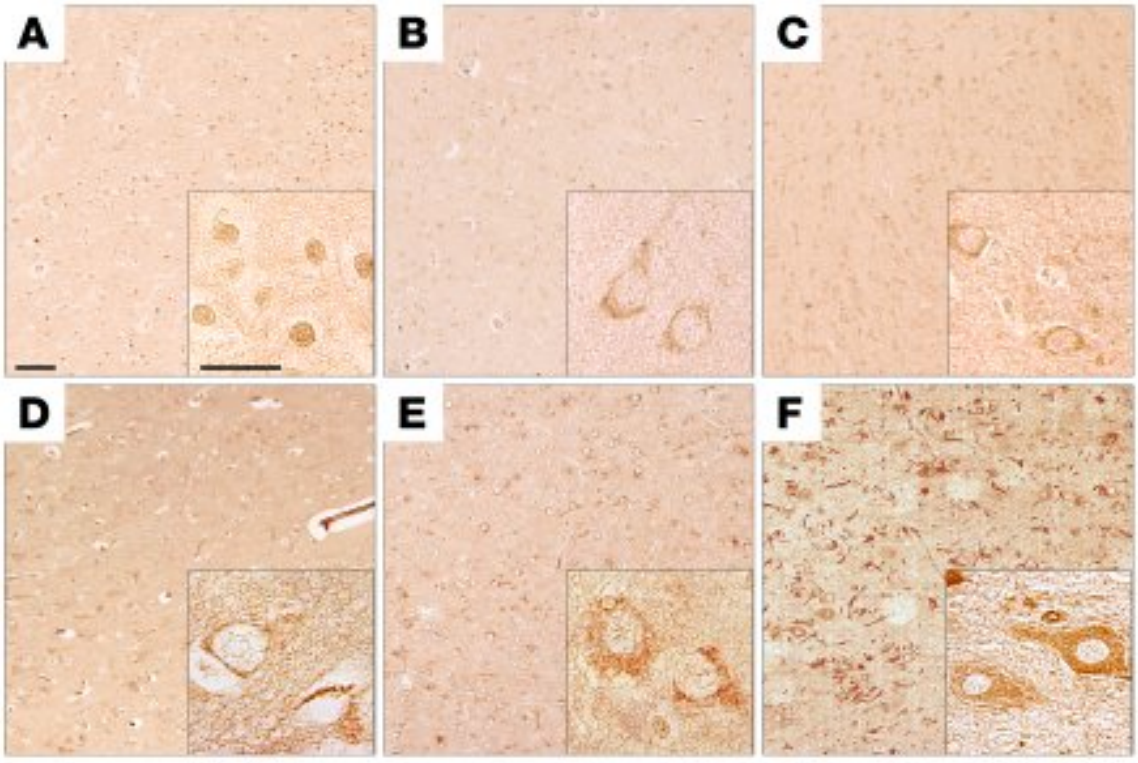

Figure 1.6. Replicating experimental in vitro and in vivo results, PMSE cortex exhibits almost exclusively nuclear LKB1 localization, in contrast to cortex samples from several other epileptic conditions. ***A,*** Approximately 95% of neurons in PMSE cortex exhbit nuclear LKB1 staining. In contrast, in ***B,*** non-epileptic control cortex as well as cortex from patients with ***C,*** cortical dysplasia focal epilepsy syndrome, ***D,*** sporadic type II focal cortical dysplasia, ***E,*** hemimegalencephaly, and ***F,*** tuberous sclerosis complex; only approximately 5% of neurons exhibit nuclear LKB1. Scale bars, 100 μm; 25 μm (insets).

CHAPTER 2

ENHANCED GROWTH FACTOR EXPRESSION IN TUBEROUS SCLEROSIS COMPLEX[2]

[2] This work was originally published in *The American Journal of Pathology*, Vol. 178, No. 1, January 2011. Parker, W.E., Orlova, K.A., Heuer, G.G., Baybis, M., Aronica, E., Frost, M., Wong, M., and Crino, P.B. Enhanced Epidermal Growth Factor, Hepatocyte Growth Factor, and Vascular Endothelial Growth Factor Expression in Tuberous Sclerosis Complex. Published by Elsevier Inc.

Abstract

Epidermal derived- (EGF), hepatocyte- (HGF), and vascular endothelial- (VEGF) growth factors regulate angiogenesis and cell growth in the developing brain. EGF, HGF, and VEGF modulate the activity of the mammalian target of rapamycin (mTOR) cascade, a pathway regulating cell growth that is aberrantly activated in tuberous sclerosis complex (TSC). We hypothesized that expression of EGF, HGF, VEGF and their receptors EGFR, c-Met, and Flt-1, respectively, would be altered in TSC. We show by cDNA array and immunohistochemical analysis that EGF, EGFR, HGF, c-Met, and VEGF, but not Flt-1, mRNA and protein expression was upregulated in *Tsc1* conditional knockout (*Tsc1*^{GFAP}CKO) mouse cortex. Importantly, these alterations closely predicted overexpression of these proteins in TSC human cortex. Expression of EGF, EGFR, HGF, c-Met and VEGF protein as well as HIF-1α, a transcription factor that regulates VEGF levels and is also modulated by mTOR cascade activity, was enhanced in subependymal giant cell astrocytomas (SEGAs; n=6) and tubers (n=10) from 15 TSC patients. Enhanced expression of these growth factors and growth factor receptors in human SEGAs and tubers and in the *Tsc1*^{GFAP}CKO mouse provides potential target molecules for therapeutic development in TSC.

Introduction

Tuberous sclerosis complex (TSC) is an autosomal dominant disorder resulting from mutations in the *TSC1* or *TSC2* genes, which encode TSC1 and TSC2 proteins, respectively (76, 77). Many individuals with TSC exhibit cognitive disability and autism (78), and over 75% of TSC patients develop seizures (79-81). Examination of the brain demonstrates cortical tubers and subependymal nodules (SENs) in over 70% of TSC patients. Tubers are developmental malformations of the cerebral cortex highly associated with epilepsy and neurocognitive abnormalities. SENs are nodular lesions (typically less than 1 cm in size) located on the surfaces of the lateral and third ventricles. In approximately 10-20% of TSC patients, subependymal giant cell astrocytomas (SEGAs) arise within the lateral ventricles, often near the foramen of Monro. SEGAs are WHO grade I tumors with low mitotic index as evidenced by Ki-67 immunoreactivity suggestive of slow cellular proliferation (82, 83). It is widely believed that SENs grow to form SEGAs, although the molecular mechanisms governing transformation from SEN to SEGA are unknown (84). Both SENs and SEGAs consist of dysmorphic glial cells, enlarged giant cells (GCs), and spindle shaped cells of unknown phenotype (85, 86). Cellular immunoreactivity for GFAP, neurofilament, S-100, neuron specific enolase, and synaptophysin proteins suggests that SEGAs contain both glial and neuronal cell types. Lineage studies have demonstrated that SEGAs express cellular markers found in progenitors derived from the subventricular zone (SVZ) adjacent to the lateral ventricles (87, 88) and that many of these markers are also expressed in cortical tubers.

The TSC1 and TSC2 proteins combine to form a heterodimer that functions as a direct upstream modulator of the mammalian target of rapamycin (mTOR) pathway,

which integrates growth factor and energy level signals to promote several cellular processes, including cell growth and proliferation (89) protein translation, and angiogenesis. *TSC1* and *TSC2* mutations are associated with loss of inhibitory modulation and consequent constitutive activation of the mTOR cascade, resulting in enhanced cell size and proliferation, especially under conditions favoring cell growth. Previous studies have suggested that altered growth factor expression may be associated with abnormal cellular architecture in the brains of TSC patients. For example, differential expression of neurotrophins and their receptors has been observed in cortical tubers (90), and TSC1-TSC2 mediated control of mTOR is modulated by insulin-like growth factor-1 (IGF-1) (91-93). Recent evidence also suggests that mTOR signaling is regulated by several growth factors such as EGF and HGF and that TSC1-TSC2 may regulate downstream expression of select angiogenic factors, such as VEGF via hypoxia inducible factor-1α (HIF-1α) (94). For example, EGF regulates smooth muscle cell proliferation via its receptor EGFR through mTOR signaling (95). VEGF expression is upregulated in the Eker rat TSC model, in mouse embryonic fibroblasts lacking TSC2, and in facial angiofibromas from TSC patients (94, 96, 97). Brain and kidney lesions in TSC exhibit abnormally enhanced expression of the vascular endothelium protein marker CD31 (98). Altered VEGF isoform D levels were observed in serum from TSC patients with lymphangioleiomyomatosis (LAM) (99). Of note, enhanced VEGF expression in TSC may occur via both mTOR-dependent and mTOR-independent mechanisms (100).

Altered expression of EGF, HGF, VEGF, and their receptors EGFR, c-Met, and Flt-1 (VEGFR1) has not been investigated in the brain in TSC, yet considerable evidence suggests that these factors play a pivotal role in the mTOR cascade's influence on cellular

phenotype, and could therefore provide insight into the mechanism of TSC cortical pathogenesis. Thus, we assayed both mRNA and protein expression in the *Tsc1* conditional knockout (*Tsc1*^{GFAP}CKO) mouse and in human TSC brain tissue specimens as a strategy to identify growth factors that could be targeted for therapeutic development in TSC.

Materials and Methods

Tsc1 Conditional Knockout Mice

Tsc1 conditional knockout (*Tsc1*^{GFAP}CKO) mice were generated as previously described (51) at The Washington University School of Medicine in accordance with the guidelines established by The Animal Studies Committee of Washington University. Samples at post-natal day 1 (P1) and P10 were analyzed for several reasons. First, at these timepoints, the active phases of embryonic neuronal migration are completed and thus, there is homeostatic expression of growth factors and receptors. Second, by P1 and P10 there is active expression of the Cre transgene in the brain and thus, adequate knockout of Tsc1 could be documented. Third, we wanted to be certain that none of the altered growth factor expression was a consequence of early seizures and altered behavioral phenotypes that occur in these animals by P20.

Extraction of mRNA from Cerebral Cortex in the Tsc1^{GFAP}*CKO Mice*

Poly(A) mRNA was extracted from the cerebral cortex of *Tsc1*^{GFAP}CKO or wild-type (WT) mice (n=5 each) as described previously (90). The entire cortex from both hemispheres was removed from the subcortical structures using a microscalpel at the level of the mid-hippocampus. Poly(A) mRNA served as a template for *in vitro* cDNA synthesis with avian myeloblastosis virus reverse transcriptase (AMVRT), and then double stranded template cDNA was synthesized with T4 DNA polymerase I (Boehringer-Mannheim) from extracted cDNA. mRNA was amplified from the double stranded cDNA with T7 RNA polymerase (Epicentre Technologies) incorporating ^{32}PCTP as a radiolabel. Amplified mRNA served as a template for a second round of

cDNA synthesis with AMVRT, dNTPs, and N(6) random hexamers (Boehringer-Mannheim). cDNA generated from amplified mRNA was made double-stranded and served as template for a second mRNA amplification, again incorporating ^{32}PCTP radiolabel. The radiolabeled, amplified mRNA was used as a probe for cDNA arrays.

cDNA Array Analysis

cDNA arrays containing full-length mouse EGF, EGFR, HGF, c-Met, VEGF, and Flt-1 cDNAs were probed with ^{32}PCTP radiolabeled mRNA amplified from the cortex (one probe per array). All hybridization reactions were performed twice for each probe. GAPDH cDNA was included to serve as positive hybridization control and pBlueScript (pBS) plasmid cDNAs were used to define background levels of hybridization on each array. Prehybridization (8 hours) and hybridization (24 hours) conditions were in 6X SSPE buffer, 5X Denhardt's solution, 50% formamide, 0.1%SDS, and salmon sperm DNA 200 mg/ml at 42^{o}C. Blots were washed in 2X SSC. mRNA probe hybridization to array cDNAs was determined by phosphorimaging and densitometry.

Human Tissue Specimens

Tuber and SEGA samples (n=15 patients; 7 females; 10 tubers, 6 SEGAs, mean age 9.9 years; in one patient a tuber and SEGA were removed *en bloc*; see **Table 2.1**) were obtained from patients with clinically diagnosed TSC. There were no significant differences in age distribution in the TSC patient specimens used in the study. Tubers were removed as part of surgery for the treatment of intractable epilepsy, and SEGAs were removed to alleviate symptomatic hydrocephalus. Surgical tissue specimens were obtained from Academic Medical Center, University of Amsterdam, The Netherlands,

and Minnesota Epilepsy Group, St. Paul, MN. Surgical localization of the tuber resection site reflected the seizure focus as determined by scalp or intracranial EEG monitoring. SEGAs were identified pre-operatively by magnetic resonance imaging as progressively enlarging lesions that exhibited enhancement with gadolinium. Three SENs were obtained post-mortem from 3 TSC patients (**Table 2.1**) who died of non-neurological causes. In these 3 specimens, morphologically normal cortex adjacent to histologically defined tubers was also obtained. Clinical mutation testing (indicated as "Genotype" in Table 1) results among the tuber, SEN, and SEGA patients revealed a *TSC1* mutation in 5 patients and a *TSC2* mutation in 10 patients; mutation data was unavailable from 3 patients (indicated as "NMI" in **Table 2.1**).

Post-mortem control brain tissue specimens (n=4; 2 females; Table 1) were procured from the Brain and Tissue Bank for Developmental Disorders, University of Maryland (http://medschool.umaryland.edu/BTBank/) from individuals who died of non-neurologic causes. Seizures were not terminal events in these patients and none had a personal or family history of epilepsy or TSC. The cytoarchitecture of these specimens was intact. Additional surgical epilepsy control tissue consisted of temporal neocortical specimens (n=5; 3 females; **Table 2.1**) obtained from individuals undergoing temporal lobectomy for intractable complex partial seizures (University of Pennsylvania Medical Center). These patients had no history or clinical findings compatible with a diagnosis of TSC and the histology of the tissue samples was intact (these specimens were classified as epilepsy controls). All human tissue was obtained in accordance with protocols approved by the University of Pennsylvania Institutional Review Board and Committee on Human Research.

Immunohistochemistry

All mouse and human tissue samples were immersion-fixed in 4% paraformaldehyde, embedded in paraffin, and sectioned at 8mm. All fixed tissue blocks were hydrated through graded ethanols. Slides were pretreated with antigen unmasking solution (Vector Labs, Burlingame, CA) prior to immunostaining reactions. Sections were probed one of the following antibodies: EGF (1:1000 dilution, rabbit polyclonal, Santa Cruz, Burlingame, CA), EGFR (1:100, rat polyclonal, Santa Cruz), EGFRvIII variant (courtesy D. O'Rourke M.D., Department of Neurosurgery, University of Pennsylvania, Philadelphia, PA), phospho-EGFR (p-EGFR, phospho Y1068, 1:250, rabbit monoclonal, Abcam, Cambridge, MA), HGF (1:500, mouse monoclonal, Abcam), c-Met (1:10 dilution, rabbit polyclonal, Abcam), VEGF (1:50, mouse monoclonal, Abcam), Flt-1 (1:100, mouse monoclonal, Santa Cruz), HIF-1a (1:1500, mouse monoclonal, Abcam), phospho-S6 ribosomal protein (p-S6, Ser235/236; 1:100, rabbit polyclonal, Cell Signaling, New England Biolabs, Beverly, MA), or S6 ribosomal protein (detects endogenous S6 expression including both phosphorylated and non-phosphorylated isoforms, 1:100, rabbit monoclonal, Cell Signaling) overnight at 4^{o}C, and with secondary antibodies at room temperature for 1 hour. The slides were visualized using avidin-biotin conjugation (Vectastain ABC Elite; Vector Labs) with 3,3'-diaminobenzidine. Following immunolabeling, sections were dehydrated through graded ethanols and xylene and coverslip-mounted (Permount).

Quantitative Cell Counts

Three representative contiguous digital photos were obtained (20X magnification) from each mouse brain tissue section using image acquisition and analysis software (Spot RT CCD camera, Diagnostic Instruments, Inc. and Phase 3 Imaging System integrated with Image Pro Plus; Media Cybernetics, Silver Spring, MD). The three images spanned a 1 mm^2 region of interest (ROI) within the lateral neocortex that was operationally defined and standardized across all cortex specimens as dorsolateral cerebral cortex at the level of the rostral hippocampus mid-way between the superior sagittal sulcus and the rhinal sulcus (Bregma coordinate -1.70mm). The area of the cortex for each ROI was determined with a glass micrometer under light microscopy.

In the human specimens, we were particularly interested in the number of GCs that expressed each protein growth factor marker. Thus, GCs were defined using maximal cell diameter based on cresyl violet and hematoxylin and eosin staining for quantitative cell counting analysis. Representative digital photos were obtained (20X magnification) under light microscopy from each tissue section (n=3 sections per case) using image acquisition and analysis software as above. Each image spanned a 1 cm^2 region of interest (ROI). Prior to final assignment as a GC by the software, each ROI was visually inspected and cellular elements erroneously included in the computerized analysis were deleted. Mean maximal diameter (cell diameter at its largest aspect) was calculated using Image Pro Plus software as expressed in pixel units that were converted to microns by direct calibration with a micrometer.

The relative optical density ratio (ODR) of labeled cells was calculated using Image Pro Plus software using a previously defined approach (90). The ODR is calculated

by determining the level of pixel staining density in labeled cells versus the pixel density of the non-cellular background (the cell densities are digitally subtracted from the image). An ODR >3 was used as a threshold to define immunopositivity for a given antibody. In the mouse, the total numbers of p-S6 immunolabeled cells were determined for each case and then expressed as a mean (±SEM) for *Tsc1*^{GFAP}CKO and control specimens. For growth factors, we used a semi-quantitative scale (0, no staining to ++++, intense labeling across most cells in each ROI) to represent labeling density in each ROI. The size of p-S6 immunolabeled cells was defined using maximum cell diameter and determining the mean (±SEM). In the human specimens, the total numbers of morphologically identified GCs were determined in each ROI for each case and the mean (±SEM) numbers of GCs in ROIs were determined across all 10 tubers and 6 SEGAs. Statistically significant differences in GCs expressing individual protein markers were determined by Student's t-test ($p<0.05$).

Western Analysis

Lysates of wildtype and *Tsc1*^{GFAP}CKO cortex were analyzed for p-S6 protein levels. A DuPont Kinetic Microplate Reader was used to approximate 15 μg total protein for each of the samples, which were individually loaded into separate wells of a 4-15% Tris-HCl polyacrylamide gel (Bio-Rad Laboratories), and electrophoresed at 60V. Proteins were then transferred overnight at 4^{o}C onto a polyvinylidene difluoride (PVDF, Millipore) membrane. Membranes were incubated in a 5% non-fat dry milk (NFDM) blocking solution for 1 hour at room temperature (RT) and then probed with rabbit anti-p-S6 ribosomal protein (Ser235/236; 1:1000, overnight at 4^{o}C, Cell Signaling) antibodies.

Rabbit anti-GAPDH (1:1000, 1 hour at RT, Cell Signaling) and rabbit anti-β-actin (1:1000, 1 hour at RT, Cell Signaling) served as protein loading controls. Membranes were then incubated for 1 hour at RT with horseradish peroxidase (HRP)-conjugated donkey anti-rabbit IgG (1:3000, GE Healthcare). Membranes were washed and developed using either ECL or ECL Plus Western Blotting Detection Reagents (Amersham, GE Healthcare), as needed for HRP visualization.

Statistical Analysis

The expression of each mRNA was determined by analysis of the radiolabeled mRNA-cDNA hybridization intensity on each array using ImageQuant5.0 software. Non-specific hybridization to pBS plasmid cDNA was subtracted from the hybridization intensity of each mRNA-cDNA to define specific hybridization intensity. The relative hybridization intensity for each mRNA was determined by averaging the phosphorimaging density of all the mRNA-cDNA hybrids on each individual array and then expressing each mRNA-cDNA hybrid as a percentage of the average hybridization intensity of the entire array. Differences in relative mRNA abundance were determined using a one-way ANOVA and a Bonferroni *post-hoc* correction was applied to each univariate ANOVA. If a significant difference was found with a Bonferroni-adjusted ANOVA, individual *post-hoc* comparisons were made using the Fischer's test ($p<0.05$ was considered significant).

Results

Enhanced S6 Phosphorylation in the Tsc1^{GFAP}*CKO Mouse Cortex and Human TSC Brain Tissue*

The expression level of Tsc1 mRNA was determined at P1 and P10 in the cerebral cortex in *Tsc1*^{GFAP}CKO mice. At P1, Tsc1 mRNA levels were reduced by 86±4% and at P10, levels were reduced by 92±7% compared to wild-type (Wt) mice (n=10 sections each in *Tsc1*^{GFAP}CKO and Wt control samples at each timepoint, $p<0.05$; **Figure 2.1*C***). Expression of Tsc2 mRNA at P1 and P10 in cortex from the *Tsc1*^{GFAP}CKO mice did not differ from that observed in Wt mice.

There was a low level of baseline p-S6 protein expression in cortical neurons and astrocytes of control Wt mice at P1 and P10. P-S6 labeled astrocytes were observed throughout all cortical layers. In neurons, p-S6 expression was observed primarily within the somatic and dendritic cytoplasm of pyramidal cells in layers III and V. At both P1 and P10, there was a clear increase in the number of p-S6 labeled cortical cells in the *Tsc1*^{GFAP}CKO mouse brain compared with control Wt brains (**Figure 2.1*A***). Quantitative cell counts of p-S6 labeled cells were performed at P1 and P10, which antedates the onset of clinical seizures in these mice. There was a significant increase in the number of p-S6 labeled cells at P1 (115 control, and 336 *Tsc1*^{GFAP}CKO mouse, $p<0.05$) and P10 (665 control, and 1319 *Tsc1*^{GFAP}CKO mouse, $p<0.05$) (**Figure 2.1*B***). Western assay revealed markedly enhanced S6 protein phosphorylation in *Tsc1*^{GFAP}CKO mice, compared to Wt control (**Figure 2.1*C***) (55). Immunolabeling of human TSC cortex also revealed an increase in phosphorylation of S6, relative to control cortex, with no corresponding

increase in endogenous S6 (both phosphorylated and non-phosphorylated isoforms) expression overall (Supplemental Figure). Increased S6 phosphorylation in tubers is consistent with previous findings in TSC and confirms mTOR hyperactivity in these lesions (40).

Increased Growth Factor mRNA Expression in Tsc1^{GFAP}CKO Mice

The expression of EGF, EGFR, HGF, c-Met, and VEGF mRNAs in cerebral cortex was increased at P1 and P10 in *Tsc1*^{GFAP}CKO mice compared with Wt mice (Fig. 2). EGFR mRNA levels were increased 9.3-fold and 7.1-fold at P1 and P10, respectively, while EGF was increased 2.1-fold and 2.8-fold, HGF was increased 3.3-fold and 4-fold, c-Met was increased 3-fold at both timepoints, and VEGF was increased 5.8-fold and 5.9-fold at P1 and P10, respectively. However, Flt-1 mRNA expression in *Tsc1*^{GFAP}CKO mice did not differ from that of Wt mice at either timepoint (not shown). Of note, GFAP mRNA expression in the cortex was increased by 3.8-fold at P1 and 6.4-fold at P10, consistent with previous reports that there is progressive increase in the number of astrocytes in the *Tsc1*^{GFAP}CKO mice (51).

Increased Growth Factor Protein Expression in Tsc1^{GFAP}CKO Mice

Low levels of EGF, EGFR, HIF-1a, c-Met, and Flt-1 expression were observed in Wt mice at P1 and P10, whereas VEGF and HGF protein expression levels were higher at both timepoints. Since a dramatic alteration of laminar architecture is not a feature of the Tsc1^{GFAP}CKO mouse cortex, we did not observe substantive changes in laminar expression of any of the growth factors or their receptors. Rather, our findings suggested enhanced expression in the expected distribution of each identified layer. For example, in

the Wt mice, EGF was expressed at low levels across the cortical plate at both P1 and P10 whereas in the $Tsc1^{GFAP}$CKO mouse, there was a global increase in EGF expression across all layers. HGF, c-Met, and VEGF exhibited an alteration in laminar expression profiles (see **Table 2.2**) with enhanced expression in deeper cortical layers in the $Tsc1^{GFAP}$CKO mouse. The expression of EGF, EGFR, HGF, c-Met, VEGF, and HIF-1a proteins was increased at P1 and P10 in $Tsc1^{GFAP}$CKO mice compared with Wt mice (**Figures 2.3-2.5**) in a profile that was similar, though not identical to mRNA expression. However, similar to its corresponding mRNA, Flt-1 expression in $Tsc1^{GFAP}$CKO mice did not differ from that of Wt mice at either timepoint (not shown). By P10, immunoreactive cells were identified in cerebral cortex across all 6 layers, and both neurons and astrocytes exhibited immunolabeling.

Increased Growth Factor Protein in Human TSC Brain Tissue

The mean maximal cell soma diameter of the GCs was 112.4 μm (range 104-125 μm) and thus, this parameter was used to generate cell counts for each individual protein marker. The expression profile for each protein marker was heterogeneous across the tubers and SEGAs. In some specimens, even when corrected for differing numbers of GCs across each case, there was robust expression of individual proteins, while in other specimens fewer numbers of cells were labeled (**Table 2.3**). For some proteins detailed below, there was enriched expression in GCs in deeper portions of the tuber (i.e., within the subcortical white matter) (**Table 2.3**, WM), whereas for others, protein expression was observed in GCs throughout the thickness of the lesion (**Table 2.3**, ALL).

Immunohistochemical analysis demonstrated that EGF, EGFR, HGF, c-Met, VEGF, and HIF-1α protein expression was markedly increased in tuber (**Figures 2.6-2.9**) and SEGA (**Figure 2.10**) specimens when compared with specimens of age-matched, post-mortem, and non-TSC epilepsy cortex. Cellular expression of growth factor proteins was observed in GCs throughout the thickness of each tuber specimen, from pial surface to subcortical white matter. For example, expression of EGF and EGFR was primarily observed in GCs in tubers (**Figure 2.6**) and SEGAs (**Figure 2.10**). Expression of the phospho-isoform of EGFR was also enhanced in tubers compared with control cortex. The EGFRvIII variant protein isoform is frequently identified as an overexpressed protein in certain types of astrocytomas and is linked to enhanced EGF signaling in these tumors. However, in contrast to native EGFR, there was no expression of EGFRvIII variant protein isoform in tubers or SEGAs (data not shown). HGF and c-Met expression was most marked in GCs and some of the surrounding dysmorphic neurons, within tubers (**Figure 2.7**) and SEGAs (**Figure 2.10**). VEGF was robustly expressed by GCs and capillary endothelial cells in tubers (**Figure 2.8**). Additionally, the level of VEGF expression in non-tuber cortex from TSC patients was increased relative to the level of VEGF expression in cortex from non-TSC epilepsy control patients (**Figure 2.9**). The distribution of HIF-1α expression was similar to that of VEGF, although HIF-1α expression was not as widespread in tubers and was often seen in small clusters of cells, especially in the subcortical white matter (**Figure 2.8**). In contrast, the levels of the VEGF receptor Flt-1 were not increased in either tubers or SEGAs (not shown).

Growth factor and growth factor receptor expression in non-tuber TSC cortex did not differ from non-TSC epilepsy control cortex, with the exception of VEGF.

Specifically, rare GCs at the edge of the resection margin exhibited VEGF expression and appeared as a stark contrast to the surrounding tissue, and there were scattered VEGF immunolabeled cells in the non-tuber TSC cortex that were more frequent in number than in control non-TSC epilepsy cortex. These findings argued against a non-specific effect of anti-seizure medications, recurrent seizures, age, or post-mortem interval on protein expression.

Additionally, an important finding was that growth factor and growth factor receptor expression was not enhanced in SENs, and appeared within these nodules to be similar to expression levels in control tissue (data not shown). These findings suggest that enhanced growth factor expression was indeed specific for tubers and SEGAs and hint toward a possible role of growth factors in the SEN to SEGA transformation.

Discussion

This is the first study to demonstrate enhanced EGF, EGFR, HGF, c-Met, and VEGF expression in association with loss of *Tsc1* in the mouse and with human TSC brain pathology. We were specifically interested in growth and angiogenic factors because of the documented enhancement of cell proliferation and angiogenesis in TSC-associated lesions such as angiomyolipomas and SEGAs. The expression of EGF, EGFR, HGF, c-Met, and VEGF mRNAs was increased at P1 and P10 in *Tsc1*^{GFAP}CKO mouse cortex, and these findings predicted similar changes in human TSC tubers and SEGAs. Increased mTOR signaling was demonstrated in *Tsc1*^{GFAP}CKO mouse brain and human TSC cortical tubers and SEGAs, as evidenced by increased phosphorylation of S6 protein. We conclude that enhanced expression of EGF, EGFR, HGF, c-Met, and VEGF is linked at least in part to altered TSC1 or TSC2 function and aberrant mTOR signaling.

The *Tsc1*^{GFAP}CKO mouse has been well-characterized, and recent studies demonstrate that mTOR antagonism with rapamycin can ameliorate seizures and prevent premature death in this strain (55). Our study is the first to define the temporal pattern of mTOR activation, as evidenced by phosphorylation of S6 protein in the cortex of these animals. There is clearly a time-dependent increase in S6 phosphorylation consistent with the ongoing effects of loss of Tsc1 following conditional inactivation. Indeed, a greater number of p-S6 immunolabeled cells were identified at P10 than P1. We submit that changes in growth factor expression in the *Tsc1*^{GFAP}CKO mice did not reflect either seizures or behavioral alterations that appear later in this strain (approximately P20-P30) and rather represent direct effects of loss of Tsc1.

In contrast, the effects of loss of TSC1 or TSC2 on expression of EGF, EGFR, HGF, c-Met, VEGF, and HIF-1α in neural cells have not yet been studied, and we are the first to report changes in these growth factors and their receptors in TSC brain tissue with defined genotypes. Our findings suggest that altered growth factor expression may be a consequence of loss of either TSC1 or TSC2. EGFR plays a pivotal role in regulating astrocyte proliferation during development and has been implicated in aberrant cell growth control in malignant gliomas. EGFR has been localized to radial glial cells in the embryonic ventricular zone and is a marker for those that differentiate into astrocytes. Both HGF and its tyrosine kinase receptor c-Met are expressed by stem cells in the subventricular zone (101), and in view of the prior demonstration of stem cell markers such as nestin in tubers (102), these growth factors could also serve to characterize tubers as phenotypically immature. Like EGFR, HGF and c-Met are expressed in human gliomas and are believed to function in cell proliferation and angiogenesis (for review see Abounader and Laterra (101)). Functional blockade of EGFR and c-Met inhibits tumor growth. Prior studies have suggested that enhanced HGF expression in proliferating hepatocytes is mTOR-dependent (103). Changes in EGF, EGFR, HGF, and c-Met expression were identified in the setting of diminished TSC1 or TSC2 function, i.e. the *Tsc1*^{GFAP}CKO mouse or human tuber or SEGA specimens, but not in surrounding non-tuber cortex and not within SENs, suggesting that complete TSC1 or TSC2 inactivation and commensurate hyperactivation of the mTOR pathway may be necessary to induce these effects.

VEGF expression is directly modulated by TSC1 and TSC2 via both mTOR-dependent and mTOR-independent pathways *in vitro* (100). Thus, among the growth

factor genes assayed, alterations in VEGF mRNA and protein levels may be most sensitive to loss of TSC1 or TSC2 (97). High levels of VEGF mRNA expression have been reported in angiomyolipomas and in serum from human TSC patients (98, 104). VEGF expression was enhanced following *Tsc1* knockout *in vivo* in mice, and we observed enhanced VEGF expression in human tubers and SEGAs as well as in peri-tuberal cortex.

Increased mTOR signaling, corresponding to loss of TSC1/TSC2 inhibition, has been demonstrated specifically in SEGAs (41) and tubers (40). Thus, the findings in human TSC tissue specimens of increased expression of EGF, HGF, VEGF, and their receptors primarily within these focal areas of mTOR cascade dysregulation suggests that reduction of TSC1 or TSC2 could lead to increased EGF, HGF, or VEGF levels via mTOR. Indeed, our results support previous observations in mouse kidney cells and fibroblasts demonstrating enhanced VEGF detected in either *Tsc2* heterozygous (+/-) or null (-/-) cells (97).

These results provide a link between aberrant mTOR cascade activation and enhancement of three new candidate growth factors that could be targeted for future therapeutic trials in TSC. EGFR, HGF, and VEGF can be blocked with specific antagonists, perhaps in association with rapamycin, as a strategy to reduce the size of tubers or SEGAs in TSC and diminish the potential toxicity of any one therapeutic compound.

Acknowledgements. This work was supported by NS045877, NS045021, and Department of Defense CDMRP-TSC Program grants (PBC); the National Epilepsy Fund - "Power of the Small," Hersenstichting Nederland (NEF 02-10 and NEF 05-11) and Stichting Michelle (M06.011; EA); and AOA and AANS medical student research awards (WEP).

Table 2.1. TSC and Control Patient Demographics

Sample	Age	Location	Genotype
Tuber	4 years	Frontal	*TSC1*
Tuber	9 years	Frontal	*TSC2*
Tuber	3 years	Temporal	*TSC2*
Tuber	9 years	Frontal	*TSC2*
Tuber	3 years	Temporal	*TSC1*
Tuber	2 years	Temporal	*TSC1*
Tuber	4 years	Frontal	NMI
Tuber	6 years	Temporal	*TSC2*
Tuber	7 years	Frontal	NMI
Tuber*	10 years	Frontal	*TSC2*
SEGA*	10 years	Lat Vent	*TSC2*
SEGA	14 years	Lat Vent	*TSC1*
SEGA	21 years	Lat Vent	*TSC2*
SEGA	22 years	Lat Vent	*TSC1*
SEGA	19 years	Lat Vent	*TSC2*
SEGA	16 years	Lat Vent	NMI
SEN	27 years	Lat Vent	*TSC2*
SEN	37 years	Lat Vent	*TSC2*
SEN	41 years	Lat Vent	*TSC2*
Epilepsy Control	6 years	Temporal	NMI
Epilepsy Control	14 years	Temporal	NMI
Epilepsy Control	12 years	Temporal	NMI
Epilepsy Control	9 years	Temporal	NMI
Epilepsy Control	16 years	Temporal	NMI
Control	4 years	Frontal	NMI
Control	9 years	Frontal	NMI
Control	11 years	Temporal	NMI
Control	11 years	Frontal	NMI

Table depicts age at time of surgery, lobar location of resection and TSC genotype. Lat Vent, lateral ventricle; NMI, no mutation identified; * specimen contained both SEGA and cortical tuber.

Table 2.2. Laminar Expression of Growth Factors in Wild-type Versus *Tsc1*^{GFAP}CKO Mice at P10

Protein	WT	Score	*Tsc1*^{GFAP}CKO	Score
EGF	ALL	+	ALL	+++
EGFR	II-IV	+	II-IV	++++
HGF	I-III	++	ALL	++++
HIF-1a	ALL	0	ALL	++
c-Met	II-III	+	ALL	+++
VEGF	II-III	++	II-V	++++

Semi-quantitative scale (0, no staining; +, very few labeled cells; ++, >20 labeled cells; +++, > 50 labeled cells; ++++, intense labeling across most cells in each ROI) to represent labeling density in each ROI. Roman numerical convention indicates expression of each growth factor within specified cortical layers; ALL, expression in all cortical layers.

Table 2.3. Growth Factor and Growth Factor Receptor Expression in Tubers

Protein	WT	Score	*Tsc1*^{GFAP}CKO	Score
EGF	ALL	+	ALL	+++
EGFR	II-IV	+	II-IV	++++
HGF	I-III	++	ALL	++++
HIF-1a	ALL	0	ALL	++
c-Met	II-III	+	ALL	+++
VEGF	II-III	++	II-V	++++

Table depicts percent of morphologically identified GCs expressing each protein marker, across all 10 tuber specimens. WM reflects relative enrichment of labeled cells in subcortical white matter; ALL reflects expression detected across all layers.

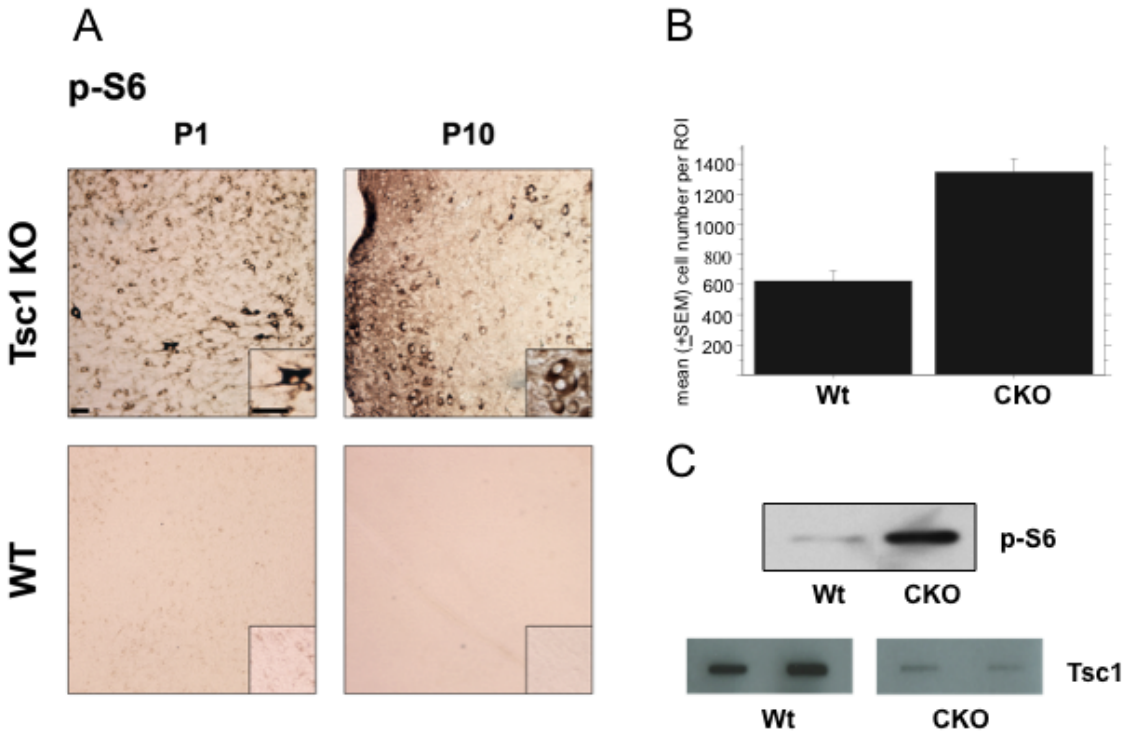

Figure 2.1. Enhanced S6 phosphorylation (p-S6) in *Tsc1*^{GFAP}CKO mouse cortex. (A), At P1 and P10 timepoints, *Tsc1*^{GFAP}CKO cortex (Tsc1 KO) shows increased p-S6 expression compared to wild-type (Wt) cortex. Photo taken at the level of the peri-rhinal sulcus; inset, magnification 40X. Scale bars, 20 μm. (B), Graph showing quantitative cell counts of p-S6 labeled cells in wild-type (Wt) and *Tsc1*^{GFAP}CKO (CKO) mice at P10. Note increased numbers of p-S6 labeled cells in CKO. (C), Western blot depicting increased p-S6 levels in *Tsc1*^{GFAP}CKO versus Wt mouse cortex homogenates, and cDNA array hybridization depicting reduced Tsc1 mRNA expression in CKO versus Wt mice.

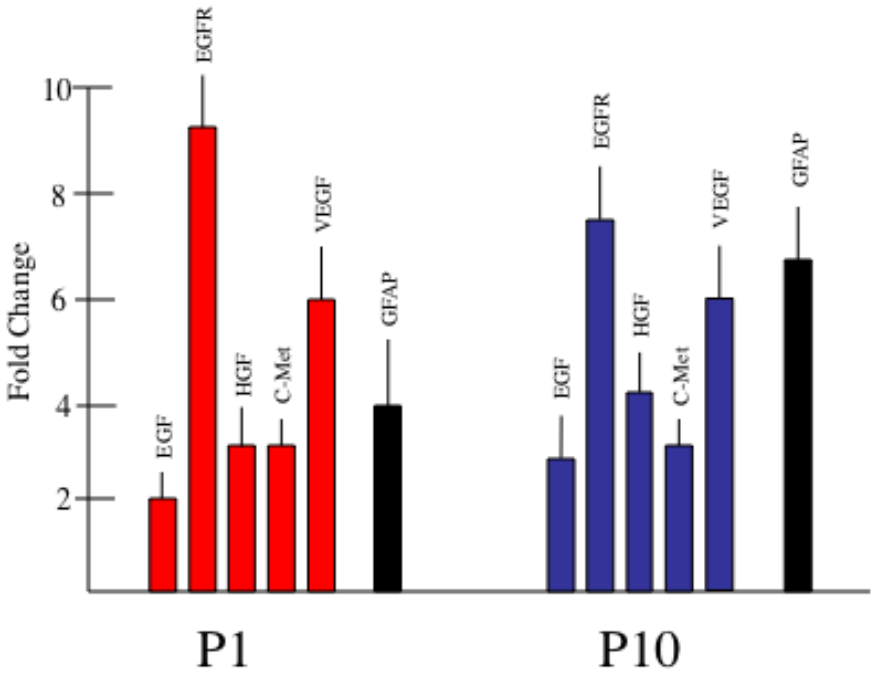

Figure 2.2. Increased expression of EGF, EGFR, HGF, c-Met, and VEGF mRNAs in *Tsc1*^{GFAP}CKO versus Wt mouse cortex at P1 (red) and P10 (blue). Bars represent mean change in relative abundance expressed as fold change relative to Wt cortex (lines above bars depict SEM; all significant $p<0.05$). Increased expression of GFAP mRNA at each timepoint is depicted in black.

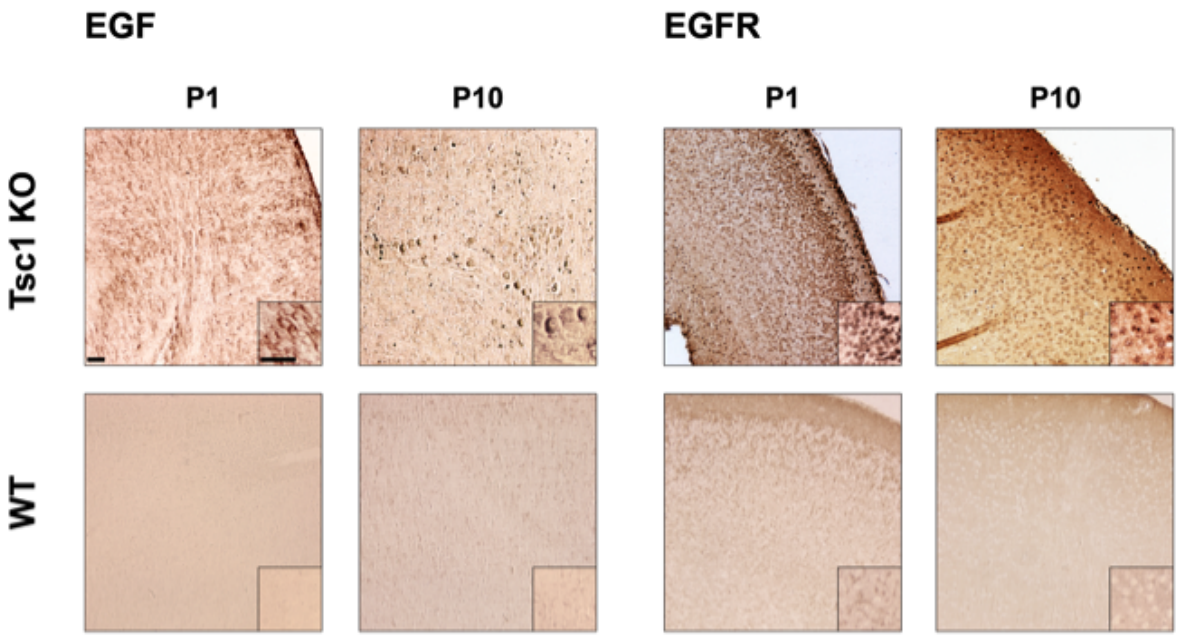

Figure 2.3. Enhanced expression of EGF and EGFR proteins in *Tsc1*^{GFAP}CKO (Tsc1 KO) mouse versus wild-type (WT) mouse cortex at P1 and P10 timepoints; inset, magnification 40X. Scale bars, 20 μm. Note EGF expression in heterotopic cells in white matter at P10.

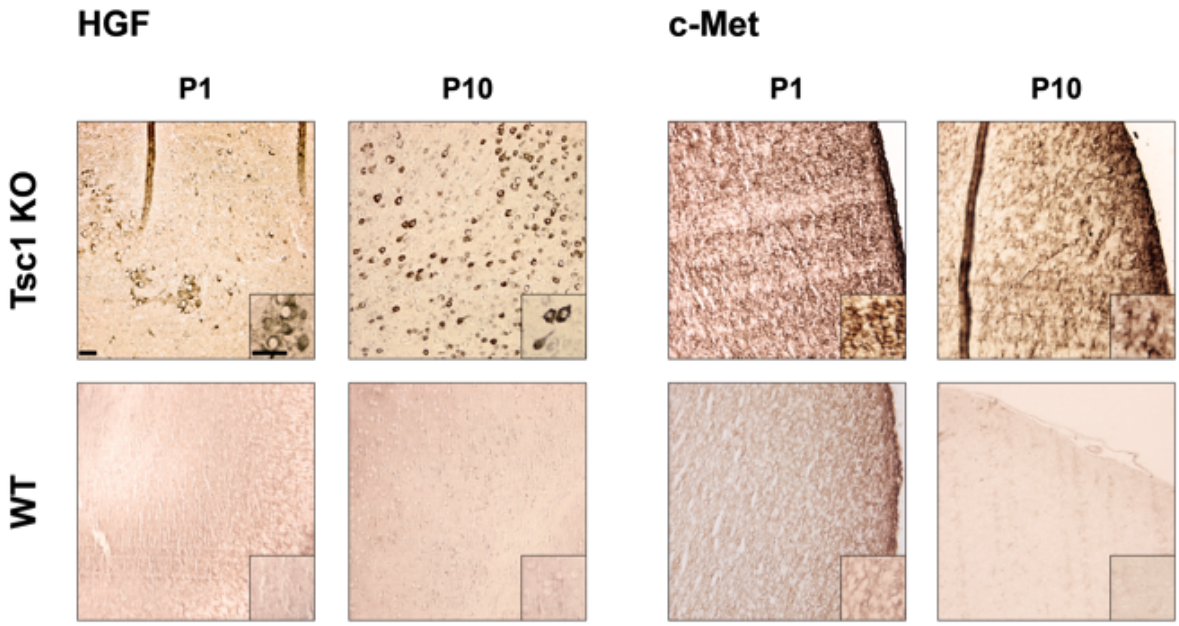

Figure 2.4. Enhanced expression of HGF and its receptor c-Met in *Tsc1*^{GFAP}CKO (Tsc1 KO) mouse versus wild-type (WT) mouse cortex at P1 and P10; inset, magnification 40X. Scale bars, 20 μm. Note expression of HGF in ectopic cell clusters depicted at P1 and throughout cortex at P10. In contrast, c-Met expression is more widespread across the cortex at both time points.

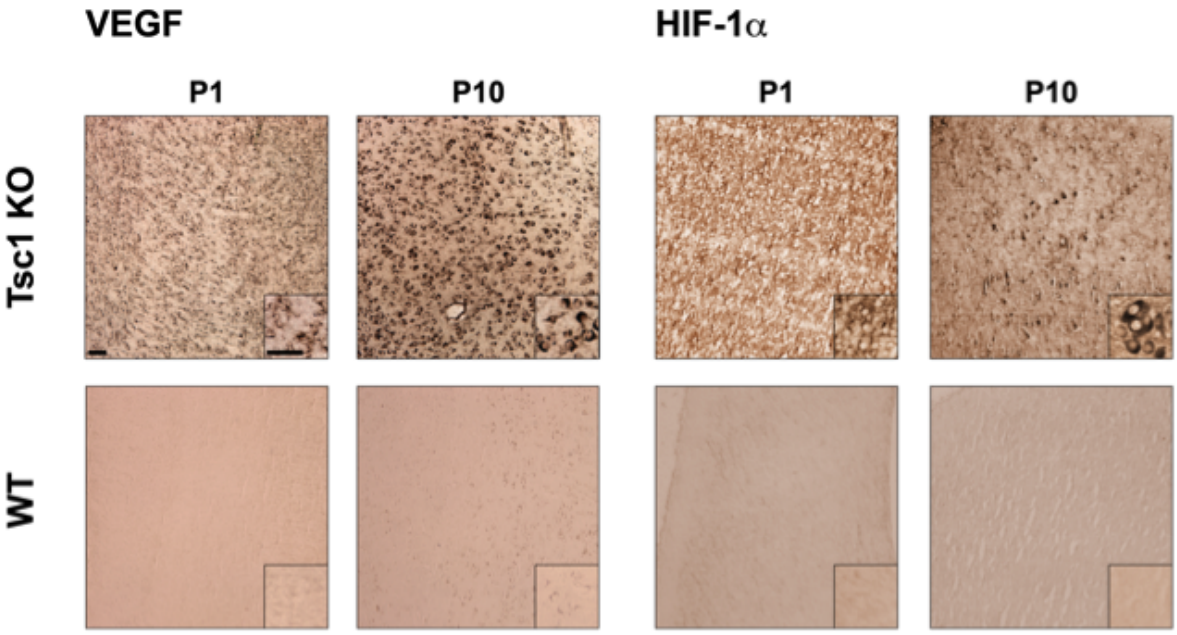

Figure 2.5. Enhanced expression of VEGF and HIF-1α proteins in *Tsc1*^{GFAP}CKO (Tsc1 KO) mouse versus wild-type (WT) mouse cortex at P1 and P10; inset, magnification 40X; depicts VEGF or HIF-1a labeling in individual cells or small clusters of cells. Scale bars, 20 μm.

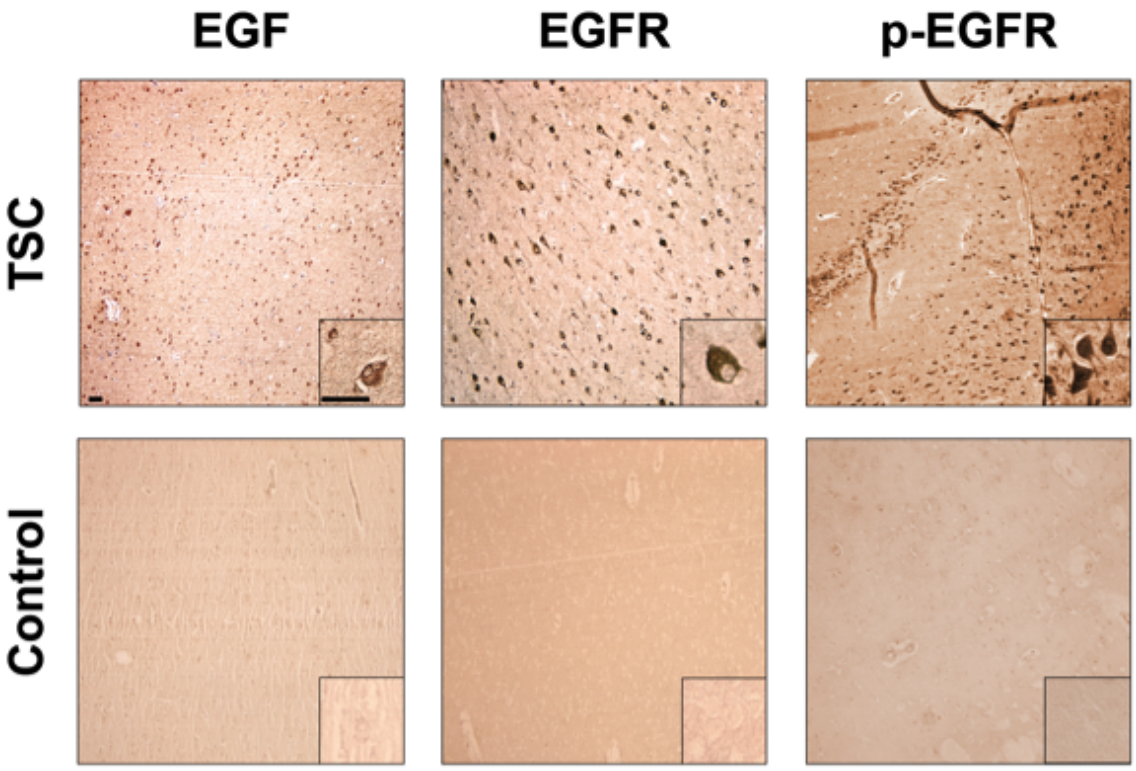

Figure 2.6. Increased EGF and EGFR (both phosphorylated and non-phosphorylated isoforms) expression in human TSC (tuber) versus control cortex; inset, magnification 40X. Scale bars, 20 μm.

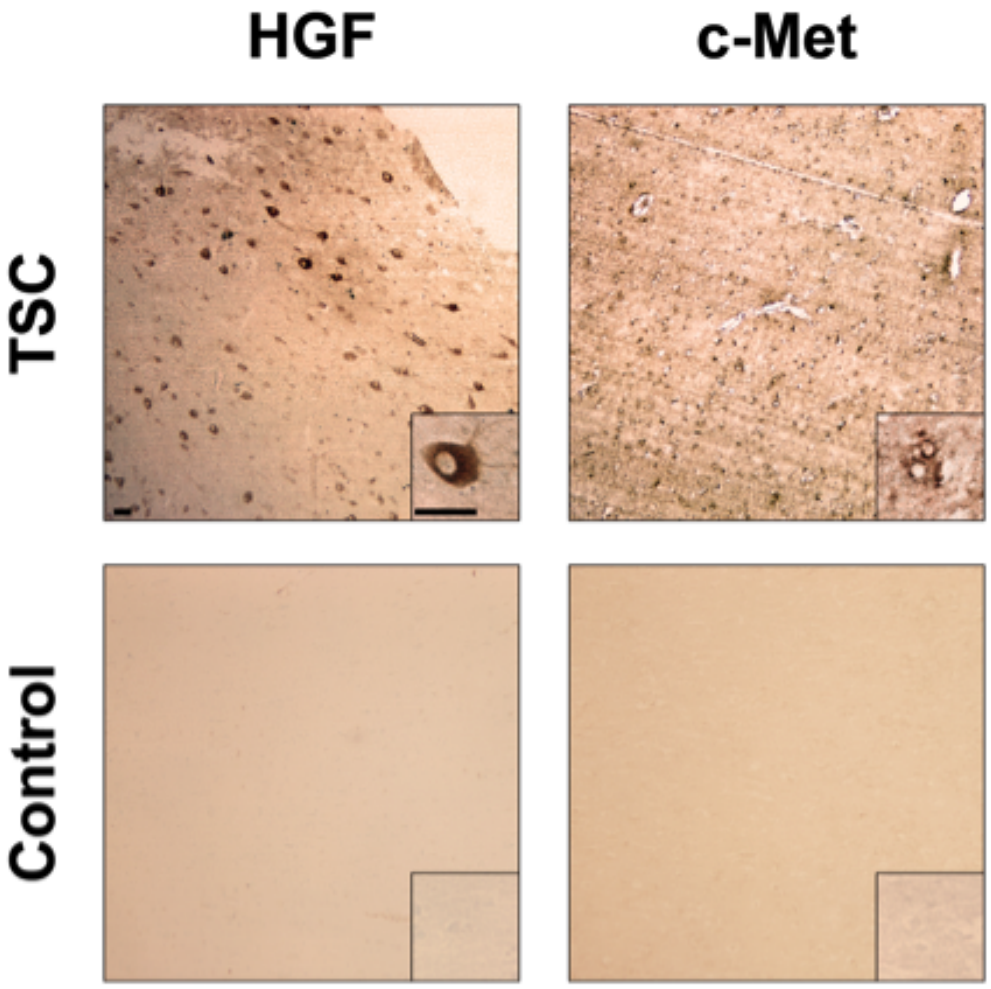

Figure 2.7. Increased HGF and c-Met expression in human TSC (tuber) versus control cortex; inset, magnification 40X. Scale bars, 20 μm.

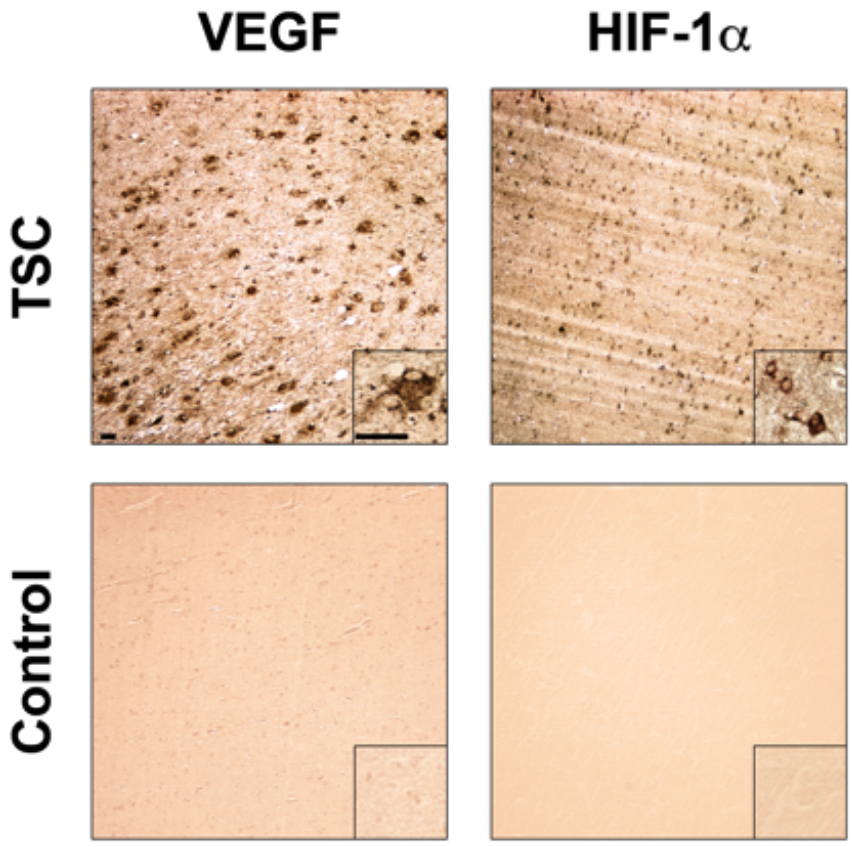

Figure 2.8. Increased VEGF and HIF-1α expression in human TSC (tuber) versus control cortex. Note VEGF expression in dysmorphic GCs as well as in capillary endothelium; inset, magnification 40X. Scale bars, 20 μm.

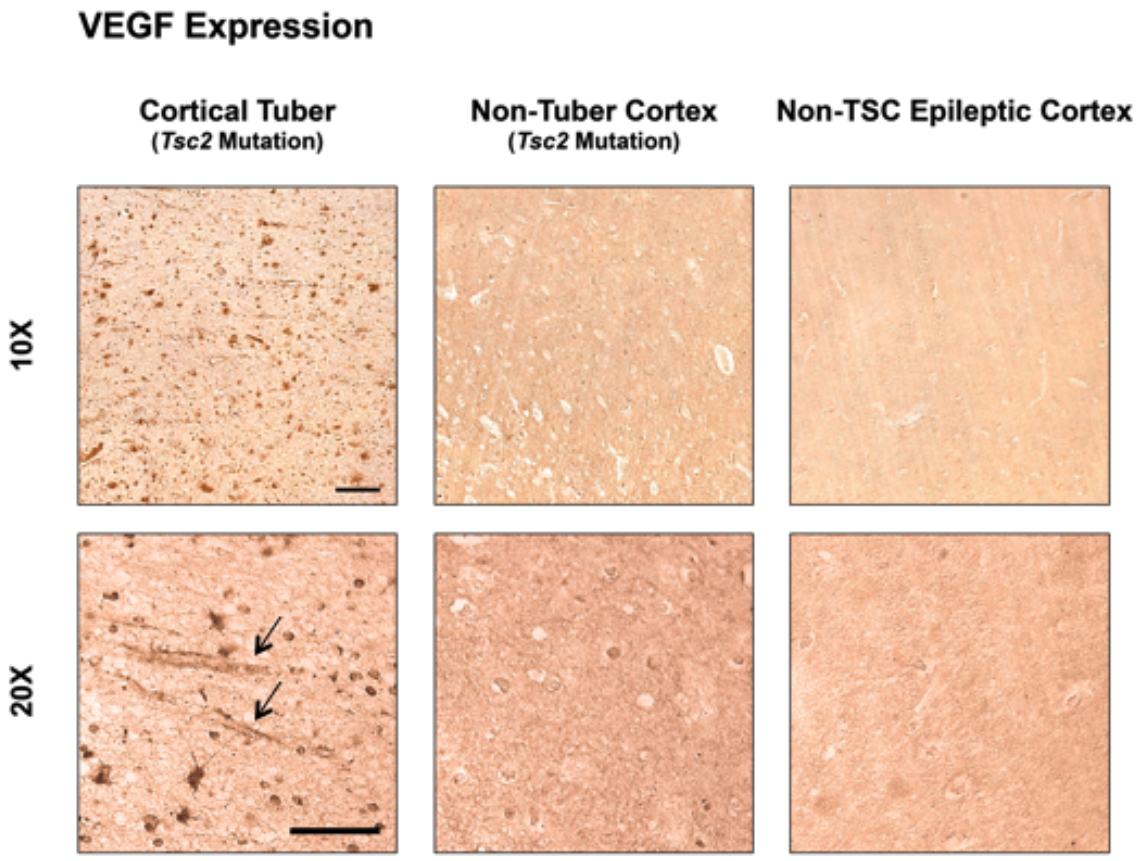

Figure 2.9. Increased expression of VEGF in a tuber specimen from a TSC patient, compared with non-tuber cortex in the same TSC patient and with non-TSC epilepsy control cortex (top row, 10X magnification; bottom row, 20X). In tuber cortex, there is robust cellular VEGF expression. In non-tuber cortex from the same TSC patient, there is overall less cellular VEGF expression than in tubers but more than in non-TSC epilepsy control cortex, in which there is little cellular VEGF expression. Scale bars, 100 μm.

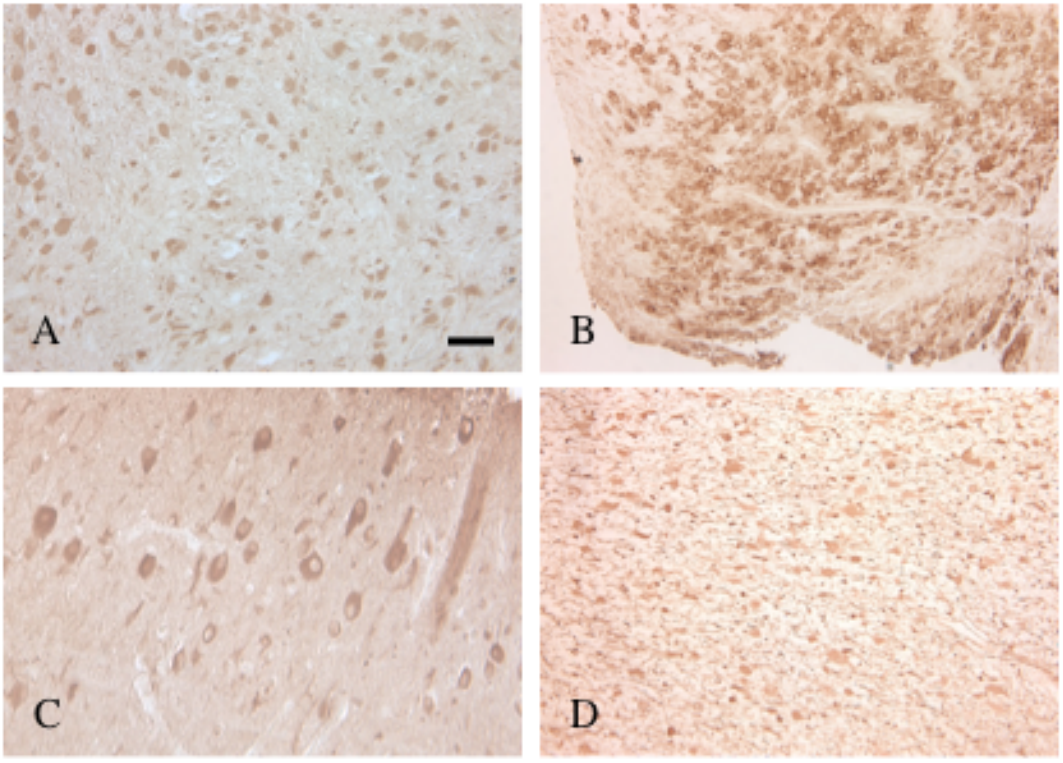

Figure 2.10. Expression of EGF (A), EGFR (B), HGF (C), and VEGF (D) in SEGAs. Scale bar, 100 μm.

CHAPTER 3

LOSS OF STRADA IN PRETZEL SYNDROME DISRUPTS NEURONAL PATHFINDING THROUGH ENHANCED IRS1 SIGNALING[3]

[3] Much of this work was originally published in *Science Translational Medicine*, Vol. 5, No. 182, April 2013. Parker, W.E., Orlova, K.A., Parker, W.H., Birnbaum, J.F., Krymskaya, V.P., Goncharov, D.A., Baybis, M., Helfferich, J., Okochi, K., Strauss, K.A., and Crino, P.B. Rapamycin Prevents Seizures After Depletion of STRADA in a Rare Neurodevelopmental Disorder. Published by AAAS.

Abstract

Heterotopic neurons in the subcortical white matter are a histopathological finding in many neurodevelopmental disorders associated with intractable epilepsy. Polyhydramnios, megalencephaly, and symptomatic epilepsy syndrome (PMSE, colloquially named "Pretzel Syndrome") is a neurodevelopmental disorder resulting from a loss-of-function mutation in STE20-related kinase adaptor alpha (*STRADA*), which encodes the pseudokinase STRADA. Postmortem PMSE brain tissue exhibits numerous heterotopic neurons, and STRADA knockdown (KD) in a mouse model results in heterotopic neurons in the subventricular zone, suggesting that STRADA may affect neuronal migration and pathfinding, although the role STRADA plays in this process has not yet been identified. We demonstrate that depletion of STRADA *in vitro* in mouse neural progenitor cells (mNPCs) results in aberrant pathfinding and disrupted polarity, associated with reduced actin polymerization. We define the mechanism for this effect as constitutive mTORC1- and p70S6K-dependent phospho-inhibition of IRS1 resulting in disinhibition of cofilin and actin depolymerization. Treatment of STRADA-deplete mNPCs with the mTORC1 inhibitor rapamycin or p70S6K inhibitor PF-4708671 rescues the pathfinding and polarity defects. We confirm the link between enhanced mTORC1 activity and cofilin signaling by demonstrating aberrant IRS1 phosphorylation in PMSE patient cortex. STRADA-deplete human fibroblasts extracted from PMSE patients exhibit disrupted migration associated with IRS1 phospho-inhibition and depolymerized actin. Finally, we demonstrate that inhibition of mTORC1 with rapamycin rescues the neural migratory defect associated with STRADA KD in the developing mouse brain.

We define STRADA as a pivotal regulator of neural pathfinding, migration, and polarity via mTORC1 and IRS1 signaling to cofilin and regulation of actin assembly.

Introduction

Heterotopic neurons within the subcortical white matter are a common histopathological finding identified in brain specimens resected from patients with intractable epilepsy (105), tuberous sclerosis complex (TSC), an autosomal dominant disorder highly associated with severe epilepsy (106), and all subtypes of focal cortical dysplasia associated with intractable pediatric epilepsy (107). Heterotopic neurons contribute to pathogenesis of epilepsy by establishing aberrant network connectivity (108). It has been proposed that heterotopic neurons result from impaired pathfinding or migration into the nascent cortical plate during corticogenesis, although the molecular mechanisms responsible for impaired movement have not been fully defined.

Loss-of-function mutation of *LYK5/STRADA* is associated with "Pretzel Syndrome" (polyhydramnios, megalencephaly, and symptomatic epilepsy syndrome, PMSE; OMIM #611087), a recessive neurodevelopmental disorder characterized by intractable epilepsy and severe cognitive impairment, identified in the Old Order Mennonite population (61). Numerous heterotopic neurons are observed in PMSE, suggesting a neural migratory defect and priming consideration of STRADA as a pivotal regulator of neuronal pathfinding and migration (12, 61). All PMSE patients share a common homozygous truncating deletion of exons 9-13 of *STRADA*, removing the protein interacting domains for complex formation with the kinase LKB1, a known regulator of mammalian target of rapamycin (mTOR) (6). It is estimated that approximately 4% of the more than 40,000 Old Order Mennonite individuals in Ohio, Pennsylvania, and New York may be hemizygous for *STRADA* deletion.

The STRADA/LKB1 protein complex inhibits mTORC1 signaling via phospho-activation of AMP-activated kinase (AMPK) and tuberous sclerosis 2 (TSC2) in gut, skin, and brain (12, 14, 16, 23). STRADA knockdown *in vitro* leads to enhanced mTORC1 signaling in lymphoblasts and neural progenitor cells, and *in vivo,* results in clusters of heterotopic neurons within the murine post-natal subventricular zone (12). Knockdown of stk25, a potential STRADA interacting protein, leads to altered Golgi assembly and polarity of mature neurons, an effect antagonized by reelin (109), and in non-neural cancer cell lines, STRADA modulates cell polarity via signaling to PAK1 (110). While LKB1 has been implicated in neuronal polarization, axon specification, and dendrite growth (10, 65), a direct assessment of a role for STRADA in migration and pathfinding of embryonic neurons or neural progenitor cells or of the cell signaling mechanisms responsible for linking STRADA to progenitor cell migration, has not been reported.

We show that STRADA is a pivotal regulatory protein that governs pathfinding in neural progenitor cells via an mTORC1-p70S6K-dependent mechanism, activating IRS1, inhibiting cofilin, and polymerizing actin, and that PAK1 and LIMK are key signaling links between STRADA, IRS1, and cofilin. mTORC1 inhibition rescues aberrant neuronal migration and pathfinding *in vitro* and *in vivo* in a mouse model of PMSE. Our data suggest that PMSE provides a novel disease model to study mechanisms leading to neuronal heterotopia.

Materials and Methods

mNPC culture and transfection

Stable transfection of puromycin-resistant shRNA plasmids in mNPCs (provided by J. Wolfe, Children's Hospital of Philadelphia, Philadelphia, Pennsylvania, USA) (111) was established using either puro-shRNA STRADA to create a stable STRADA KD line or puro-shRNA scram to create a control line (KM41633P; SABiosciences), as previously described (12). Cells were cultured on poly-D-lysine-coated plates (10 μg/ml; Sigma-Aldrich) in complete media consisting of DMEM/F12 (Invitrogen) supplemented with 1% N2 (Invitrogen), 1% FBS (Sigma-Aldrich), 1% penicillin/streptomycin (Invitrogen), 20 ng/ml basic fibroblast growth factor (Promega), and 5 μg/ml heparin (Sigma-Aldrich). To maintain stable transfection, selective pressure was applied with 6 μg/ml puromycin (Invitrogen).

Mouse embryonic fibroblasts (*MEFs)*

Lkb1$^{+/+}$ and *Lkb1*$^{-/-}$ MEFs were a gift from the laboratories of L. Cantley (Beth Israel Deaconess Medical Center, Boston, Massachusetts, USA) and R. Shaw (Salk Institute for Biological Sciences, La Jolla, California, USA) (19, 23). Cells were cultured in DMEM (Invitrogen) supplemented with 10% FBS (Sigma-Aldrich) and 1% penicillin/streptomycin (Invitrogen). For protein quantification assays, MEFs were serum starved overnight to attenuate basal mTORC1 activity and pre-treated with AICAR (2 mM; Cell Signaling) to stimulate AMPK for 2 hours prior to lysis (12).

Human fibroblast extraction and culture

PMSE patient (3), parent (2), and normal control (1) fibroblasts were obtained from skin-punch biopsies at the Clinic for Special Children in Lancaster, Pennsylvania, USA, following informed consent. Fibroblasts were extracted from tissue samples by incubation in 0.25% Trypsin/EDTA (Gibco) overnight at 4^{o}C. The next day, epidermis was removed, and dermis was digested with Collagenase P (Roche) buffered in 130 mM sodium chloride (Sigma-Aldrich), 10 mM calcium acetate (Sigma-Aldrich), and 20 mM HEPES buffer (Gibco) for 30 minutes at 37^{o}C. Then 0.5% Trypsin/EDTA (Gibco) was added, and the mixture was incubated at 37^{o}C for an additional 10 minutes before neutralization with fibroblast culturing media, composed of DMEM (Gibco) supplemented with 10% FBS (Sigma-Aldrich), 10 mM HEPES buffer (Gibco), 1% penicillin/streptomycin (10,000 u/ml penicillin, 10 mg/ml streptomycin stock; Gibco), and 1% fungizone (250 μg/ml stock; Gibco). Fibroblasts were pelleted through centrifugation for 5 minutes at 1500 rpm, and the pellet was resuspended in fibroblast culturing media to obtain the desired cells. For protein quantification assays, fibroblast media was supplemented with CAMKK inhibitor STO-609 (5 μM; Tocris) and AMPK activator AICAR (2 mM; Cell Signaling) at 6 hours and 4 hours, respectively, prior to cell lysis, to enable isolation of STRADA-dependent inhibition of mTORC1 signaling. Rapamycin (100 nM; Cell Signaling) or p70S6Ki (PF-4708671, 10 μM; Pfizer Pharmaceuticals) was applied for 2 hours prior to cell lysis.

Western blotting

Cells were lysed and lysates electrophoresed according to previously-established protocol (12). The following primary antibodies were used: rabbit polyclonal to LYK5 (1:500; Abcam), rabbit monoclonal to phospho-S6 ribosomal protein (Ser235/236, 1:1000; Cell Signaling), rabbit monoclonal to phospho-4EBP1 (Thr37/46, 1:1000; Cell Signaling), rabbit polyclonal to IRS1 (phospho S636 + S639, 1:500; Abcam), rabbit polyclonal to phospho-PAK1 (Ser144)/PAK2 (Ser141) (1:1000; Cell Signaling), rabbit polyclonal to phospho-LIMK1 (Thr508)/LIMK2 (Thr505) (1:1000; Cell Signaling), rabbit monoclonal to phospho-cofilin (Ser3, 1:1000; Cell Signaling), and rabbit monoclonal to GAPDH (1:1000; Cell Signaling).

Immunocytochemistry

Scram and STRADA KD mNPCs plated on coverslips and subjected to the described migration assay were fixed in 4% PFA at room temperature for 20 minutes, permeabilized with 0.3% Triton X-100 (Sigma) in PBS (Gibco), and blocked for 2 hours in 5% normal goat serum (Vector Laboratories). Cells were incubated in mouse anti-GM130 monoclonal Ab (1:100; BD Transduction Laboratories) overnight at 4^{o}C. Alexa-Fluor 488 goat anti-mouse secondary Ab (Invitrogen) was applied for 1 hour at room temperature. Cells were then blocked in 1% bovine serum albumin (BSA; Sigma-Aldrich) for 30 minutes. Phalloidin (1:40; Invitrogen) was applied for 20 minutes, followed by Hoechst nuclear stain (0.0001 μg/μl; Invitrogen). Cells were visualized and images captured using fluorescence microscopy, as specified above. Golgi-specific

labeling was confirmed by co-staining a subset of coverslips with rabbit anti-Giantin polyclonal Ab (1:500; Abcam) and Alexa-Fluor 594 goat anti-rabbit secondary Ab (Invitrogen).

Human brain immunohistochemistry

A single postmortem PMSE brain of a 7-month old female was procured from the Clinic for Special Children (Lancaster, Pennsylvania, USA). Cortical dysplasia and focal epilepsy syndrome cortex served as a non-PMSE epileptic control specimen (112). The specimens were fixed in 4% paraformaldehyde (PFA), embedded in paraffin, and cut into 7-μm sections. Sections were probed with rabbit polyclonal anti-IRS1 (phospho S636+S639; Abcam) and processed for immunohistochemistry as reported previously (12).

Migration assay

mNPCs, MEFS, or human fibroblasts were plated on 6-well plates, chamber slides, or laminin-coated cover slips, coated with poly-D-lysine (mNPCs; Sigma-Aldrich) or poly-L-lysine (fibroblasts; Sigma-Aldrich) and cultured in complete mNPC or human fibroblast media (specified above). Prior to the migration assay, cells were cultured for 24 hours in serum-deplete media (1 ml complete media : 4 ml basal media; DMEM/F12 for mNPCs or DMEM for fibroblasts; Gibco) to attenuate basal mTORC1 activity. Serum-deplete media was maintained for the duration of the migration assay. Rapamycin

(50 nM for mNPCs, 100 nM for fibroblasts) or p70S6Ki (10 μM) was applied for one hour prior to and throughout the duration of the experiment. A 200-μl micropipette tip was used to create a linear scratch across a confluent monolayer of cells (113). In PAK inhibitor migration analysis, doses ranging from 1-10 μM IPA-3 (Tocris Bioscience) were applied to Scram mNPCs for one hour prior to and throughout the duration of the experiment. Confirmatory Western p-cofilin signaling analysis was performed using 10 mM IPA-3 for one hour and pre-treating with the ROCK inhibitor Y-27632 (10 μM; BioVision) for 12 hours prior to cell lysis, to isolate PAK-dependent LIMK phosphorylation.

Treatment with AraC

Mitotic inhibitor arabinofuranosyl cytosine (AraC, Cytosine β-D-Arabinofuranoside; Sigma) was used to inhibit mitosis of migrating cells, and demonstrate that the migration deficit seen with STRADA KD and rapamycin rescue were independent of any effects on cell proliferation. Wildtype (WT) mNPCs were plated in serum-starve media in 6-well plates, and pre-treated with AraC for 24 hours, after which a fresh dose of AraC was applied for 0h, 15h, or 20h, in order to replicate the time course of the migration assay. Cells were enzymatically de-adhered using 0.25% Trypsin-EDTA (Gibco) at each indicated treatment time, and Trypan Blue (Sigma) was used to visualize and count cells under light microscopy. The optimal effective anti-proliferative, non-apoptotic AraC dose (20 μM) was applied to Scram and STRADA KD mNPCs for 24 hours prior to and throughout the duration of the migration assay with rapamycin treatment.

Video capture in migration assay

Migration of STRADA KD and Scram mNPCs was determined in chamber slides, within a micro-incubator (model CSMI; Harvard Apparatus; at 37^{o}C) on an inverted microscope (Nikon TE300) equipped with a digital video camera (Evolution QEi; Media Cybernetics) (114). Images were taken every 5 minutes in the phase-contrast channel for 20 hours. For each condition, three or four videos were taken across the scratch.

G:F Actin Assay

Cell lysates were prepared and actin was extracted and separated into G and F fractions using differential ultracentrifugation and a G-actin/F-actin In Vivo Assay Kit (Cytoskeleton), according to the manufacturer's protocol. G and F actin fractions were then electrophoresed on a 4-15% SDS-PAGE gel (Bio-Rad) and transferred onto a PVDF membrane (Millipore) at 4^{o}C overnight. G-actin/F-actin was assayed by Western blot using rabbit anti-actin polyclonal Ab (1:500; Cytoskeleton).

In utero *electroporation*

We used *in utero* electroporation (IUE) to transfect ventricular zone/subventricular zone (VZ/SVZ) cells in E14.0 C57BL/6J mouse embryos with GFP-tagged STRADA shRNA plasmid (8 μg/μl), as described previously (115). A subset of pregnant dams was injected

intraperitoneally with rapamycin (5 mg/kg, in vehicle solution composed of 5% PEG 400, 5% Tween 80, 0.9% NaCl in sterile water; LC Laboratories) daily from E15.0 through E18.0. Animals were sacrificed using CO_2 overdose on E19.0, at which time brains were extracted from the embryos, fixed in 4% PFA, cryoprotected in a sucrose gradient, and frozen in Optimal Cutting Temperature solution (OCT, Tissue Tek). 20-μm coronal sections were cut on a cryostat (Leica CM 1950), stained with Hoechst 33342 nuclear stain (0.0001 μg/μl; Invitrogen), and coverslipped in mounting media (Fluoromount-G; Southern Biotech). Images were taken using a Leica DMI6000 B fluorescent microscope with a Leica DFC360 FX camera.

Quantitative Analysis

Three independent observers quantified the percentage of GFP^+ cells reaching the cortical plate, using the Image-Pro Plus 7.0 (Media Cybernetics) automatic count function for bright objects within an outlined region of interest, and this was verified by hand count. Localization of the cortical plate (CP) was determined by relative nuclear density.

In still-image migration assays, three independent coverslip scratches were made per treatment condition per shRNA or disease condition, and three images were taken across each scratch at each timepoint. A blinded observer recorded ten measurements per image, yielding 90 measures per timepoint per condition (using Photoshop CS2; Adobe or Image-Pro Plus 7.0). Migration distances were determined by subtracting the distance between edges of the scratch at 15h from the distance at 0h and halving this value.

For video migration assays, a blinded observer evaluated five representative leading-edge cells per video, and measured the distance translocated and directional angle at each 30-minute timepoint for the same cell, using Image-Pro Plus 7.0 software. Migration distance for each cell over the 20 hours recorded was measured as the sum of all 30-minute measures. Directional variance for each cell was calculated as the variance in the set of directional angles. Greater directional variance was determined to indicate reduced linear directionality.

In the Golgi compaction assay, a blinded observer used the outlining tool and area measurement function in Image-Pro Plus 7.0 to define Golgi area in each cell. The crescentic angle of Golgi subtended around the nucleus was calculated by measuring the angle between two rays each passing through one end of the Golgi, with a vertex at the center point of the nucleus.

To define relative levels of G and F actin, densitometric analysis was performed using ImageJ (NIH) software. Band densities were standardized to background pixel density for each image, and data are represented as a ratio of G:F actin (for STRADA depletion conditions) or F:G actin (for LKB1 depletion) in the respective KD or KO versus control.

Statistics

Data are presented in Table 1 as mean $\pm$ s.e.m. Excel (Microsoft) and Prism 5 (GraphPad) software programs were used for statistical analysis. In all comparisons, a *P*

value less than 0.05 was considered significant. Unpaired 2-tailed Student's *t* tests were performed to determine significance for all individual measures, and served as the sole method of analysis for experiments set up as binary comparisons, including IUE and video migration measures. For all still migration measures and measures of Golgi area and crescentic angle, significance was determined by a 1-way ANOVA with a Bonferroni correction for multiple comparisons in the migration assays or a Dunnett post-hoc analysis to determine the extent of rapamycin or p70S6Ki rescue in the Golgi measures.

All animal experiments were approved by the Institutional Animal Care and Use Committee of the University of Pennsylvania. All human studies were approved by the Institutional Review Board of Lancaster General Hospital (Lancaster, Pennsylvania, USA). Parents provided informed consent prior to their own and their children's participation.

Results

STRADA KD in mNPCs causes an mTORC1 and p70S6K-dependent migration defect *in vitro*

We hypothesized that loss of STRADA causes a primary failure of neural progenitor cell migration. Thus, we developed a system to model cell migration in the setting of STRADA loss *in vitro*. We established stably-transfected mNPC lines, using puromycin-resistant STRADA shRNA (STRADA shRNA-puro^R, STRADA KD) for STRADA KD and control puromycin-resistant scrambled shRNA (Scram shRNA-puro^R, Scram). STRADA depletion (more than 90%) and enhanced mTORC1 signaling (evidenced by enhanced phosphorylation of downstream effectors ribosomal S6 and 4EBP1 proteins) in the STRADA shRNA-puro^R line was confirmed by Western analysis (**Figure 3.1*A***).

Cell migration in STRADA KD and Scram mNPC lines was defined in a modified wound-healing assay previously described in fibroblasts (113). A 200-ml micropipette tip was used to create a scratch gap in confluent mNPCs. The gap established opposing migratory leading edges so that measurements of cell migration across the gap could be determined from the time of the scratch (0h) to 15 hours later (15h). STRADA KD significantly reduced the gap closure at 15h, compared with Scram cells, suggesting that STRADA KD impairs mNPC migration. We next show that the effect of STRADA KD on gap closure can be rescued by the mTORC1 inhibitor rapamycin (50 nM) at 15h (**Figure 3.1*B,D*; Table 3.1**). In order to rule out the possibility that STRADA KD or rapamycin treatment produced differences in gap closure by altering cell mitotic rate, we applied the mitotic inhibitor arabinofuranosyl cytosine

(AraC, 20 μM) 24 hours prior to and during the course of migration. Following AraC treatment, STRADA-deplete mNPCs continued to exhibit a significant migration deficit, rescued by rapamycin, suggesting that STRADA's role in mNPC migration is mTORC1-dependent and not altered by changes in cell mitosis (**Table 3.1**).

To further define the signaling mechanisms causing impaired migration, we next hypothesized that altered migration observed in STRADA KD mNPCs was mediated by the mTORC1 substrate p70S6K, due to its putative association with actin dynamics and cell migration (116, 117). mNPCs were treated with a novel selective p70S6K inhibitor (p70S6Ki), PF-4708671 (72). P70S6Ki (10 μM) was applied one hour prior to the initiation of the assay (-1h) and maintained until 15h. Treatment with p70S6Ki provided a full rescue of the STRADA KD-associated migration defect and resulted in a significantly greater distance migrated by STRADA KD cells at 15h (**Figure 3.1*C-D*, Table 3.1**). Thus, altered migration of STRADA KD mNPCs is mediated through a p70S6K-dependent mechanism.

STRADA KD impairs mNPC pathfinding

We next analyzed the distance migrated and directionality of individual STRADA KD mNPCs in real time using video time-lapse microscopy. Movement of multiple, individual STRADA KD and Scram mNPCs was captured every five minutes for 20 hours. A blinded observer evaluated five representative leading-edge cells per video and measured for each cell the distance traveled and direction angle relative to a unit circle, over each 30-minute epoch. Total distance traveled for each cell was calculated as the

sum of all distances measured over 20 hours, and directionality was calculated as the variance of the set of angles over that time period.

While most Scram cells moved forward in a linear fashion, STRADA KD cells moved in divergent, non-linear directions, often oriented away from the opposing cell front (**Figure 3.2*A***). In fact, to our surprise, STRADA KD mNPCs translocated a *greater* overall *distance* than Scram cells (**Figure 3.2*B*, Table 3.1**). However, compared to Scram cells, STRADA KD resulted in a profound impairment in directionality, with STRADA KD mNPCs exhibiting significantly greater directional variance than controls (**Figure 3.2*D*, Table 3.1**). STRADA KD mNPCs migrated on average 1.5-fold greater distance and exhibited a nearly 3-fold increase in directional variance compared to Scram cells. Thus, in the absence of functional STRADA, individual mNPCs lose the ability to follow a linear migratory pathway. These results demonstrate that STRADA plays a pivotal role in establishing linear directionality and pathfinding of migrating mNPCs.

STRADA mediates mNPC pathfinding via mTORC1 signaling

We next hypothesized that STRADA regulates mNPC pathfinding via mTORC1 inhibition. Indeed, rapamycin treatment significantly reduced total distance migrated by STRADA KD cells, as well as diminished directional variance compared with untreated STRADA KD mNPCs. (**Figure 3.2*C,E*; Table 3.1**). Overall, rapamycin enhanced linear directionality, and enabled more uniform migration of STRADA KD mNPCs. Thus, STRADA drives migrating cell directionality by inhibiting mTORC1 signaling.

STRADA regulates mNPC polarization through mTORC1/p70S6K signaling

Since STRADA KD impairs mNPC directionality, and since pathfinding depends in large measure on appropriate establishment of cell polarity, we next investigated whether STRADA KD alters mNPC polarity. It is well established that the Golgi apparatus is compacted and localized forward of the nucleus in the direction of migration, i.e., the cell's leading edge, during active motility of fibroblasts and neurons (118) and that cell polarity depends on intact structure, function, and localization of the Golgi apparatus (119) (69, 73). Therefore, we used Golgi compaction as a bioassay to measure polarization of mNPCs.

Ten hours after initiation of migration, cells were fixed and immunostained for the Golgi marker GM130, and co-labeled with Hoechst nuclear stain and phalloidin for actin cytoskeleton visualization. A blinded observer measured Golgi area and the crescentic angle subtended by the Golgi around each cell's nucleus. We hypothesized that if STRADA KD disrupted neural progenitor polarization, STRADA-deplete mNPCs would exhibit Golgi dispersion (greater area and crescentic angle). In fact, STRADA KD significantly increased Golgi area and the crescentic angle of the Golgi around the nucleus compared with Scram cells (**Figure 3.3*A-B,E-F*; Table 3.1**). In a separate experiment, Scram and STRADA KD mNPCs were treated with rapamycin (50 nM) or p70S6Ki (10 μM). Enhanced Golgi area and crescentic angle in STRADA KD mNPCs was partially rescued with rapamycin and fully rescued with p70S6Ki treatment (**Figure 3.3*C-F*; Table 3.1**). Thus, reduced Golgi compaction associated with STRADA

depletion suggests that STRADA plays a critical role in polarizing migrating mNPCs, in an mTORC1- and p70S6K-dependent manner.

STRADA promotes inhibitory cofilin phosphorylation through IRS1

We hypothesized that STRADA contributes to cell polarization and pathfinding in mNPCs via p70S6K phosphorylation of IRS1, a recognized downstream target of p70S6K that signals to the actin cytoskeleton machinery via cofilin (67, 120). Indeed, Western analysis demonstrated that STRADA KD in mNPCs led to enhanced P-IRS1 levels (**Figure 3.4*B***). To confirm our findings in human brain, we investigated the level of IRS1 phosphorylation in PMSE patient cortex and found that P-IRS1 was enhanced in PMSE compared with control cortex (**Figure 3.4*A***). Next, we evaluated the cofilin signaling pathway, which is modulated by IRS1 signaling via PAK1 and LIMK. In the setting of STRADA depletion and enhanced inhibitory phosphorylation of IRS1, PAK1 phospho-activation (indicated by autophosphorylation at Ser 144 residue) was reduced, leading to diminished LIMK phosphorylation and diminished phospho-inhibition of cofilin (**Figure 3.4*B***). To validate p70S6K/IRS1 as a mechanistic link between mTORC1 and the cofilin signaling pathway, we evaluated the phosphorylation status of IRS1 and cofilin in a subset of STRADA KD mNPCs treated with p70S6Ki (10 μM). Inhibition of p70S6K rescued enhanced IRS1 phosphorylation as well as diminished cofilin phosphorylation in the STRADA-deplete cells, indicating that STRADA's role in cofilin signaling operates through p70S6K/IRS1 (**Figure 3.4*C***).

Because signaling from IRS1 to LIMK/cofilin occurs via PAK1, which in normal cells is activated during migration, we hypothesized that pharmacological blockade with a PAK1 inhibitor would attenuate mNPC motility. Indeed, application of the PAK inhibitor IPA-3 (121) caused a migration deficit in Scram mNPCs similar to that seen in the STRADA KD line, and reduced distance migrated in a dose-dependent manner (**Figure 3.4*D*, Table 3.1**). Using a Rho kinase (ROCK) inhibitor (Y-27632) (122) to attenuate compensatory LIMK phosphorylation in the absence of PAK1 activation, we further show that PAK1 inhibition results in a decrease in phosphorylated cofilin in Scram mNPCs, mirroring the signaling pattern of STRADA KD (**Figure 3.4*E***). These data demonstrate that STRADA inhibits mTORC1/p70S6K activity, resulting in active IRS1 and consequent PAK1 phosphorylation of LIMK, which phosphorylates and inhibits cofilin (mechanism proposed in **Figure 3.5**). STRADA inhibition of cofilin promotes migrating cell linear directionality. Conversely, loss of STRADA leads to enhanced IRS1 phosphorylation, reduced phospho-inhibition of cofilin, and impaired motility.

STRADA and LKB1 exhibit dissociable effects on cofilin

Loss of LKB1 in cancer cell lines as well as in Lkb1-null MEFs is associated with *enhanced* cell migration, in direct contrast to our results demonstrating *impaired* migration in STRADA KD mNPCs. Thus, since STRADA has only been defined previously as an activator of LKB1 (1, 6-8, 14, 23), we investigated several signaling nodes both upstream and downstream of PAK1 in *Lkb1*$^{-/-}$ versus *Lkb1*$^{+/+}$ MEFs (19, 23),

for comparison with signaling patterns in our STRADA KD mNPCs. In fact, in contrast to STRADA KD mNPCs, *Lkb1*$^{-/-}$ MEFs exhibited distinct and opposite patterns of PAK1, LIMK, and cofilin phosphorylation, with enhanced P-PAK1 (Ser 144), P-LIMK and P-cofilin, suggestive of activated PAK1 (**Figure 3.4*B***). These results demonstrate that phosphorylation patterns associated with STRADA versus LKB1 depletion diverge at the level of PAK1, suggest opposing influences of STRADA and LKB1 on signaling to cofilin, consistent with opposite functional effects of STRADA and LKB1 on cell migration.

Fibroblasts from PMSE patients exhibit aberrant IRS1/cofilin signaling

We next hypothesized that the effects of STRADA loss on IRS1 and cofilin phosphorylation in mNPCs would be replicated in human PMSE cells. Thus, we generated fibroblasts from skin punch biopsy samples from control (*STRADA*$^{+/+}$; n=1) and PMSE (*STRADA*$^{-/-}$; n=3) subjects (**Figure 3.6*A***). Compared to control cells, PMSE fibroblasts exhibit enhanced S6 and IRS1 phosphorylation and diminished cofilin phosphorylation, directly corroborating the signaling mechanism defined in STRADA KD mNPCs (**Figure 3.4*F***). These results were in contrast to the phosphorylation profile of cofilin seen in *Lkb1*$^{-/-}$ MEFs, suggesting a STRADA-specific effect.

PMSE patient fibroblasts exhibit a migration defect

We next performed the wound-healing migration assay in human PMSE and control fibroblasts as a strategy to further corroborate the effects of STRADA KD in mNPCs. PMSE and control fibroblasts were treated with rapamycin (100 nM) or p70S6Ki (10 μM) throughout the duration of the assay (ending at 15h). The distance migrated by PMSE fibroblasts was significantly reduced relative to control fibroblasts, and this effect was reversed with rapamycin or p70S6Ki treatment, suggesting a dependence on mTORC1/p70S6K signaling (**Figure 3.6*B-C*, Table 3.1**). Thus, both the signaling and functional effects of STRADA loss identified in mNPCs are robustly replicated in human PMSE cells. We then evaluated the effects of p70S6Ki treatment of these cells on the phosphorylation status of S6 and IRS1, and found that inhibiting p70S6K in PMSE fibroblasts reduces phosphorylation of both effectors, also consistent with our proposed mechanism (**Figure 3.6*D***). Importantly, parallel signaling patterns and migration deficit phenotypes in STRADA KD mNPCs and PMSE fibroblasts demonstrate that our *in vitro* murine data provide translational insights into PMSE pathogenesis and the role of STRADA in human brain development.

STRADA and LKB1 differentially regulate actin polymerization

We hypothesized that if STRADA functions to regulate cofilin activity, loss of STRADA should change the composition of actin structure. Notably, polymerized or filamentous (F) actin plays a critical role in establishing polarity of migrating cells (73). To test this, we measured the relative contents of depolymerized globular (G) versus polymerized F actin in STRADA KD and Scram mNPCs using a differential centrifugation assay. As

expected, in association with reduced cofilin phosphorylation in STRADA KD mNPCs, the ratio of G:F actin was approximately 2.91 times greater in STRADA KD than in Scram mNPCs (**Figure 3.7*A***). Thus, loss of cofilin inhibition associated with STRADA KD in migrating neurons disrupts actin polymerization and establishment of F actin. We next performed the differential centrifugation actin assay on PMSE versus control fibroblasts, and found that PMSE fibroblasts exhibit an approximately 12.59-fold greater ratio of G:F actin than control cells (**Figure 3.7*B***). We submit that STRADA promotes the phosphorylation and inhibition of cofilin, enabling actin polymerization and consequent migrating cell polarization and linear directionality. Importantly, these results demonstrate that impaired actin polymerization is a common mechanism highly associated with the absence of STRADA both in human PMSE fibroblasts and in STRADA KD mNPCs. Interestingly, *Lkb1*$^{-/-}$ MEFs exhibited the opposite pattern, with a predominance of *polymerized* actin. Compared with *Lkb1*$^{+/+}$ MEF control cells, the *Lkb1*$^{-/-}$ line exhibited a 2.78-fold greater ratio of *F:G actin* (in contrast to the trend seen in conditions of STRADA depletion), consistent with enhanced cofilin phosphorylation and increased migration associated with LKB1 depletion (**Figure 3.7*C***).

Rapamycin prevents heterotopic neurons associated with STRADA KD in developing cortex

Since STRADA modulates IRS1 signaling through mTORC1 inhibition, we hypothesized that pharmacological mTORC1 inhibition could rescue aberrant cortical lamination in a mouse PMSE model (12). STRADA shRNA knockdown (KD; GFP-

tagged shRNA plasmid targeting STRADA) by IUE on embryonic day 14 (E14) in the mouse cortex results in heterotopic neurons in the VZ/SVZ that fail to migrate to the CP by E19. Transfected pregnant dams were treated with daily intraperitoneal injections of rapamycin (5 mg/kg) or vehicle control solution (0.9% saline) from E15 until sacrifice at E19. While vehicle-treated pups exhibited a cortical malformation with the majority of STRADA KD neurons failing to migrate into the CP at E19, rapamycin treatment significantly rescued the cortical migratory defect and enabled STRADA KD neurons to reach the CP (**Figure 3.8, Table 3.1**). These findings support a mechanistic link between enhanced mTORC1 signaling and aberrant neuronal migration in PMSE.

Discussion

We demonstrate that STRADA functions as pivotal regulator of polarity and pathfinding in migrating neurons by signaling from IRS1 to cofilin and promoting actin polymerization. Loss of STRADA in PMSE patient fibroblasts or following shRNA knockdown in mNPCs leads to mTORC1 activation and enhanced phospho-inhibition of IRS1 via p70S6K, which in turn diminishes PAK1 phospho-activation of LIMK. Activated PAK1 phosphorylates and activates LIMK, which phosphorylates and inhibits cofilin, promoting actin polymerization, an essential process in leading edge formation and establishment of polarity in migrating neurons and fibroblasts (73, 123-125). Reduced LIMK activation leads to diminished phospho-inhibition of cofilin and enhanced actin depolymerization. Thus we submit that STRADA depletion disrupts neuronal polarity and consequently, pathfinding and migration via effects on actin. Detection of enhanced P-IRS1 in human PMSE cortex supports the hypothesis that disruption of this signaling mechanism occurs in PMSE during brain development, resulting in failed neuronal migration and consequent heterotopic neurons in the subcortical white matter. The rescue of heterotopic neurons following STRADA KD with rapamycin suggests dependence of PMSE phenotype on mTORC1-p70S6K signaling and yields an important therapeutic target.

Our studies define STRADA as a critical modulator of mTORC1-p70S6K-IRS1 signaling in neural progenitor cells. The rescue of impaired migration with rapamycin following STRADA KD *in vitro* and *in vivo* strongly supports an mTORC1-dependent mechanism, further substantiated by rescue *in vitro* with an inhibitor of p70S6K, which

reverses the phospho-inhibition of IRS1. p70S6K signaling has been identified as an essential pathway in cell migration, contributing to cell motility and actin filament remodeling (116). P-p70S6K phosphorylates IRS1, driving a decrease in PI3K-mediated activation of the Rho GTPases Rac1 and Cdc42 and corresponding decrease in PAK1 activation, an effect associated with impaired cell migration in TSC2-depleted fibroblasts, downstream of STRADA (66, 67, 126). TSC2-null MEFs exhibit impaired cell motility and enhanced mTORC1 activation, suggesting a link between enhanced mTORC1-p70S6K-IRS1 signaling and diminished cell motility (66). In our STRADA KD studies, diminished downstream phospho-signaling through PAK1 and LIMK leads to decreased cofilin phosphorylation and disrupted actin polymerization, evidenced by an increase in the relative proportions of G to F actin, which is corroborated in PMSE patient fibroblasts. In fact, the phenotype of STRADA KD in mNPCs is reminiscent of cells expressing mutant PAK1, which exhibit disrupted pathfinding (127).

Our findings of *impaired* cell migration in the setting of STRADA depletion are in direct contrast to *enhanced* cell migration reported in LKB1 depletion models (128), suggesting dissociable effects of LKB1 on cell migration in the presence or absence of STRADA that shed light on these phenotypic differences. We thus propose a new model for the interaction between STRADA and LKB1, wherein STRADA binding LKB1 modulates LKB1 to preferentially activate AMPK and therefore inhibit mTOR, providing a downstream activation of PAK1 via IRS1, PI3K, and Rho GTPases. When STRADA is present, PAK1 activation through the mTORC1 pathway is dominant and cofilin is phosphorylated and inhibited, favoring actin polymerization and establishment of migrating cell polarity. In contrast, in the absence of STRADA, PAK1 is inhibited dually,

through enhanced mTORC1 signaling and consequent inhibition of IRS1/p70S6K-dependent activation of PAK1, and possibly through direct LKB1 inhibition of PAK1. Indeed, a recent study has defined a direct inhibitory link between LKB1 and PAK1, through phosphorylation at PAK1 Thr 109 (128). In the absence of LKB1, the predominant effect is PAK1 activation, as a consequence of removing LKB1 direct inhibition of PAK1. In this case, cofilin phospho-inhibition by activated LIMK is increased, resulting in enhanced actin polymerization and increased migration. Thus, we propose that under normal circumstances, STRADA binding to LKB1 favors PAK1 activation to drive polarity and pathfinding in migrating neurons. This is consistent with previous studies demonstrating that induction of STRADA in intestinal epithelial cells was sufficient to cause cell-autonomous establishment of polarity in an LKB1-dependent manner (71). Interestingly, a recent study has demonstrated that overexpressing STRADA in the setting of LKB1 loss in cancer cells could activate PAK1 and induce cell polarization (110). The dependence of this effect on mTORC1/p70S6K and IRS1 signaling, as suggested by our work, will need to be considered in further experiments. In a previous study, we have shown that STRADA depletion is associated with a predominance of LKB1 in the nucleus, consistent with a role for STRADA in nucleo-cytoplasmic transport of LKB1 (7, 8, 12). Because each component of our defined signaling mechanism (**Figure 3.5**) can function in nucleus as well as cytoplasm, further studies are needed to determine the particular effects of subcellular localization on the interaction between LKB1 and PAK1, and the consequent polymerization state of actin (1, 129).

Using PMSE as a model disease, we have defined a novel mechanism linking STRADA and mTOR signaling to actin assembly, cell polarization, neuronal migration, and cortical development, which may be functional in other mTORC1-associated neurodevelopmental disorders. We propose that STRADA plays a critical role in neural progenitor cell migration during cortical development, and likely accounts for heterotopic neurons in PMSE. In the future, targeting functional nodes along the STRADA/mTORC1 cascade could offer plausible therapeutic approaches to inhibit aberrant IRS1/cofilin signaling in other mTORC1-associated neurodevelopmental disorders such as TSC or autism-macrocephaly syndrome.

Table 3.1. Data Quantification and Statistical Measures for STRADA Migration

Corresponding Figure	Cell Type	Condition	Treatment	Mean	S.E.M.	Unit Measured	n	Comparison	p-value
1B	mNPCs	Scram	Untreated	313.62	3.67	µm	3 wells, 90 measures	Scram vs. STRADA KD-untreated	<0.00001
		STRADA KD	Untreated	244.77	4.42	µm	3 wells, 90 measures	STRADA KD-untreated vs. STRADA KD-Rapa	0.000016
			Rapamycin (50 nM)	268.4	9.03	µm	3 wells, 90 measures		
1C	mNPCs	Scram	Untreated	135.99	3.61	µm	3 wells, 90 measures	Scram vs. STRADA KD-untreated	<0.00001
		STRADA KD	Untreated	113.66	2.9	µm	3 wells, 90 measures	Scram vs. STRADA KD-p70S6Ki	0.74
			p70S6Ki (10 µM)	134.35	2.51	µm	3 wells, 90 measures		
Supplement to Fig. 1 Data for AraC Migration	mNPCs	WT	AraC only	560.05	11.66	µm	3 wells, 90 measures	WT-AraC vs. Scram AraC	0.14
		Scram	AraC only	534.61	13.13	µm	3 wells, 90 measures	Scram-AraC vs. STRADA KD-AraC	<0.00001
		STRADA KD	AraC only	421.47	15.68	µm	3 wells, 90 measures	STRADA KD-AraC vs. - STRADA KD-AraC+Rapa	<0.00001
		STRADA KD	AraC+Rapamycin (50 nM)	564.65	20.83	µm	3 wells, 90 measures	Scram-AraC vs. STRADA KD-AraC+Rapa	0.2
2B	mNPCs	Scram	Untreated	508.59	26.63	µm	20 cells	Scram vs. STRADA KD	<0.00001
		STRADA KD	Untreated	688.74	64.13	µm	15 cells		
2C	mNPCs	STRADA KD	Untreated	397.46	23.89	µm	20 cells	STRADA KD-untreated vs. STRADA KD-Rapa	0.0001
		STRADA KD	Rapamycin (50 nM)	348.31	21.98	µm	20 cells		
2D	mNPCs	Scram	Untreated	784.88	92.93	degrees^2	20 cells	Scram vs. STRADA KD	<0.00001
		STRADA KD	Untreated	2050.1	129.39	degrees^2	15 cells		
2E	mNPCs	STRADA KD	Untreated	2254.38	111.08	degrees^2	20 cells	STRADA KD-untreated vs. STRADA KD-Rapa	<0.00001
		STRADA KD	Rapamycin (50 nM)	1481.8	84.12	degrees^2	20 cells		
3E	mNPCs	Scram		78.83	1.33	µm^2	640 cells	Scram vs. STRADA KD-untreated	<0.00001
		STRADA KD	Untreated	98.8	1.95	µm^2	600 cells	STRADA KD-untreated vs. STRADA KD-Rapa	0.00204
		STRADA KD	Rapamycin (50 nM)	88.66	2.51	µm^2	300 cells	STRADA KD-untreated vs. STRADA KD-p70S6Ki	<0.00001
		STRADA KD	p70S6Ki (10 µM)	77.87	1.94	µm^2	360 cells	Scram vs. STRADA KD-p70S6Ki	0.67
3F	mNPCs	Scram		98.56	1.86	degrees	640 cells	Scram vs. STRADA KD-untreated	<0.00001
		STRADA KD	Untreated	112.82	2.35	degrees	600 cells	STRADA KD-untreated vs. STRADA KD-Rapa	0.037
		STRADA KD	Rapamycin (50 nM)	104.93	2.56	degrees	300 cells	STRADA KD-untreated vs. STRADA KD-p70S6Ki	0.033
		STRADA KD	p70S6Ki (10 µM)	104.86	2.8	degrees	360 cells		
4D, 10h	mNPCs	STRADA KD	Untreated	142.57	3.79	µm	3 wells, 90 measures	Scram-untreated vs. STRADA KD-untreated	0.000029
		Scram	Untreated	178.56	7.48	µm	3 wells, 90 measures	Scram-untreated vs. Scram-IPA-3 (1 µM)	0.0015
		Scram	IPA-3 (1 µM)	148.55	5.51	µm	3 wells, 90 measures	Scram-untreated vs. Scram-IPA-3 (2.5 µM)	<0.00001
		Scram	IPA-3 (2.5 µM)	129.99	3.77	µm	3 wells, 90 measures	Scram-untreated vs. Scram-IPA-3 (5 µM)	<0.00001
		Scram	IPA-3 (5 µM)	124.86	4.26	µm	3 wells, 90 measures	Scram-untreated vs. Scram-IPA-3 (10 µM)	<0.00001
		Scram	IPA-3 (10 µM)	66.34	4.64	µm	3 wells, 90 measures		
4D, 20h	mNPCs	STRADA KD	Untreated	256.71	3.61	µm	3 wells, 90 measures	Scram-untreated vs. STRADA KD-untreated	<0.00001
		Scram	Untreated	315.5	7.36	µm	3 wells, 90 measures	Scram-untreated vs. Scram-IPA-3 (1 µM)	0.07
		Scram	IPA-3 (1 µM)	298.57	5.65	µm	3 wells, 90 measures	Scram-untreated vs. Scram-IPA-3 (2.5 µM)	0.0022
		Scram	IPA-3 (2.5 µM)	282.34	4.82	µm	3 wells, 90 measures	Scram-untreated vs. Scram-IPA-3 (5 µM)	<0.00001
		Scram	IPA-3 (5 µM)	260.5	4.49	µm	3 wells, 90 measures	Scram-untreated vs. Scram-IPA-3 (10 µM)	<0.00001
		Scram	IPA-3 (10 µM)	179.88	5.39	µm	3 wells, 90 measures		
6C	Hu Fibroblasts	CTL		231.71	6.97	µm	3 wells, 90 measures	CTL vs. PMSE-untreated	0.0019
		PMSE	Untreated	201.55	6.14	µm	3 wells, 90 measures	PMSE-untreated vs. PMSE-Rapa	<0.00001
		PMSE	Rapamycin (100 nM)	269.29	9.54	µm	3 wells, 90 measures	PMSE-untreated vs. PMSE-p70S6Ki	<0.00001
		PMSE	p70S6Ki (10 µM)	285.75	7.58	µm	3 wells, 90 measures		
8E	mNPCs *in vivo*	STRADA KD	Vehicle Control (saline)	26.35	5.37	% GFP+ cells in CP	5 animals	Vehicle Control vs. Rapamycin-treated	0.000051
		STRADA KD	Rapamycin (5 mg/kg)	67.78	2.8	% GFP+ cells in CP	6 animals		

Figure 3.1. STRADA KD is associated with migration deficit in mNPCs, in an mTORC1- and p70S6K-dependent manner.

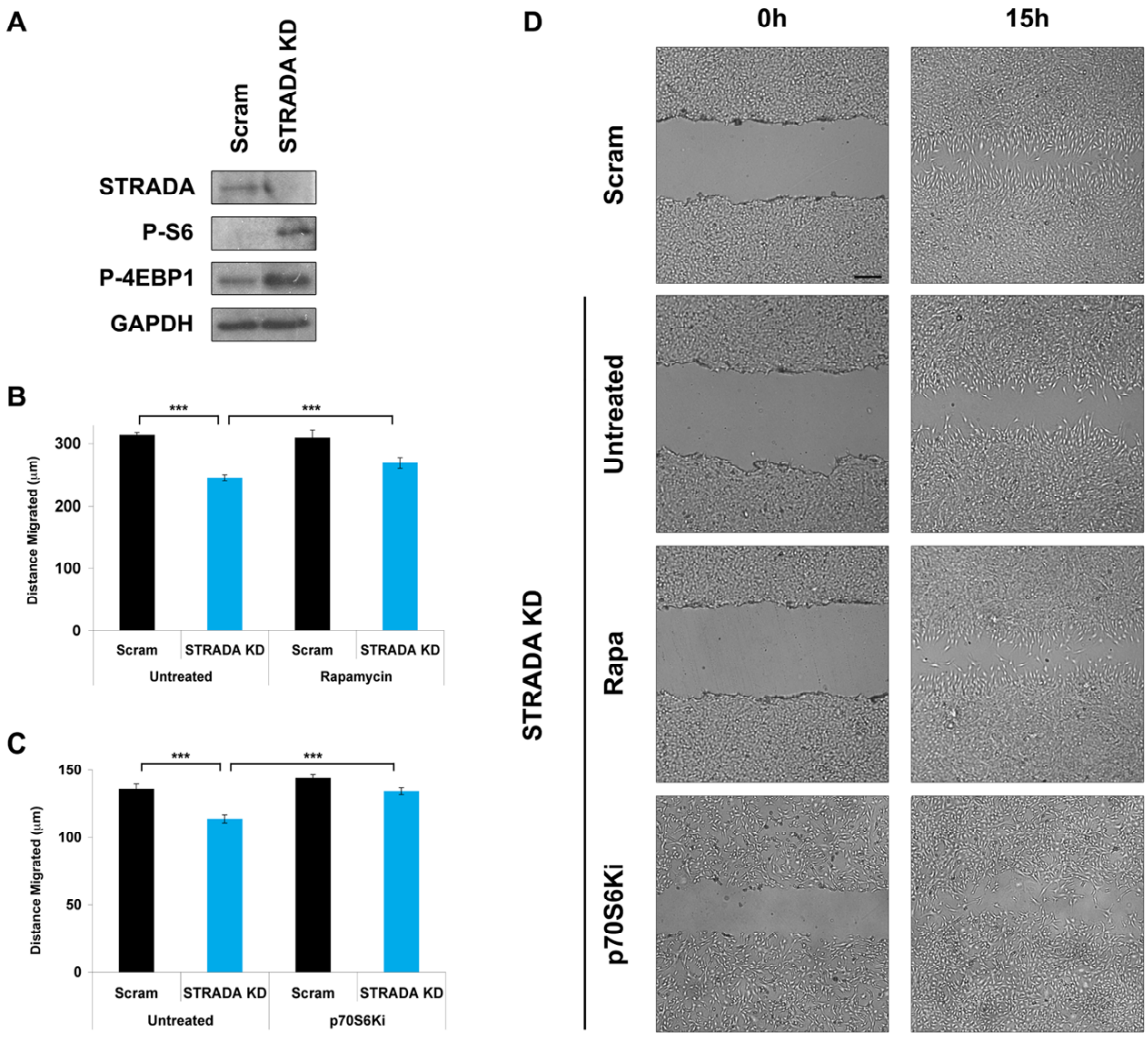

Figure 3.1. STRADA KD is associated with migration deficit in mNPCs, in an mTORC1- and p70S6K-dependent manner. ***A,*** STRADA depletion and enhanced mTORC1 signaling in a stably-transfected STRADA shRNA-puro^R (STRADA KD) mNPC line used for migration assays. STRADA KD cells exhibit reduced expression of STRADA and enhanced phosphorylated S6 (P-S6) and 4EBP1 (P-4EBP1) protein levels, indicating mTORC1 activity, relative to Scram shRNA-puro^R (Scram) control cells. GAPDH was used as an internal loading control. ***B,*** Untreated STRADA KD mNPCs exhibit reduced migration in a wound-healing migration assay, relative to Scram mNPCs. n = 3 wells, 90 measures per condition at each timepoint, ***$P < 0.001$. Treatment with either rapamycin or ***C,*** p70S6Ki significantly increases the distance migrated by STRADA KD cells, confirming that STRADA regulates mNPC migration through mTORC1/p70S6K signaling. n = 3 wells, 90 measures per condition at each timepoint, ***$P < 0.001$. ***D,*** Representative images depict gap closure in each transfection (Scram or STRADA KD) and treatment (Untreated, Rapa, and p70S6Ki) condition from the time the scratch is made (0h) to the endpoint of measurement (15h). Scale bar: ***D,*** 250 μm.

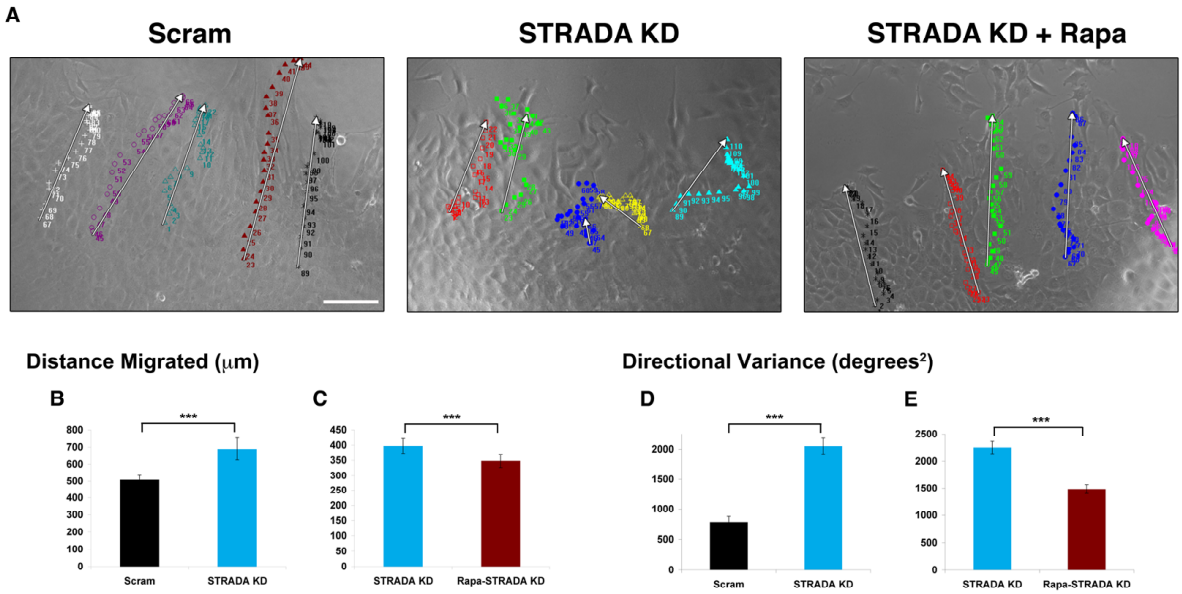

Figure 3.2. STRADA-deplete migrating mNPCs exhibit impaired linear directionality. ***A***, The migratory paths of individual cells recorded every 30 minutes for 20 hours in each panel are represented by individual colors, and white arrows indicate the composite migration vectors of each cell. Scram mNPCs migrate in a predominantly uniform linear manner to close the gap created in the wound-healing migration assay. STRADA KD mNPCs migrate in a haphazard fashion without consistent linear direction. Treatment with rapamycin restores linear directionality in these cells. ***B-E***, Quantitative analysis reveals a significant increase in ***B***, overall distance migrated as well as ***D***, directional variance in STRADA KD mNPCs. ***C,E***, These effects are both attenuated with rapamycin treatment. n = 15 cells for untreated STRADA KD, 20 cells for each other condition, ***$P < 0.001$. Scale bar: ***A,*** 100 μm.

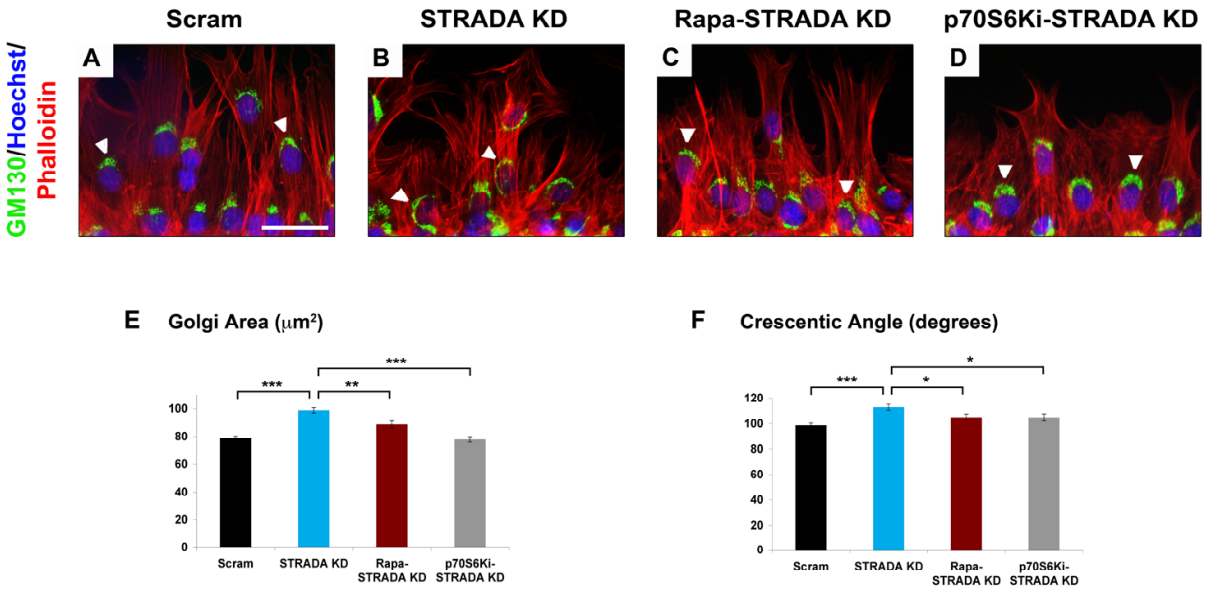

Figure 3.3. STRADA depletion in mNPCs impairs polarization capacity, evidenced by Golgi dispersion. ***A,*** Representative immunofluorescent images demonstrate compaction of Golgi (indicated by GM130) forward of the nucleus toward the leading edge in migrating Scram mNPCs, and ***B,*** dispersion of the Golgi around the nucleus with failure to establish cell polarity in migrating STRADA KD mNPCs. Golgi compaction is largely restored in STRADA KD cells with ***C,*** rapamycin or ***D,*** p70S6Ki treatment. White arrowheads indicate representative Golgi bodies in each panel. ***E,*** Quantification of Golgi area as a measure of compaction reveals significantly increased area in STRADA KD compared with Scram mNPCs, attenuated with rapamycin or p70S6Ki treatment. n = 640 cells for Scram, 600 cells for untreated STRADA KD, 300 cells for Rapa-treated STRADA KD, 360 cells for p70S6Ki-treated STRADA KD, ***$P < 0.001$, **$P < 0.01$. ***F,*** Similarly, quantification of crescentic angle subtended by Golgi around the nucleus reveals greater dispersion (larger angle) in STRADA KD mNPCs, attenuated with rapamycin or p70S6Ki treatment. Taken together, these results suggest that STRADA mediates migrating mNPC capacity to polarize, in an mTORC1-/p70S6K-dependent manner. n = 640 cells for Scram, 600 cells for untreated STRADA KD, 300 cells for Rapa-treated STRADA KD, 360 cells for p70S6Ki-treated STRADA KD, ***$P < 0.001$, *$P < 0.05$. Scale bar: (in ***A***) ***A-D,*** 50 μm.

Figure 3.4. STRADA regulates cell migration through IRS1 signaling to cofilin, dissociable from LKB1's regulation of cofilin.

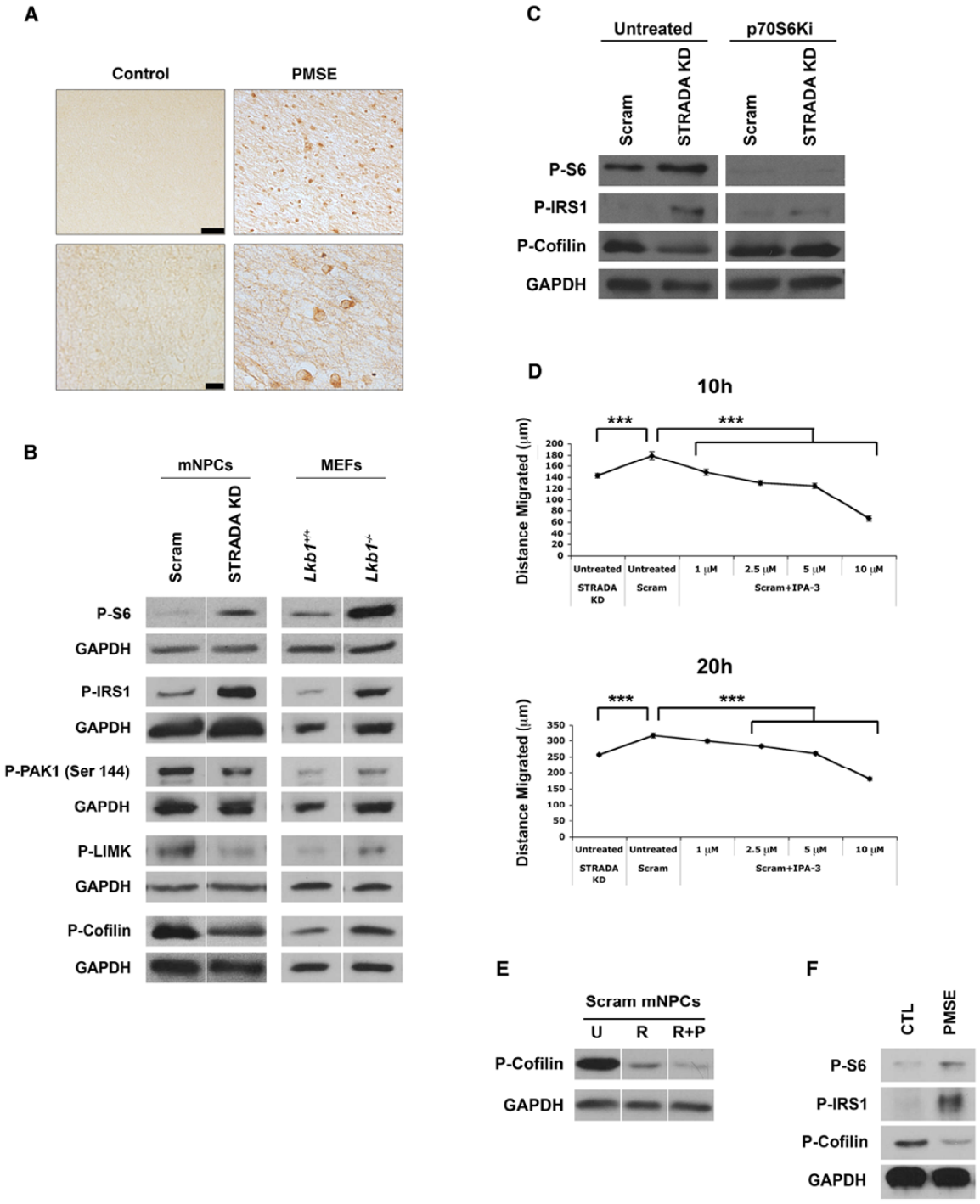

Figure 3.4. STRADA regulates cell migration through IRS1 signaling to cofilin, dissociable from LKB1's regulation of cofilin. ***A,*** PMSE patient cortex exhibits enhanced expression of P-IRS1 relative to control epileptic cortex, linking aberrant mTORC1 signaling associated with STRADA loss in the brain to the cofilin signaling pathway, via IRS1. ***B,*** Western analysis reveals enhanced phosphorylation of S6 and IRS1, and diminished autophosphorylation of PAK1 (Ser 144) and phosphorylation of LIMK and cofilin, in STRADA KD mNPCs. In contrast, the phosphorylation pattern of *Lkb1*$^{-/-}$ MEFs diverges from that of STRADA KD at the level of PAK1. *Lkb1*$^{-/-}$ MEFs exhibit enhanced phosphorylation of S6 and IRS1, but also enhanced phosphorylation of PAK1, LIMK, and cofilin, indicating dissociable roles for STRADA and LKB1 in the cofilin signaling pathway. GAPDH serves as an internal loading control. ***C,*** p70S6Ki rescues aberrant IRS1/Cofilin signaling in STRADA KD mNPCs. Compared with Scram control cells, untreated STRADA KD mNPCs exhibit enhanced phosphorylation of S6 and IRS1, with diminished inhibitory phosphorylation of cofilin. Treatment with p70S6Ki rescues these effects, indicating a p70S6K dependence of this mechanism. GAPDH serves as an internal loading control. ***D,*** Application of the PAK inhibitor IPA-3 at increasing doses (1-10 μM) in Scram mNPCs produces a migration defect at 10h and 20h that mimics that caused by STRADA KD, implicating PAK1 as a key operator in this effect, consistent with the signaling mechanism proposed. n = 3 wells, 90 measures per condition at each timepoint, ***P < 0.001. ***E,*** Reduced cofilin phosphorylation caused by PAK inhibition with ROCK inhibition. To isolate the effects of PAK inhibition with IPA-3 treatment on cofilin phosphorylation, ROCK inhibitor Y-27632 (10 μM) was applied 12 hours prior to 1-hour treatment with IPA-3 (10 μM). ROCK inhibition alone (R) reduces cofilin phosphorylation relative to untreated cells (U), and PAK inhibition (R+P) provides further reduction, indicating an independent effect of PAK on cofilin phosphorylative inhibition. GAPDH serves as an internal loading control. ***F,*** PMSE patient fibroblasts (PMSE; *STRADA*$^{-/-}$) exhibit enhanced phosphorylation of S6 and IRS1, and diminished phosphorylation of cofilin, relative to control (CTL; *STRADA*$^{+/+}$) fibroblasts, supporting the mechanism established in STRADA KD mNPCs. GAPDH serves as an internal loading control. Scale bars: ***A,*** 50 μm (top), 10 μm (bottom).

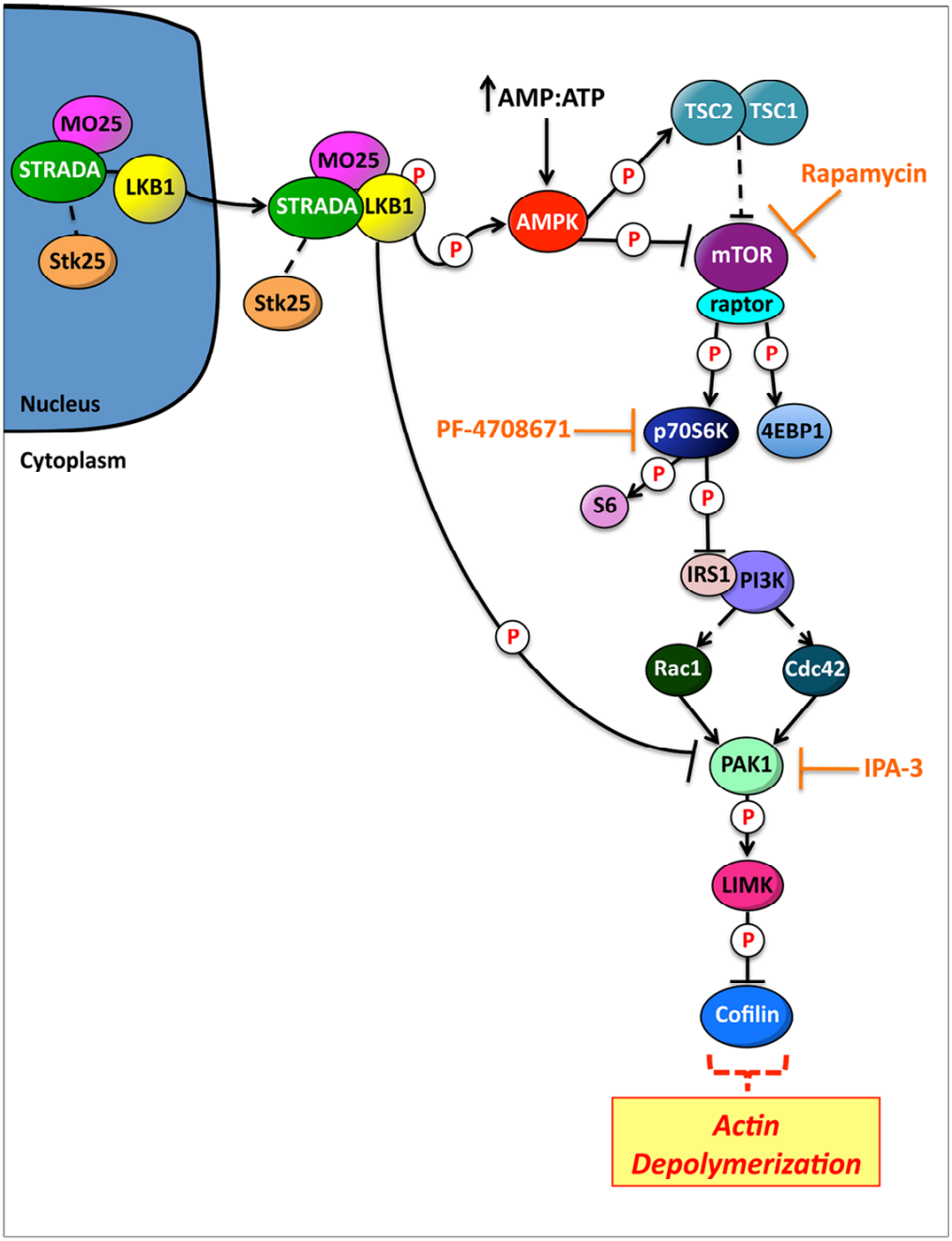

Figure 3.5. We propose that STRADA inhibits mTORC1/p70S6K, which promotes Rac1/Cdc42 activation of PAK1 through P-IRS1/PI3K signaling, activating LIMK, and inhibiting cofilin. STRADA-dependent phosphorylative inhibition of cofilin promotes actin polymerization, which enables migrating cells to polarize by establishing an F-actin based leading edge to drive linear directionality. LKB1 independently phosphorylates and inhibits PAK1, producing the opposite pattern of phosphorylation at the level of and downstream of this node as a consequence of LKB1 versus STRADA depletion.

Figure 3.6. PMSE fibroblasts exhibit enhanced mTORC1/p70S6K activity and IRS1 phosphorylation and impaired migration, rescued with mTORC1 or p70S6K inhibition.

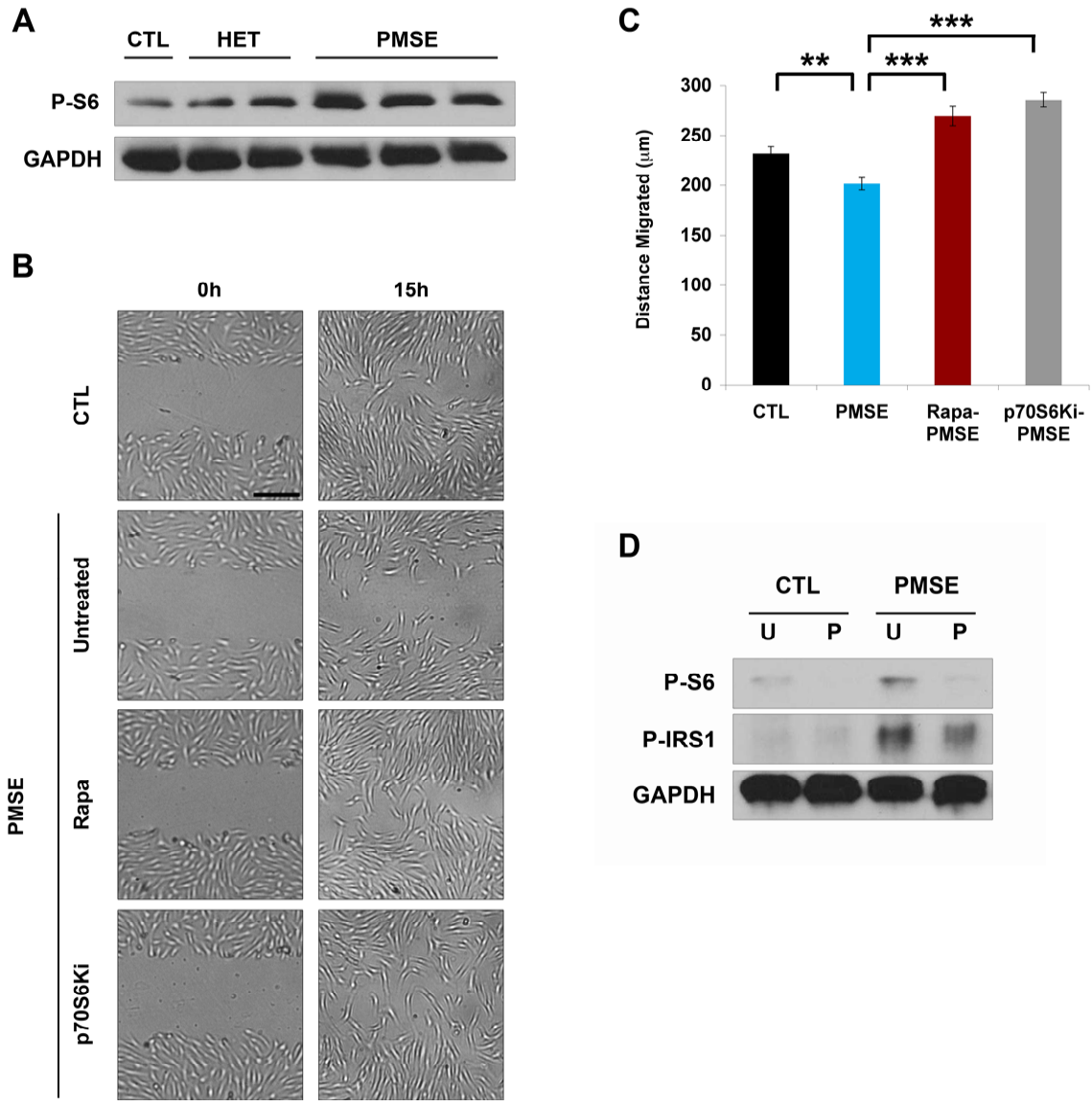

Figure 3.6. PMSE fibroblasts exhibit enhanced mTORC1/p70S6K activity and IRS1 phosphorylation and impaired migration, rescued with mTORC1 or p70S6K inhibition. ***A,*** Enhanced mTORC1 activity in PMSE fibroblasts. Western analysis performed on control (CTL; $STRADA^{+/+}$), heterozygous STRADA (HET; $STRADA^{+/-}$), and PMSE patient (PMSE; $STRADA^{-/-}$) fibroblasts reveals enhanced P-S6, indicative of mTORC1 activity level, in HET compared to CTL fibroblasts, and further enhanced P-S6 in PMSE fibroblasts. Each band represents a fibroblast line derived from a separate donor. GAPDH serves as an internal loading control. ***B,*** In a wound-healing migration assay, untreated PMSE fibroblasts demonstrate impaired migration at 15h, compared with controls, corroborating the deficit associated with STRADA KD in mNPCs. ***C,*** PMSE fibroblast migration is fully rescued by treatment with rapamycin or p70S6Ki. n = 3 wells, 90 measures per condition at each timepoint, $***P < 0.001$, $**P < 0.01$. ***D,*** p70S6K inhibition reduces enhanced S6 and IRS1 phosphorylation in PMSE fibroblasts. Western analysis was used to quantify P-S6 and P-IRS1 in Control (CTL) and PMSE patient (PMSE) fibroblasts, with (P) and without (U) p70S6Ki treatment. Untreated PMSE fibroblasts exhibit greater P-S6 and P-IRS1 than CTL cells, and these effects are attenuated with p70S6K inhibition, suggesting the efficacy of this mechanism as a potential therapeutic approach. GAPDH serves as an internal loading control. Scale bar: ***B,*** 250 μm.

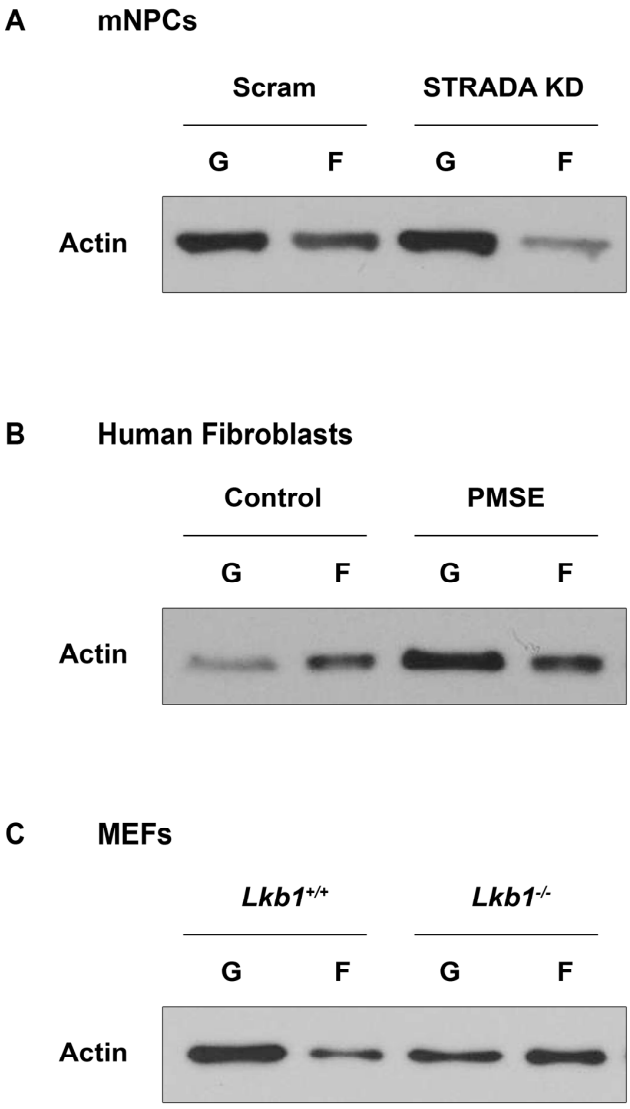

Figure 3.7. STRADA and LKB1 differentially regulate actin dynamics. ***A,*** Analysis of G and F actin fractions reveals a 2.91-fold greater G:F ratio in STRADA KD compared with Scram mNPCs, suggesting diminished capacity of cells to polymerize actin in the absence of STRADA, consistent with enhanced cofilin activity. ***B,*** Actin analysis reveals that PMSE fibroblasts exhibit a 12.59-fold enhanced G:F actin ratio compared with controls, supporting the actin-based mechanism of aberrant migration proposed in mNPCs and confirming this STRADA-specific role in actin polymerization across different cell types, fibroblasts in addition to mNPCs. ***C,*** In contrast to STRADA-depleted mNPCs and PMSE fibroblasts, *Lkb1*$^{-/-}$ MEFs show the opposite pattern of actin polymerization, with a 2.78-fold greater F:G ratio compared with *Lkb1*$^{+/+}$ controls, consistent with diminished cofilin activity.

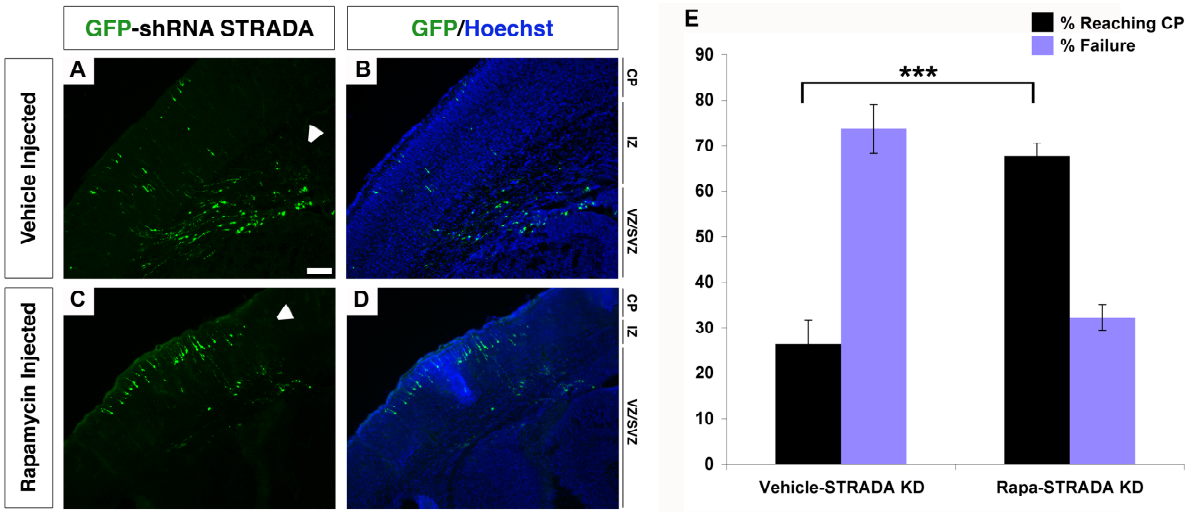

Figure 3.8. Inhibition of mTORC1 with rapamycin rescues the cortical lamination defect associated with STRADA KD in the developing mouse brain. ***A-B,*** Vehicle-(0.9% saline) injection does not alter cortical lamination defect at E19 induced by IUE transfection with GFP-shRNA STRADA at E14. The majority of transfected cells remain in the ventricular/subventricular zone (VZ/SVZ) and fail to reach the cortical plate (CP). ***C-D,*** Rapamycin treatment of GFP-shRNA STRADA transfected animals from E15 to E18 prevents the laminar defect, and the majority of GFP^+ cells reach the CP by E19. ***E,*** Percentage of GFP-shRNA STRADA transfected cells reaching the CP at E19 following rapamycin (Rapa) versus saline (Vehicle) treatment. ***$P < 0.001$. White arrowheads indicate regions of GFP^+ cells in each panel. Scale bar: (in ***A***) ***A-D,*** 100 μm.

CHAPTER 4

GENERATING A TRANSGENIC MOUSE MODEL OF PMSE

PMSE patients present with intractable, multifocal epilepsy, starting in infancy (61). Similarly, seizures are a common phenotypic manifestation of TSC, often presenting in association with cortical tubers (29, 130, 131). In order to most effectively model PMSE and investigate the role of STRADA in cortical development and epilepsy, we are generating *de novo* a STRADA knockout (KO) mouse, in collaboration with Penn Transgenic Facility.

We designed a transgenic floxed construct to replicate the deletion seen in PMSE patients, with loxP sequences flanking exons 9-13 of the *STRADA* gene, which shares a high degree of homology between mice and humans. In humans, this deletion results in a lack of STRADA expression, producing an unstable variant of the protein (5, 12). Our construct was transformed into embryonic stem (ES) cells generated from a C57BL/6 mouse, neomycin selection was applied, and resulting clones were confirmed to carry the transgene via Southern analysis (**Figure 4.1**). The transformed ES cells were injected into the blastocyst of a BALB-C albino mouse, and chimeric mice were generated, with white fur indicating BALB-C background and black fur indicating the presumed percentage of transgenic C57BL/6 carriage (for a diagram of this process, see **Figure 4.2**). Chimeric males with ≥75% black fur were mated to wildtype (WT) C57BL/6 females, and black F1 offspring were selected from agouti littermates and genotyped using Southern analysis. We confirmed carriage of the *STRADA* KO transgene in two F1 offspring ($STRADA^{+/fl}$), which we are breeding to generate a KO line (**Figure 4.3**). Subsequent generations are evaluated for carriage of the transgenic floxed *STRADA* allele through PCR detection of the neomycin resistance gene (Neo^R) (**Figure 4.4**). Carriers are then evaluated for heterozygosity or homozygosity through Southern analysis.

Homozygous floxed mice (*STRADA*$^{fl/fl}$) will be mated to Cre recombinase-expressing (Cre) mice to yield the knockout (*STRADA*$^{fl/fl}$*;Cre*$^{+/-}$ or *STRADA*$^{fl/fl}$*;Cre*$^{+/+}$), and homozygous floxed mice not mated to Cre partners will be used as controls (*STRADA*$^{fl/fl}$*;Cre*$^{-/-}$) (See **Figure 4.5** for a schematic). If our KO mouse is non-viable, we will create a conditional KO by mating the *STRADA*$^{fl/fl}$ mouse to a nestin promoter-driven or drug-inducible promoter-driven Cre mouse. Additionally, we will perform focal KO in cortex using IUE with a Cre plasmid in the *STRADA*$^{fl/fl}$ mice not mated to Cre partners, in order to assess specifically the effects of *STRADA* gene KO in the developing brain, in a cell-autonomous manner.

We anticipate that focal KO in the *STRADA*$^{fl/fl}$ mice will provide an effective way to evaluate the implications of failed neuronal migration in cortical epileptogenesis and thus model seizures in PMSE. Bai and colleagues demonstrated that knockdown of Doublecortin (DCX), a microtubule-associated protein that plays a key role in migration, using RNAi in IUE results in a subcortical band heterotopia (SBH) (132). Interestingly, this is associated with aberrant neural firing patterns in the region of cortex overlying the SBH. Calcium imaging recording of neurons in the cortical area of failed migration revealed that these cells display both greater activity and greater co-activity, indicating enhanced synchronization, suggestive of epileptogenic activity (133). Preliminary electrophysiological analysis using calcium imaging in slice preparations from our IUE-generated STRADA KD mice suggests that STRADA loss is associated with regional hyperactivity in cortical areas overlying retention of transfected cells in VZ/SVZ. Particularly in a high-potassium (5.5 mM K^+) artificial cerebrospinal fluid (aCSF) solution, we found a pattern similar to that generated by DCX knockdown, of enhanced

neural firing and neural synchronicity, in the cortical area experiencing failed migration of STRADA KD cells (**Figure 4.6**). Since we have demonstrated that STRADA depletion impairs neuronal migration (see Chapter 3), and since appropriate neuronal migration during development is critical to the establishment of effective cortical networks, we hypothesize that this mechanism may account at least in part for the severe epilepsy experienced by patients with PMSE (108, 133). Evaluation of behavioral patterns and neural activity in the STRADA KO animals will provide an ideal platform for investigation of this mechanism.

With the generation of a STRADA KO mouse, we will be able to evaluate more effectively the phenotype associated with STRADA loss and test multiple therapeutic options. Lifespan, head circumference, brain and body weights, metabolic panels, and behavioral phenotype will be evaluated in this strain. A likely epileptic phenotype will be assessed through video/EEG recording and calcium imaging of cortical and hippocampal slice preparations. Additionally, it will be important to determine the capacity for treatment with rapamycin and other mTOR inhibitors. Immunohistochemical analysis of mTOR activity, cortical lamination, and neuronal differentiation profiles in KO brain specimens will allow comparison between this model and the neuropathological patterns seen in PMSE brain. Through our endeavors, we hope to delineate the role of STRADA in cortical development and epilepsy, and optimize biologically-targeted therapies for patients with mTOR-associated neurodevelopmental disorders, who are often refractory to standard antiepileptic drugs.

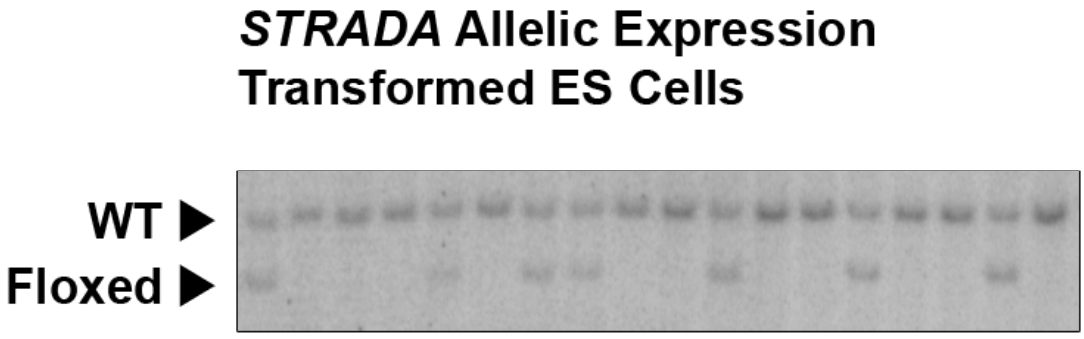

Figure 4.1. Southern blotting confirms several clones of transformed ES cells to carry the transgenic *STRADA* (*STRADA*^{fl}) allele. Each column of bands represents DNA extracted from a single clone of transformed ES cells and probed for *STRADA*. Higher molecular weight bands (MW) represent wild-type (WT) *STRADA*, while lower MW bands represent the transgenic floxed *STRADA* allele.

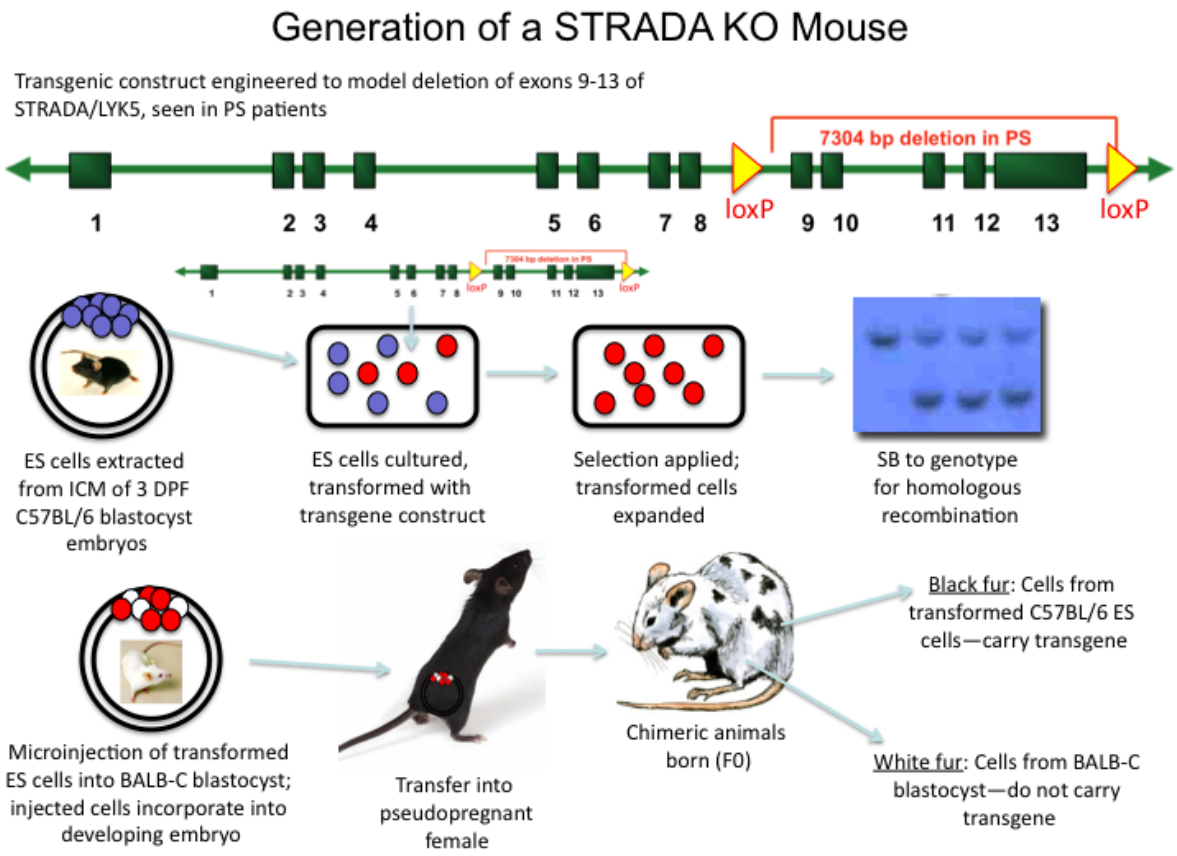

Figure 4.2. Generation of a *STRADA*$^{+/fl}$ carrier mouse. As indicated in the diagram, we replicated the deletion of *STRADA* exons 9-13, as seen in PMSE patients, to create the transgenic *STRADA* allele, with this region flanked by loxP sites for later Cre recombination. The transgene was engineered to carry this sequence as well as a neomycin resistance (*Neo*^{R}) gene, for selection. Embryonic stem (ES) cells were extracted from the inner cell mass (ICM) of a C57BL/6 blastocyst, at 3 days post-fertilization (DPF). These cells were cultured and transformed with the transgene. Neomycin selection was applied, and viable colonies were expanded and genotyped to confirm carriage of the transgene, via Southern blotting (SB). Transformed ES cells were microinjected into the blastocyst of a BALB-C albino mouse and incorporated into the developing embryo. This embryo was transferred to a host pseudopregnant female for gestation and delivery. Resulting offspring expressed a chimeric phenotype, with white fur color linked to non-transgenic cells from the BALB-C mouse, and black fur color linked to transgenic ES cells transformed from the original C57BL/6 mouse.

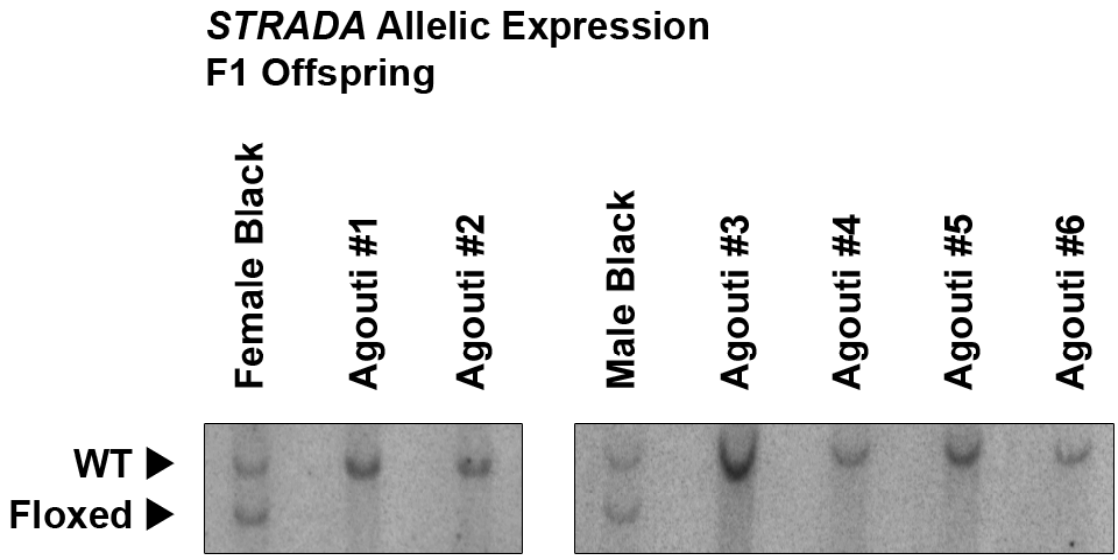

Figure 4.3. Southern blotting confirms F1 offspring to carry the transgenic *STRADA* (*STRADA*^{fl}) allele heterozygously. Each column of bands represents DNA extracted from a single animal and probed for *STRADA*. Higher molecular weight bands (MW) represent wild-type (WT) *STRADA*, while lower MW bands represent the transgenic floxed *STRADA* allele (Floxed). "Female Black" and "Male Black" refer to mice with black fur in the F1 generation, sired by P-generation chimeric males. Agouti mice served as littermate controls, carrying only the WT *STRADA* allele.

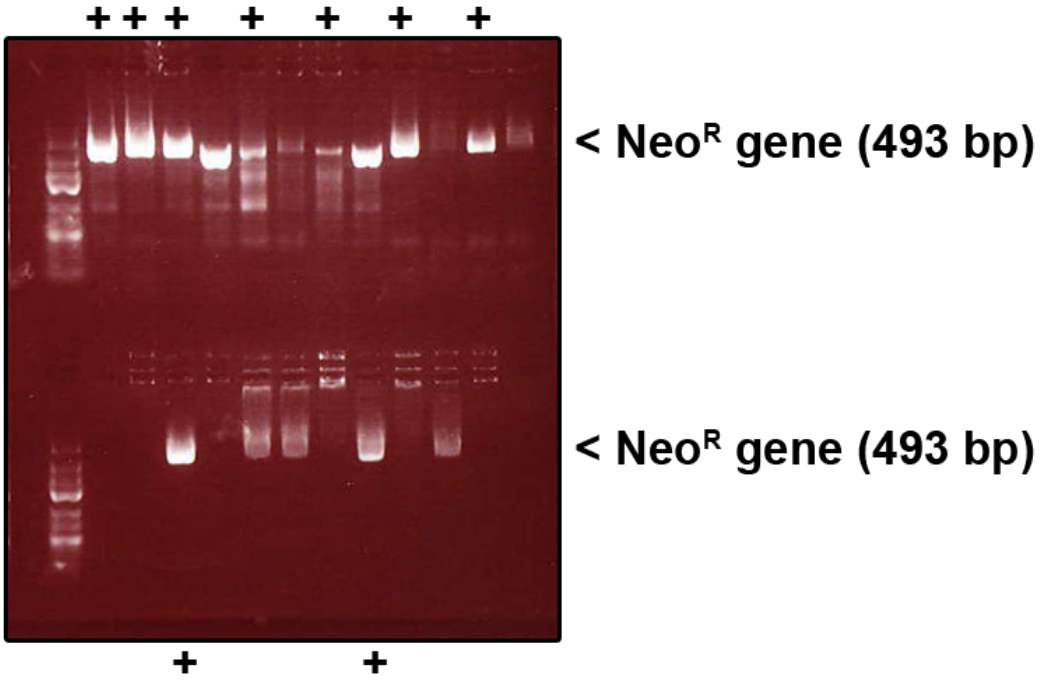

Figure 4.4. Polymerase chain reaction (PCR) indicates the presence of transgenic *STRADA*^{fl} allele in F2 animals. Each column represents DNA extracted from a separate animal. Plus signs identify animals carrying the 493 bp neomycin resistance (*Neo*^{R}) gene, which indicates presence of the *STRADA* floxed transgene.

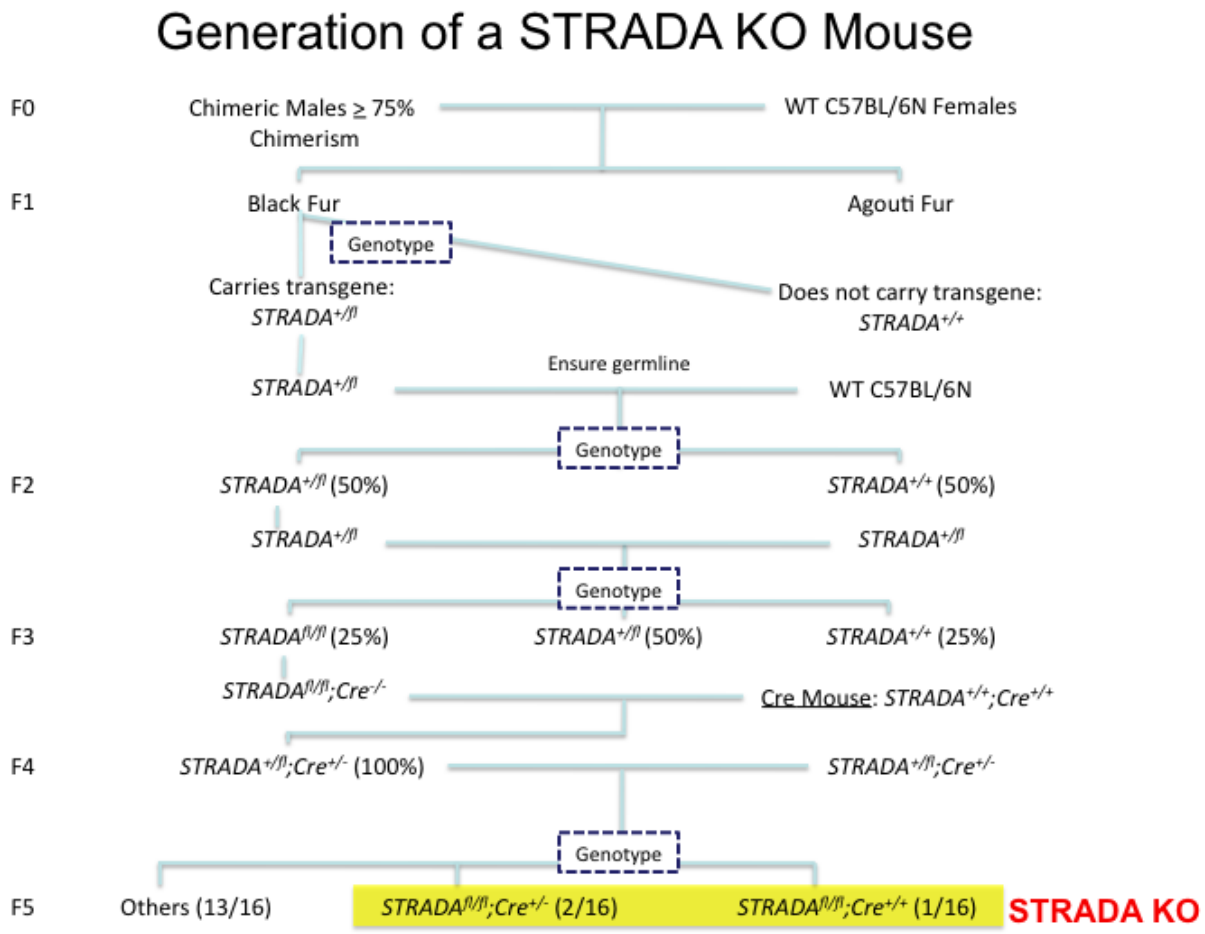

Figure 4.5. Diagram outlines the process of generating a STRADA KO mouse from the chimeric P/F0 generation. Refer to the text for details.

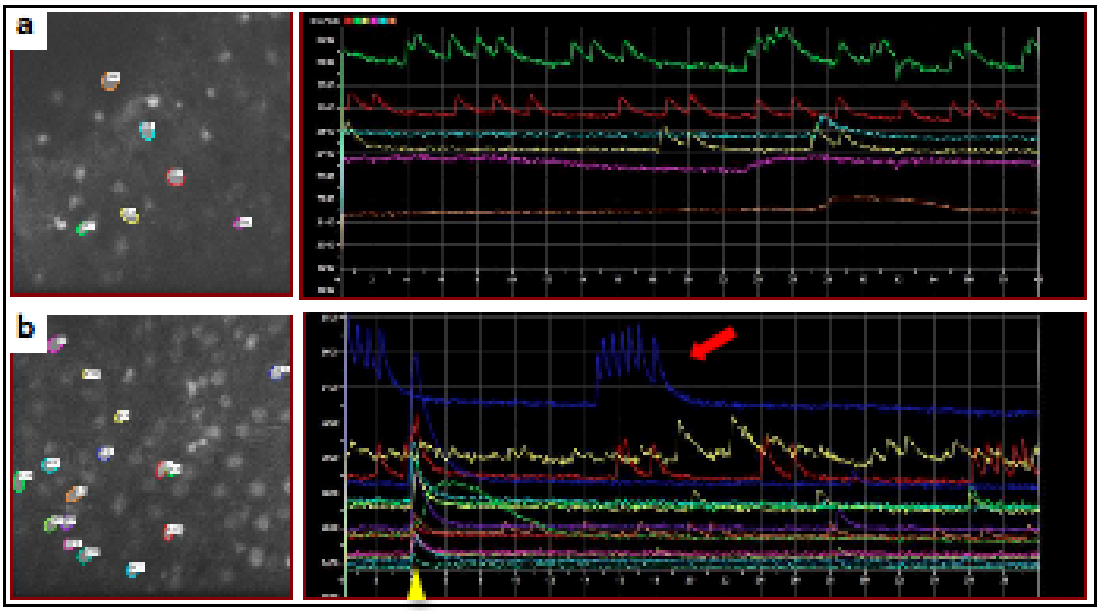

Figure 4.6. Calcium imaging of the cortical plate layer 2/3 (CP 2/3) region overlying heterotopic STRADA KD mNPCs reveals aberrant neuronal firing patterns. IUE was used to transfect animals at embryonic day 14 (E14) with GFP-tagged STRADA shRNA, to effect STRADA KD. At postnatal day 7 (P7), animals were sacrificed, and 350 μm coronal sections were cut on a microtome. Fluorescent microscopy was used to define the region of heterotopic GFP^+ mNPCs located in the ventricular/subventricular zone (VZ/SVZ), as well as the overlying CP 2/3 region, representing the appropriate destination area to which the STRADA-deplete cells failed to migrate. Coronal slices were bathed in artificial CSF (aCSF) solution or a potassium-supplemented (5 mM K^+) aCSF activating solution. In both solutions, the CP 2/3 region overlying the STRADA KD heterotopia exhibited considerably higher levels of neuronal firing. This was especially evident in the high-K^+ solution (pictured), in which neurons in the CP overlying the heterotopia exhibited evidence of epileptiform activity. Cells in this region showed synchronous firing (indicated by yellow arrowhead) as well as burst spiking (red arrow). ***A,*** Top panel demonstrates cortical neuronal firing outside the area of failed migration in a focal STRADA KD animal at P7. ***B,*** Bottom panel demonstrates enhanced cortical neuronal firing in the area of failed migration.

CHAPTER 5

DISCUSSION AND CLINICAL TRANSLATION[4]

[4] The PMSE patient data reported here was originally published in *Science Translational Medicine*, Vol. 5, No. 182, April 2013. Parker, W.E., Orlova, K.A., Parker, W.H., Birnbaum, J.F., Krymskaya, V.P., Goncharov, D.A., Baybis, M., Helfferich, J., Okochi, K., Strauss, K.A., and Crino, P.B. Rapamycin Prevents Seizures After Depletion of STRADA in a Rare Neurodevelopmental Disorder. Published by AAAS.

So often, rare genetic disorders can offer key insights into the normal functioning and role of a biological pathway based upon understanding the pathogenesis resulting from what is lacked. Here, we have employed one such disorder, PMSE, to elucidate the role of STRADA and mTOR signaling in cortical development. Although PMSE provides us with a fortuitous opportunity to understand an important biological process, we understand that this comes at a cost to those who suffer from the disorder without effective treatment options. This chapter will summarize the conclusions of our work, place STRADA into the larger context of mTOR-regulatory proteins, offer future directions, and finally discuss the implications of our findings for treatment of PMSE and other mTOR-associated neurodevelopmental disorders.

STRADA Plays a Critical Role in Cortical Development Through Directing Neuronal Migration: A Summary of Our Results and Proposal of Future Studies

The landmark study by Puffenberger and colleagues, defining PMSE as a *STRADA* mutation and describing the clinical and pathological phenotype of the disease, identified periventricular nodules on MRI scans of two patients (61). Histopathological analysis of tissue from a postmortem PMSE brain showed evidence of cytomegaly, mTOR hyperactivity through enhanced P-S6, and the presence of heterotopic neurons in the subcortical white matter, highly suggestive of failed neuronal migration (12, 61). Further work in our lab was able to recapitulate the cytomegalic phenotype of PMSE through shRNA knockdown of STRADA in mNPCs, and this effect could be prevented with rapamycin treatment, indicating mTORC1 dependence (12). Additionally, we showed that STRADA knockdown *in vivo,* results in clusters of heterotopic neurons

within the murine post-natal VZ/SVZ, similar to heterotopia in PMSE (See Chapter 1) (12). The VZ/SVZ heterotopic neurons expressed enhanced mTORC1 activation, suggesting this as a possible mechanism. In a set of experiments outlined in Chapter 3, we chose to investigate the hypothesis that aberrant mTORC1 signaling actually causes aberrant cortical lamination in a STRADA-deplete experimental model. Additionally based on the evidence of neuronal heterotopia in PMSE human and STRADA KD mouse brain, we explored the hypothesis that STRADA affects cortical lamination through directing neuronal migration.

First, we sought to determine whether a disruption in migration *per se* could account for aberrant cortical lamination in the setting of STRADA loss. To do this, we devised a minimalistic *in vitro* approach. We extracted mNPCs from neonatal murine VZ/SVZ and transfected them with an shRNA targeting STRADA to induce STRADA KD. We then subjected these cells to a wound-healing scratch migration assay, and saw a significant decrease in distance migrated associated with STRADA KD. Importantly, this effect could be prevented by treatment with rapamycin or p70S6Ki, indicating dependence on mTORC1/p70S6K signaling. Next, we characterized this migration defect as a disruption of neuronal pathfinding, using video microscopy, which revealed a loss of directionality in migrating mNPCs with STRADA KD. This too was rescued by rapamycin treatment, suggesting dependence of this effect on mTORC1. To corroborate this finding, we used immunocytochemistry to evaluate the size and position of the Golgi body relative to the nucleus of leading-edge migrating cells, and found an mTORC1-/p70S6K-dependent disruption in cell polarity corresponding to STRADA KD. To confirm mTORC1-dependence of failed neuronal migration in a mouse model, we

subjected embryos to STRADA KD through IUE, and found that treatment with rapamycin was able to rescue the capacity of transfected cells to reach their appropriate destination in the CP.

We next hypothesized that STRADA regulates neuronal pathfinding through modulating cofilin and actin dynamics, downstream of mTORC1. In a series of protein quantification experiments, we defined phosphorylation profiles of several nodes in this pathway consistent with enhanced IRS1 phosphorylation and a dysregulation of cofilin signaling and consequent actin depolymerization in the setting of STRADA depletion. Interestingly, profiling the phosphorylation status of nodes on this pathway in the setting of LKB1 depletion in MEFs revealed a divergence at PAK1, consistent with a recent report that LKB1 can directly phosphorylate and inhibit PAK1 at a separate phosphorylation site (128), resulting in enhanced actin polymerization. This is also consistent with a well-documented association of LKB1 loss with enhanced cell migration in certain forms of metastatic cancers and in LKB1-null MEFs.

It is interesting to consider the mechanisms through which LKB1 depletion and STRADA depletion might have opposite effects on cell migration. We speculate that STRADA might in fact not be a universal activator of LKB1 as previously postulated (7). We propose that it is likely that STRADA binding LKB1 activates the kinase specifically toward phosphorylating certain downstream substrates, AMPK inclusive. When STRADA is present, LKB1 activity toward the cofilin pathway is driven primarily through mTOR, activating AMPK, inhibiting mTOR, activating PAK1, and inhibiting cofilin, resulting in actin polymerization. In the absence of STRADA, however, the

inhibitory influence of LKB1 on PAK1 appears stronger. We postulate that without STRADA, LKB1 can not appreciably activate AMPK and thus can not inhibit mTOR, resulting in a lack of PAK1 activation through the mTOR pathway. Secondarily, LKB1's direct phosphorylative inhibition of PAK1 goes unopposed, resulting in a second-hit inhibition of PAK1, disinhibiting cofilin and depolymerizing actin, opposing effective cell polarization and pathfinding. Further experiments, particularly employing mutation of phosphorylation sites on PAK1 and AMPK in the presence and absence of STRADA and LKB1 individually and together, will be necessary to delineate the specific mechanism and test our hypotheses.

Evaluation of Our Proposed Mechanism of Cell Migration in PMSE: Summary of Our Results in Patient Cells and Establishment of Preclinical Data

In order to be able to apply our proposed mechanism and role for STRADA in neuronal migration to the human disease, we extracted fibroblasts from PMSE patients, heterozygous parents, and controls. Western analysis of the phosphorylation profiles of key nodes in our signaling pathway revealed a corroboration of our mNPC results. Compared with control cells, PMSE fibroblasts exhibited enhanced phosphorylation of mTORC1 targets S6 and IRS1, and diminished phosphorylative inhibition of cofilin. Importantly, this was associated with actin depolymerization and a defect in cell migration, rescued with rapamycin or p70S6Ki. To confirm the link from mTORC1 signaling into our defined pathway, we immunostained postmortem PMSE cortical tissue for phosphorylated IRS1 and found enhanced P-IRS1 in PMSE compared with control cortex.

Importantly, our results show that abnormal brain development in PMSE can be attributed significantly to a defect in neuronal migration resulting from STRADA loss. This defect results from enhanced mTORC1 signaling, as evidenced by rescue with both mTORC1 inhibition through rapamycin and inhibition of its direct effector p70S6K. Through our experiments *in vitro* and *in vivo* in mice, corroborated by parallel effects in cells extracted from PMSE patients, we provide sufficient preclinical data for the consideration of targeting the mTORC1/p70S6K pathway as a treatment strategy for PMSE.

Modeling Epilepsy in PMSE: Future Directions

Our experiments extensively address the role of STRADA in neuronal migration, and failed neuronal migration has been proposed as a mechanism for epileptogenesis (108). Our preclinical data evaluating cortical activity in the region of failed neuronal migration resulting from STRADA knockdown suggests that this may be an important mechanism in our model as well, since this region exhibits neuronal hyperactivity and enhanced synchronization (see Chapter 4). However, we have not yet addressed the direct effects of STRADA depletion on altering the firing potential of individual neurons. Recent studies by Filippi and colleagues have shown that STRADA's binding partner MO25 can induce an approximately 100-fold activation of SPAK/OSR1 kinases, enhancing their ability to phosphorylate the ion cotransporters NKCC1, NKCC2, and NKCC (134). Knockdown of MO25 inhibited phosphorylation of NKCC1 by SPAK/OSR1, and this was rescued by MO25 re-expression. Alteration of NKCC1 and NKCC2 expression can dramatically alter membrane potential and thus likelihood of a

neuron to fire an action potential. In fact, it is precisely a change in the ratio of NKCC1 to NKCC2 membrane expression that is thought to change the response of early neurons in the developing brain to GABA from excitation to inhibition, based on a switch from predominantly intracellular to predominantly extracellular chloride concentrations (135). Importantly, NKCC1 has recently been suggested as a potentially attractive pharmacological target in epilepsy (136). Common loop diuretics, particularly bumetanide, can be used to inhibit this transporter and consequently reduce intracellular chloride concentration and susceptibility to depolarization upon opening of chloride channels. Given the compelling link to MO25, it is worth investigating how the absence of STRADA in PMSE might impact MO25 function, and particularly NKCC1 activation and neuronal firing potential. Finally, it will be important to determine whether easily accessible and generally well-tolerated loop diuretics might be able to impact neuronal firing and treat seizures in PMSE patients.

To evaluate the effects of STRADA loss on NKCC1 activity and neuronal firing, as well as the treatment potential of loop diuretics, we are establishing cultures of derived PMSE patient and control neurons, in collaboration with Dr. Jack Parent at the University of Michigan. PMSE patient and control fibroblasts were reprogrammed into pluripotent lines through transduction of four transcription factors, including Oct4, Sox2, Klf4, and c-Myc (137, 138). Induced pluripotent stem cells (iPSCs) originating from PMSE patients and controls were established, then differentiated into Tuj1-positive PMSE neurons (**Figures 5.1 and 5.2**). Importantly, this will allow single-cell recording in a human neuronal line to determine if STRADA loss affects the firing potential of individual neurons independently of network dynamics, as well as evaluation of

treatment options, without requiring invasive procedures to obtain these cells from patients.

mTOR Dysregulation, Neurodevelopmental Disease, and Epilepsy: Toward Effective Therapy

mTOR signaling plays a critical role in corticogenesis. Tight regulation of this cascade is essential to normal development, and disruption of this process can result in myriad developmental disorders. Interestingly, loss of function mutations in mTOR-inhibitory genes such as *TSC1* or *TSC2*, or gain of function mutations in mTOR activators such as *AKT3* result in aberrant brain development and intractable seizures (28, 29, 139). Since epilepsy in these patients is so often refractory to treatment with anti-epileptic drugs, it has been suggested that directly targeting the mTOR pathway might prove more effective (140, 141). Indeed, recent clinical trials have been promising. The mTORC1 inhibitor rapamycin (sirolimus) has been shown to induce the regression of astrocytomas on MRI in TSC patients, while cessation of treatment was associated with mass regrowth until treatment was resumed (142). Additionally, rapamycin treatment has been shown to reduce seizure frequency in TSC patients with otherwise medically intractable epilepsy (143). Recently, treating TSC patients with the rapamycin analogue everolimus was associated with reduction of subependymal giant cell astrocytoma (SEGA) volume and seizure frequency (144).

PMSE is a rare genetic disorder, yet it can offer key insights into the role of aberrant mTOR signaling in several more common neurodevelopmental disorders. We propose that PMSE serves as an important model of mTOR-associated brain disease

since all PMSE patients share the same deletion in STRADA and thus represent a homogeneous study group, and since this is to date the only identified mTOR-associated disorder resulting from a genetic homozygous deletion.

PMSE is disorder with 100% penetrance. All patients will develop intractable seizures and cognitive decline, and no effective treatment strategies have yet been reported. Based on our pre-clinical results demonstrating rescue of cell size and migration defects with rapamycin treatment, we administered rapamycin (sirolimus) to 5 PMSE patients at the Clinic for Special Children in Lancaster, PA, in collaboration with their physician Dr. Kevin Strauss. Rapamycin treatment was tolerated by all 5 patients and no adverse events to necessitate cessation of the treatment were experienced (**Table 5.1**). Compared with historical PMSE controls (n=16, ages 7 months to 28 years), of whom 100% currently experience ongoing and intractable seizures at least monthly, and in many cases daily, rapamycin-treated patients experienced a profound decrease in seizures, with only one child in the cohort experiencing one seizure, at a time of febrile illness, during the most recent year of rapamycin therapy (61). Of note, Patient 1 in our cohort has never had a seizure at age 8 months, whereas rapamycin-naïve PMSE patients typically start to seize between 3 and 6 months of age. Patient 3, who was previously burdened with 180 seizures per year, has been seizure free over the last year on rapamycin. In both the historical control group and our rapamycin-treated cohort, the Denver Developmental Screening Test II was used to measure psychomotor development, and provisional developmental differences between the two groups were noted in receptive language and social domains. Anecdotally, parents of PMSE children report that those on rapamycin seem more interactive and more emotionally engaged than

those not treated with the drug. Long-term effects will need to be evaluated in order to make safe clinical recommendations, but promising early results suggest that targeting mTORC1 signaling might be the key to effectively treating seizures and other disease manifestations in these otherwise-intractable patients.

Through PMSE, we were able to model STRADA depletion and define the role of STRADA and mTORC1 signaling in neuronal migration and brain development, as well as characterize the effects of STRADA's absence and consequently aberrant mTORC1 signaling in disrupted corticogenesis. Thus, we have added STRADA to the list of key regulators of neuronal migration and mTOR signaling during cortical development. By evaluating the rescue potential of rapamycin and p70S6Ki throughout our experiments, we established pre-clinical precedent for targeting mTORC1 signaling as a therapeutic strategy to treat PMSE as well as other mTOR-associated neurodevelopmental disorders. Our promising early clinical data in the PMSE population suggests that pharmacological mTOR inhibition could be a highly effective treatment strategy and a key to preventing seizures and cognitive decline in these patients.

Table 5.1. Clinical Summary of PMSE Patients Treated With Sirolimus

Patient	Age (yr/mo)	BMI (kg/m2)	Sirolimus Start (mo)	Current dose (mg/m2)	Ave. sirolimus trough (ng/mL)	AED 1	AED 2	GTC/SE	Worst # seizures/yr	# seizures in last 12 mos*	Developmental Quotient†				
											Gross Motor	Adaptive	Expressive Language	Receptive Language	Social
1	8m	15.0	3	1.0	18.5	OXC		0	0	0	0.76	0.69	0.63	0.63	0.69
2	1y 7m	16.2	8	1.8	1.3	OXC	PB	0	4	0	0.44	0.56	0.44	0.44	0.60
3	3y 6m	14.4	6	1.1	12.9	LEV	TOP	22	180	0	0.24§	0.24	0.14¶	0.41¶	0.33
4	4y 6m	13.3	3	3.9	4.6	CBZ		1	1	0	0.14§	0.27	0.12¶	0.49¶	0.33
5	4y 8m	15.0	4	4.9	3.6	OXC	TOP	2	4	1	0.22§	0.22	0.14¶	0.40¶	0.27
Average (SD)	3y 0m (1y 8m)	14.8 (1.1)	4.8 (2.2)	2.5 (1.8)	8.2 (7.2)			6 (11)	38 (80)	0.2 (0.4)	0.37 (0.22)	0.40 (0.21)	0.29 (0.23)	0.47 (0.10)	0.44 (0.19)

*For patient <1 year of age, this column lists the number of seizures since birth.

†Developmental Quotient is defined as developmental age, determined by the Denver Developmental Screening Test II, divided by chronological age. A score of 1.0 represents psychomotor development commensurate with age.

§Gross motor development of STRADA-deficient children is hindered by congenital absence of anterior cruciate ligaments, which leads to recurrent knee dislocations and typically precludes ambulation.

¶All STRADA-deficient patients are mute; we therefore determined separate Developmental Quotients for expressive or "spoken" langauge and receptive or "understood" language, the latter represented by pointing to or otherwise indicating pictures, body parts, named family members, etc.

Abbreviations: AED, antiepileptic drug; CBZ, carbamazepine; GTC/SE, generalized tonic-clonic seizure +/- status epilepticus;LEV, levetiracetam; OXC, oxcarbazepine; PB, phenobarbital; TOP, topiramate.

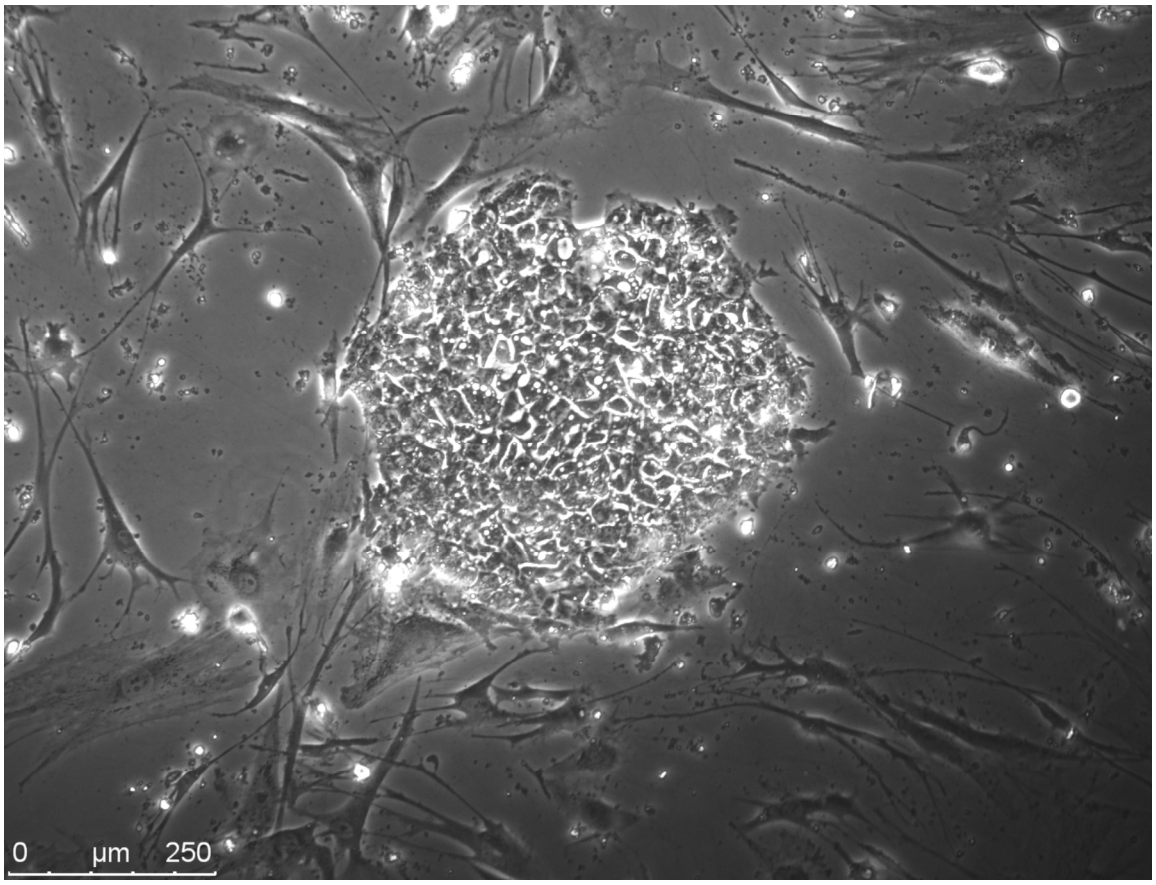

Figure 5.1. A colony of reprogrammed PMSE iPSCs. The colony sits atop a layer of fibroblast feeder cells. Courtesy of Jack Parent, University of Michigan.

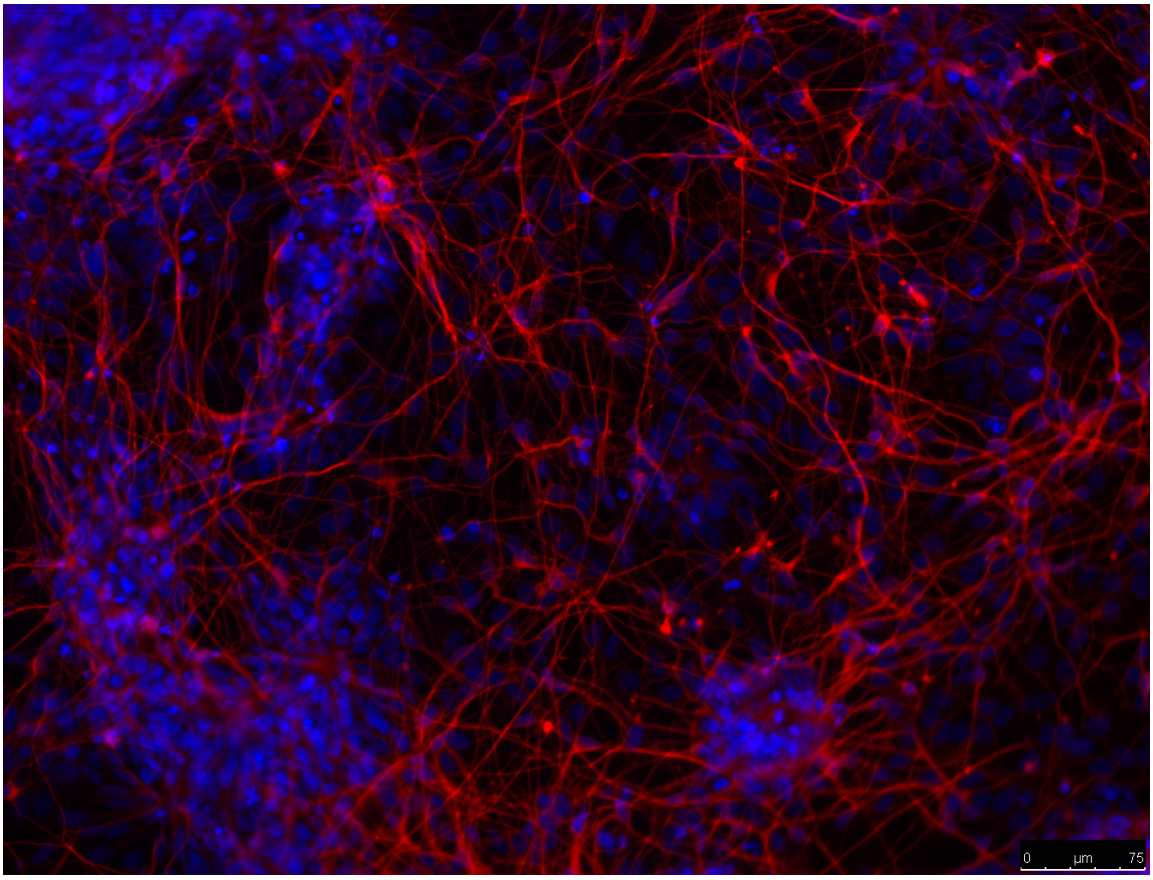

Figure 5.2. PMSE derived neurons, with red fluorescence indicating Tuj1 staining for neuronal maturity, and blue fluorescence indicating nuclear DNA. Courtesy of Jack Parent, University of Michigan.

BIBLIOGRAPHY

1. Baas AF, Boudeau J, Sapkota GP, Smit L, Medema R, Morrice NA, et al. Activation of the tumour suppressor kinase LKB1 by the STE20-like pseudokinase STRAD. EMBO J. 2003;22(12):3062-72. PMCID: 162144.

2. Johnston AM, Naselli G, Gonez LJ, Martin RM, Harrison LC, DeAizpurua HJ. SPAK, a STE20/SPS1-related kinase that activates the p38 pathway. Oncogene. 2000;19(37):4290-7.

3. Sanna MG, da Silva Correia J, Luo Y, Chuang B, Paulson LM, Nguyen B, et al. ILPIP, a novel anti-apoptotic protein that enhances XIAP-mediated activation of JNK1 and protection against apoptosis. J Biol Chem. 2002;277(34):30454-62.

4. Nishigaki K, Thompson D, Yugawa T, Rulli K, Hanson C, Cmarik J, et al. Identification and characterization of a novel Ste20/germinal center kinase-related kinase, polyploidy-associated protein kinase. J Biol Chem. 2003;278(15):13520-30.

5. Zeqiraj E, Filippi BM, Goldie S, Navratilova I, Boudeau J, Deak M, et al. ATP and MO25alpha regulate the conformational state of the STRADalpha pseudoki nase and activation of the LKB1 tumour suppressor. PLoS Biol. 2009;7(6):e1000126. PMCID: 2686265.

6. Zeqiraj E, Filippi BM, Deak M, Alessi DR, van Aalten DM. Structure of the LKB1-STRAD-MO25 complex reveals an allosteric mechanism of kinase activation. Science. 2009;326(5960):1707-11.

7. Boudeau J, Baas AF, Deak M, Morrice NA, Kieloch A, Schutkowski M, et al. MO25alpha/beta interact with STRADalpha/beta enhancing their ability to bind, activate and localize LKB1 in the cytoplasm. EMBO J. 2003;22(19):5102-14. PMCID: 204473.

8. Dorfman J, Macara IG. STRADalpha regulates LKB1 localization by blocking access to importin-alpha, and by association with Crm1 and exportin-7. Mol Biol Cell. 2008;19(4):1614-26. PMCID: 2291406.

9. Tiainen M, Vaahtomeri K, Ylikorkala A, Makela TP. Growth arrest by the LKB1 tumor suppressor: induction of p21(WAF1/CIP1). Hum Mol Genet. 2002;11(13):1497-504.

10. Barnes AP, Lilley BN, Pan YA, Plummer LJ, Powell AW, Raines AN, et al. LKB1 and SAD kinases define a pathway required for the polarization of cortical neurons. Cell. 2007;129(3):549-63.

11. Shelly M, Cancedda L, Heilshorn S, Sumbre G, Poo MM. LKB1/STRAD promotes axon initiation during neuronal polarization. Cell. 2007;129(3):565-77.

12. Orlova KA, Parker WE, Heuer GG, Tsai V, Yoon J, Baybis M, et al. STRADalpha deficiency results in aberrant mTORC1 signaling during corticogenesis in humans and mice. J Clin Invest. 2010;120(5):1591-602. PMCID: 2860905.

13. Milburn CC, Boudeau J, Deak M, Alessi DR, van Aalten DM. Crystal structure of MO25 alpha in complex with the C terminus of the pseudo kinase STE20-related adaptor. Nat Struct Mol Biol. 2004;11(2):193-200.

14. Hawley SA, Boudeau J, Reid JL, Mustard KJ, Udd L, Makela TP, et al. Complexes between the LKB1 tumor suppressor, STRAD alpha/beta and MO25 alpha/beta are upstream kinases in the AMP-activated protein kinase cascade. J Biol. 2003;2(4):28. PMCID: 333410.

15. Boudeau J, Scott JW, Resta N, Deak M, Kieloch A, Komander D, et al. Analysis of the LKB1-STRAD-MO25 complex. J Cell Sci. 2004;117(Pt 26):6365-75.

16. Lizcano JM, Goransson O, Toth R, Deak M, Morrice NA, Boudeau J, et al. LKB1 is a master kinase that activates 13 kinases of the AMPK subfamily, including MARK/PAR-1. EMBO J. 2004;23(4):833-43. PMCID: 381014.

17. Hardie DG, Scott JW, Pan DA, Hudson ER. Management of cellular energy by the AMP-activated protein kinase system. FEBS Lett. 2003;546(1):113-20.

18. Kemp BE, Stapleton D, Campbell DJ, Chen ZP, Murthy S, Walter M, et al. AMP-activated protein kinase, super metabolic regulator. Biochem Soc Trans. 2003;31(Pt 1):162-8.

19. Shaw RJ, Kosmatka M, Bardeesy N, Hurley RL, Witters LA, DePinho RA, et al. The tumor suppressor LKB1 kinase directly activates AMP-activated kinase and regulates apoptosis in response to energy stress. Proc Natl Acad Sci U S A. 2004;101(10):3329-35. PMCID: 373461.

20. Corton JM, Gillespie JG, Hawley SA, Hardie DG. 5-aminoimidazole-4-carboxamide ribonucleoside. A specific method for activating AMP-activated protein kinase in intact cells? Eur J Biochem. 1995;229(2):558-65.

21. Zhou G, Myers R, Li Y, Chen Y, Shen X, Fenyk-Melody J, et al. Role of AMP-activated protein kinase in mechanism of metformin action. J Clin Invest. 2001;108(8):1167-74. PMCID: 209533.

22. Hawley SA, Gadalla AE, Olsen GS, Hardie DG. The antidiabetic drug metformin activates the AMP-activated protein kinase cascade via an adenine nucleotide-independent mechanism. Diabetes. 2002;51(8):2420-5.

23. Shaw RJ, Bardeesy N, Manning BD, Lopez L, Kosmatka M, DePinho RA, et al. The LKB1 tumor suppressor negatively regulates mTOR signaling. Cancer Cell. 2004;6(1):91-9.

24. Alessi DR, Sakamoto K, Bayascas JR. LKB1-dependent signaling pathways. Annu Rev Biochem. 2006;75:137-63.

25. Inoki K, Zhu T, Guan KL. TSC2 mediates cellular energy response to control cell growth and survival. Cell. 2003;115(5):577-90.

26. Wullschleger S, Loewith R, Hall MN. TOR signaling in growth and metabolism. Cell. 2006;124(3):471-84.

27. Garami A, Zwartkruis FJ, Nobukuni T, Joaquin M, Roccio M, Stocker H, et al. Insulin activation of Rheb, a mediator of mTOR/S6K/4E-BP signaling, is inhibited by TSC1 and 2. Mol Cell. 2003;11(6):1457-66.

28. Marcotte L, Crino PB. The neurobiology of the tuberous sclerosis complex. Neuromolecular Med. 2006;8(4):531-46.

29. Crino PB, Nathanson KL, Henske EP. The tuberous sclerosis complex. N Engl J Med. 2006;355(13):1345-56.

30. Crino PB. mTOR: A pathogenic signaling pathway in developmental brain malformations. Trends Mol Med. 2011;17(12):734-42.

31. Loewith R, Jacinto E, Wullschleger S, Lorberg A, Crespo JL, Bonenfant D, et al. Two TOR complexes, only one of which is rapamycin sensitive, have distinct roles in cell growth control. Mol Cell. 2002;10(3):457-68.

32. Foster KG, Fingar DC. Mammalian target of rapamycin (mTOR): conducting the cellular signaling symphony. J Biol Chem. 2010;285(19):14071-7. PMCID: 2863215.

33. Gwinn DM, Shackelford DB, Egan DF, Mihaylova MM, Mery A, Vasquez DS, et al. AMPK phosphorylation of raptor mediates a metabolic checkpoint. Mol Cell. 2008;30(2):214-26. PMCID: 2674027.

34. Jacinto E, Loewith R, Schmidt A, Lin S, Ruegg MA, Hall A, et al. Mammalian TOR complex 2 controls the actin cytoskeleton and is rapamycin insensitive. Nat Cell Biol. 2004;6(11):1122-8.

35. Sarbassov DD, Ali SM, Sengupta S, Sheen JH, Hsu PP, Bagley AF, et al. Prolonged rapamycin treatment inhibits mTORC2 assembly and Akt/PKB. Mol Cell. 2006;22(2):159-68.

36. Jaeschke A, Hartkamp J, Saitoh M, Roworth W, Nobukuni T, Hodges A, et al. Tuberous sclerosis complex tumor suppressor-mediated S6 kinase inhibition by phosphatidylinositide-3-OH kinase is mTOR independent. J Cell Biol. 2002;159(2):217-24. PMCID: 2173059.

37. Ruvinsky I, Sharon N, Lerer T, Cohen H, Stolovich-Rain M, Nir T, et al. Ribosomal protein S6 phosphorylation is a determinant of cell size and glucose homeostasis. Genes Dev. 2005;19(18):2199-211. PMCID: 1221890.

38. Ruvinsky I, Meyuhas O. Ribosomal protein S6 phosphorylation: from protein synthesis to cell size. Trends Biochem Sci. 2006;31(6):342-8.

39. Gingras AC, Raught B, Gygi SP, Niedzwiecka A, Miron M, Burley SK, et al. Hierarchical phosphorylation of the translation inhibitor 4E-BP1. Genes Dev. 2001;15(21):2852-64. PMCID: 312813.

40. Baybis M, Yu J, Lee A, Golden JA, Weiner H, McKhann G, 2nd, et al. mTOR cascade activation distinguishes tubers from focal cortical dysplasia. Ann Neurol. 2004;56(4):478-87.

41. Chan JA, Zhang H, Roberts PS, Jozwiak S, Wieslawa G, Lewin-Kowalik J, et al. Pathogenesis of tuberous sclerosis subependymal giant cell astrocytomas: biallelic inactivation of TSC1 or TSC2 leads to mTOR activation. J Neuropathol Exp Neurol. 2004;63(12):1236-42.

42. Hsu PP, Kang SA, Rameseder J, Zhang Y, Ottina KA, Lim D, et al. The mTOR-regulated phosphoproteome reveals a mechanism of mTORC1-mediated inhibition of growth factor signaling. Science. 2011;332(6035):1317-22. PMCID: 3177140.

43. Yu Y, Yoon SO, Poulogiannis G, Yang Q, Ma XM, Villen J, et al. Phosphoproteomic analysis identifies Grb10 as an mTORC1 substrate that negatively regulates insulin signaling. Science. 2011;332(6035):1322-6. PMCID: 3195509.

44. Miyata H, Chiang AC, Vinters HV. Insulin signaling pathways in cortical dysplasia and TSC-tubers: tissue microarray analysis. Ann Neurol. 2004;56(4):510-9.

45. Krsek P, Maton B, Korman B, Pacheco-Jacome E, Jayakar P, Dunoyer C, et al. Different features of histopathological subtypes of pediatric focal cortical dysplasia. Ann Neurol. 2008;63(6):758-69.

46. Blumcke I, Thom M, Aronica E, Armstrong DD, Vinters HV, Palmini A, et al. The clinicopathologic spectrum of focal cortical dysplasias: a consensus classification proposed by an ad hoc Task Force of the ILAE Diagnostic Methods Commission. Epilepsia. 2011;52(1):158-74. PMCID: 3058866.

47. Crino PB, Miyata H, Vinters HV. Neurodevelopmental disorders as a cause of seizures: neuropathologic, genetic, and mechanistic considerations. Brain Pathol. 2002;12(2):212-33.

48. Orlova KA, Tsai V, Baybis M, Heuer GG, Sisodiya S, Thom M, et al. Early progenitor cell marker expression distinguishes type II from type I focal cortical dysplasias. J Neuropathol Exp Neurol. 2010;69(8):850-63.

49. Ljungberg MC, Bhattacharjee MB, Lu Y, Armstrong DL, Yoshor D, Swann JW, et al. Activation of mammalian target of rapamycin in cytomegalic neurons of human cortical dysplasia. Ann Neurol. 2006;60(4):420-9.

50. Hentges KE, Sirry B, Gingeras AC, Sarbassov D, Sonenberg N, Sabatini D, et al. FRAP/mTOR is required for proliferation and patterning during embryonic development in the mouse. Proc Natl Acad Sci U S A. 2001;98(24):13796-801. PMCID: 61121.

51. Uhlmann EJ, Wong M, Baldwin RL, Bajenaru ML, Onda H, Kwiatkowski DJ, et al. Astrocyte-specific TSC1 conditional knockout mice exhibit abnormal neuronal organization and seizures. Ann Neurol. 2002;52(3):285-96.

52. Meikle L, Talos DM, Onda H, Pollizzi K, Rotenberg A, Sahin M, et al. A mouse model of tuberous sclerosis: neuronal loss of Tsc1 causes dysplastic and ectopic neurons, reduced myelination, seizure activity, and limited survival. J Neurosci. 2007;27(21):5546-58.

53. Way SW, McKenna J, 3rd, Mietzsch U, Reith RM, Wu HC, Gambello MJ. Loss of Tsc2 in radial glia models the brain pathology of tuberous sclerosis complex in the mouse. Hum Mol Genet. 2009;18(7):1252-65. PMCID: 2655769.

54. Zeng LH, Rensing NR, Zhang B, Gutmann DH, Gambello MJ, Wong M. Tsc2 gene inactivation causes a more severe epilepsy phenotype than Tsc1 inactivation in a mouse model of Tuberous Sclerosis Complex. Hum Mol Genet. 2010.

55. Zeng LH, Xu L, Gutmann DH, Wong M. Rapamycin prevents epilepsy in a mouse model of tuberous sclerosis complex. Ann Neurol. 2008;63(4):444-53.

56. Chalhoub N, Baker SJ. PTEN and the PI3-kinase pathway in cancer. Annu Rev Pathol. 2009;4:127-50. PMCID: 2710138.

57. Kwon CH, Luikart BW, Powell CM, Zhou J, Matheny SA, Zhang W, et al. Pten regulates neuronal arborization and social interaction in mice. Neuron. 2006;50(3):377-88.

58. Ogawa S, Kwon CH, Zhou J, Koovakkattu D, Parada LF, Sinton CM. A seizure-prone phenotype is associated with altered free-running rhythm in Pten mutant mice. Brain Res. 2007;1168:112-23.

59. Ljungberg MC, Sunnen CN, Lugo JN, Anderson AE, D'Arcangelo G. Rapamycin suppresses seizures and neuronal hypertrophy in a mouse model of cortical dysplasia. Dis Model Mech. 2009;2(7-8):389-98. PMCID: 2707106.

60. Zhou J, Blundell J, Ogawa S, Kwon CH, Zhang W, Sinton C, et al. Pharmacological inhibition of mTORC1 suppresses anatomical, cellular, and behavioral abnormalities in neural-specific Pten knock-out mice. J Neurosci. 2009;29(6):1773-83.

61. Puffenberger EG, Strauss KA, Ramsey KE, Craig DW, Stephan DA, Robinson DL, et al. Polyhydramnios, megalencephaly and symptomatic epilepsy caused by a homozygous 7-kilobase deletion in LYK5. Brain. 2007;130(Pt 7):1929-41.

62. Feliciano DM, Su T, Lopez J, Platel JC, Bordey A. Single-cell Tsc1 knockout during corticogenesis generates tuber-like lesions and reduces seizure threshold in mice. J Clin Invest. 2011;121(4):1596-607. PMCID: 3069783.

63. Tsai V, Parker WE, Orlova KA, Baybis M, Chi AWS, Berg BD, et al. Fetal Brain mTOR Pathway Activation in Tuberous Sclerosis Complex. Cerebral Cortex. 2012;In Press.

64. Way SW, Rozas NS, Wu HC, McKenna J, 3rd, Reith RM, Hashmi SS, et al. The differential effects of prenatal and/or postnatal rapamycin on neurodevelopmental defects and cognition in a neuroglial mouse model of tuberous sclerosis complex. Hum Mol Genet. 2012;21(14):3226-36. PMCID: 3384384.

65. Asada N, Sanada K, Fukada Y. LKB1 regulates neuronal migration and neuronal differentiation in the developing neocortex through centrosomal positioning. J Neurosci. 2007;27(43):11769-75.

66. Larson Y, Liu J, Stevens PD, Li X, Li J, Evers BM, et al. Tuberous sclerosis complex 2 (TSC2) regulates cell migration and polarity through activation of CDC42 and RAC1. J Biol Chem. 2010;285(32):24987-98. PMCID: 2915734.

67. Um SH, Frigerio F, Watanabe M, Picard F, Joaquin M, Sticker M, et al. Absence of S6K1 protects against age- and diet-induced obesity while enhancing insulin sensitivity. Nature. 2004;431(7005):200-5.

68. Konno D, Yoshimura S, Hori K, Maruoka H, Sobue K. Involvement of the phosphatidylinositol 3-kinase/rac1 and cdc42 pathways in radial migration of cortical neurons. J Biol Chem. 2005;280(6):5082-8.

69. Solecki DJ, Govek EE, Tomoda T, Hatten ME. Neuronal polarity in CNS development. Genes Dev. 2006;20(19):2639-47.

70. Kemphues KJ, Priess JR, Morton DG, Cheng NS. Identification of genes required for cytoplasmic localization in early C. elegans embryos. Cell. 1988;52(3):311-20.

71. Baas AF, Kuipers J, van der Wel NN, Batlle E, Koerten HK, Peters PJ, et al. Complete polarization of single intestinal epithelial cells upon activation of LKB1 by STRAD. Cell. 2004;116(3):457-66.

72. Pearce LR, Alton GR, Richter DT, Kath JC, Lingardo L, Chapman J, et al. Characterization of PF-4708671, a novel and highly specific inhibitor of p70 ribosomal S6 kinase (S6K1). Biochem J. 2010;431(2):245-55.

73. Govek EE, Hatten ME, Van Aelst L. The role of Rho GTPase proteins in CNS neuronal migration. Dev Neurobiol. 2011;71(6):528-53. PMCID: 3188326.

74. Thoreen CC, Kang SA, Chang JW, Liu Q, Zhang J, Gao Y, et al. An ATP-competitive mammalian target of rapamycin inhibitor reveals rapamycin-resistant functions of mTORC1. J Biol Chem. 2009;284(12):8023-32. PMCID: 2658096.

75. Liu Q, Chang JW, Wang J, Kang SA, Thoreen CC, Markhard A, et al. Discovery of 1-(4-(4-propionylpiperazin-1-yl)-3-(trifluoromethyl)phenyl)-9-(quinolin-3-yl)benz o[h][1,6]naphthyridin-2(1H)-one as a highly potent, selective mammalian target of rapamycin (mTOR) inhibitor for the treatment of cancer. J Med Chem. 2010;53(19):7146-55.

76. Consortium TECTS. Identification and characterization of the tuberous sclerosis gene on chromosome 16. Cell. 1993;75(7):1305-15.

77. van Slegtenhorst M, de Hoogt R, Hermans C, Nellist M, Janssen B, Verhoef S, et al. Identification of the tuberous sclerosis gene TSC1 on chromosome 9q34. Science. 1997;277(5327):805-8.

78. Bolton PF, Park RJ, Higgins JN, Griffiths PD, Pickles A. Neuro-epileptic determinants of autism spectrum disorders in tuberous sclerosis complex. Brain. 2002;125(Pt 6):1247-55.

79. Gomez MR, Sampson JR, Whittemore VH. Tuberous sclerosis complex. 3rd ed. New York: Oxford University Press; 1999.

80. Koh S, Jayakar P, Dunoyer C, Whiting SE, Resnick TJ, Alvarez LA, et al. Epilepsy surgery in children with tuberous sclerosis complex: presurgical evaluation and outcome. Epilepsia. 2000;41(9):1206-13.

81. Sparagana SP, Roach ES. Tuberous sclerosis complex. Curr Opin Neurol. 2000;13(2):115-9.

82. Sharma M, Ralte A, Arora R, Santosh V, Shankar SK, Sarkar C. Subependymal giant cell astrocytoma: a clinicopathological study of 23 cases with special emphasis on proliferative markers and expression of p53 and retinoblastoma gene proteins. Pathology. 2004;36(2):139-44.

83. Gyure KA, Prayson RA. Subependymal giant cell astrocytoma: a clinicopathologic study with HMB45 and MIB-1 immunohistochemical analysis. Mod Pathol. 1997;10(4):313-7.

84. Kim SK, Wang KC, Cho BK, Jung HW, Lee YJ, Chung YS, et al. Biological behavior and tumorigenesis of subependymal giant cell astrocytomas. J Neurooncol. 2001;52(3):217-25.

85. Lopes MB, Altermatt HJ, Scheithauer BW, Shepherd CW, VandenBerg SR. Immunohistochemical characterization of subependymal giant cell astrocytomas. Acta Neuropathol. 1996;91(4):368-75.

86. Mizuguchi M, Takashima S. Neuropathology of tuberous sclerosis. Brain Dev. 2001;23(7):508-15.

87. Lee A, Maldonado M, Baybis M, Walsh CA, Scheithauer B, Yeung R, et al. Markers of cellular proliferation are expressed in cortical tubers. Ann Neurol. 2003;53(5):668-73.

88. Ess KC, Kamp CA, Tu BP, Gutmann DH. Developmental origin of subependymal giant cell astrocytoma in tuberous sclerosis complex. Neurology. 2005;64(8):1446-9.

89. Fingar DC, Blenis J. Target of rapamycin (TOR): an integrator of nutrient and growth factor signals and coordinator of cell growth and cell cycle progression. Oncogene. 2004;23(18):3151-71.

90. Kyin R, Hua Y, Baybis M, Scheithauer B, Kolson D, Uhlmann E, et al. Differential cellular expression of neurotrophins in cortical tubers of the tuberous sclerosis complex. Am J Pathol. 2001;159(4):1541-54. PMCID: 1850517.

91. Harrington LS, Findlay GM, Gray A, Tolkacheva T, Wigfield S, Rebholz H, et al. The TSC1-2 tumor suppressor controls insulin-PI3K signaling via regulation of IRS proteins. J Cell Biol. 2004;166(2):213-23. PMCID: 2172316.

92. Shah OJ, Wang Z, Hunter T. Inappropriate activation of the TSC/Rheb/mTOR/S6K cassette induces IRS1/2 depletion, insulin resistance, and cell survival deficiencies. Curr Biol. 2004;14(18):1650-6.

93. Shah OJ, Hunter T. Turnover of the active fraction of IRS1 involves raptor-mTOR- and S6K1-dependent serine phosphorylation in cell culture models of tuberous sclerosis. Mol Cell Biol. 2006;26(17):6425-34. PMCID: 1592824.

94. Brugarolas J, Kaelin WG, Jr. Dysregulation of HIF and VEGF is a unifying feature of the familial hamartoma syndromes. Cancer Cell. 2004;6(1):7-10.

95. Lesma E, Grande V, Ancona S, Carelli S, Di Giulio AM, Gorio A. Anti-EGFR antibody efficiently and specifically inhibits human TSC2-/- smooth muscle cell proliferation. Possible treatment options for TSC and LAM. PLoS One. 2008;3(10):e3558. PMCID: 2570214.

96. Nguyen-Vu PA, Fackler I, Rust A, DeClue JE, Sander CA, Volkenandt M, et al. Loss of tuberin, the tuberous-sclerosis-complex-2 gene product is associated with angiogenesis. J Cutan Pathol. 2001;28(9):470-5.

97. El-Hashemite N, Walker V, Zhang H, Kwiatkowski DJ. Loss of Tsc1 or Tsc2 induces vascular endothelial growth factor production through mammalian target of rapamycin. Cancer Res. 2003;63(17):5173-7.

98. Arbiser JL, Brat D, Hunter S, D'Armiento J, Henske EP, Arbiser ZK, et al. Tuberous sclerosis-associated lesions of the kidney, brain, and skin are angiogenic neoplasms. J Am Acad Dermatol. 2002;46(3):376-80.

99. McCormack FX. Lymphangioleiomyomatosis: a clinical update. Chest. 2008;133(2):507-16.

100. Brugarolas JB, Vazquez F, Reddy A, Sellers WR, Kaelin WG, Jr. TSC2 regulates VEGF through mTOR-dependent and -independent pathways. Cancer Cell. 2003;4(2):147-58.

101. Abounader R, Laterra J. Scatter factor/hepatocyte growth factor in brain tumor growth and angiogenesis. Neuro Oncol. 2005;7(4):436-51. PMCID: 1871724.

102. Crino PB, Trojanowski JQ, Dichter MA, Eberwine J. Embryonic neuronal markers in tuberous sclerosis: single-cell molecular pathology. Proc Natl Acad Sci U S A. 1996;93(24):14152-7. PMCID: 19509.

103. Palmes D, Zibert A, Budny T, Bahde R, Minin E, Kebschull L, et al. Impact of rapamycin on liver regeneration. Virchows Arch. 2008;452(5):545-57.

104. Young LR, Inoue Y, McCormack FX. Diagnostic potential of serum VEGF-D for lymphangioleiomyomatosis. N Engl J Med. 2008;358(2):199-200.

105. Inage Y, Halliday WC, Go C, Ochi A, Akiyama T, Akiyama M, et al. Histopathology of cortex and white matter in pediatric epileptic spasms: comparison with those of partial seizures. Brain Dev. 2012;34(2):118-23.

106. Marcotte L, Aronica E, Baybis M, Crino PB. Cytoarchitectural alterations are widespread in cerebral cortex in tuberous sclerosis complex. Acta Neuropathol. 2012;123(5):685-93.

107. Muhlebner A, Coras R, Kobow K, Feucht M, Czech T, Stefan H, et al. Neuropathologic measurements in focal cortical dysplasias: validation of the ILAE 2011 classification system and diagnostic implications for MRI. Acta Neuropathol. 2012;123(2):259-72.

108. Chevassus-au-Louis N, Represa A. The right neuron at the wrong place: biology of heterotopic neurons in cortical neuronal migration disorders, with special reference to associated pathologies. Cell Mol Life Sci. 1999;55(10):1206-15.

109. Matsuki T, Matthews RT, Cooper JA, van der Brug MP, Cookson MR, Hardy JA, et al. Reelin and stk25 have opposing roles in neuronal polarization and dendritic Golgi deployment. Cell. 2010;143(5):826-36. PMCID: 3033572.

110. Eggers CM, Kline ER, Zhong D, Zhou W, Marcus AI. STE20-related kinase adaptor protein alpha (STRADalpha) regulates cell polarity and invasion through PAK1 signaling in LKB1-null cells. J Biol Chem. 2012;287(22):18758-68. PMCID: 3365778.

111. Magnitsky S, Walton RM, Wolfe JH, Poptani H. Magnetic resonance imaging detects differences in migration between primary and immortalized neural stem cells. Acad Radiol. 2008;15(10):1269-81. PMCID: 2573997.

112. Strauss KA, Puffenberger EG, Huentelman MJ, Gottlieb S, Dobrin SE, Parod JM, et al. Recessive symptomatic focal epilepsy and mutant contactin-associated protein-like 2. N Engl J Med. 2006;354(13):1370-7.

113. Liang CC, Park AY, Guan JL. In vitro scratch assay: a convenient and inexpensive method for analysis of cell migration in vitro. Nat Protoc. 2007;2(2):329-33.

114. Goncharova E, Goncharov D, Noonan D, Krymskaya VP. TSC2 modulates actin cytoskeleton and focal adhesion through TSC1-binding domain and the Rac1 GTPase. J Cell Biol. 2004;167(6):1171-82. PMCID: 2172598.

115. Saito T. In vivo electroporation in the embryonic mouse central nervous system. Nat Protoc. 2006;1(3):1552-8.

116. Qian Y, Corum L, Meng Q, Blenis J, Zheng JZ, Shi X, et al. PI3K induced actin filament remodeling through Akt and p70S6K1: implication of essential role in cell migration. Am J Physiol Cell Physiol. 2004;286(1):C153-63.

117. Berven LA, Willard FS, Crouch MF. Role of the p70(S6K) pathway in regulating the actin cytoskeleton and cell migration. Exp Cell Res. 2004;296(2):183-95.

118. Kupfer A, Louvard D, Singer SJ. Polarization of the Golgi apparatus and the microtubule-organizing center in cultured fibroblasts at the edge of an experimental wound. Proc Natl Acad Sci U S A. 1982;79(8):2603-7. PMCID: 346248.

119. Yadav S, Puri S, Linstedt AD. A primary role for Golgi positioning in directed secretion, cell polarity, and wound healing. Mol Biol Cell. 2009;20(6):1728-36. PMCID: 2655245.

120. Arber S, Barbayannis FA, Hanser H, Schneider C, Stanyon CA, Bernard O, et al. Regulation of actin dynamics through phosphorylation of cofilin by LIM-kinase. Nature. 1998;393(6687):805-9.

121. Deacon SW, Beeser A, Fukui JA, Rennefahrt UE, Myers C, Chernoff J, et al. An isoform-selective, small-molecule inhibitor targets the autoregulatory mechanism of p21-activated kinase. Chem Biol. 2008;15(4):322-31.

122. Narumiya S, Ishizaki T, Uehata M. Use and properties of ROCK-specific inhibitor Y-27632. Methods Enzymol. 2000;325:273-84.

123. Edwards DC, Sanders LC, Bokoch GM, Gill GN. Activation of LIM-kinase by Pak1 couples Rac/Cdc42 GTPase signalling to actin cytoskeletal dynamics. Nat Cell Biol. 1999;1(5):253-9.

124. Tahirovic S, Bradke F. Neuronal polarity. Cold Spring Harb Perspect Biol. 2009;1(3):a001644. PMCID: 2773638.

125. Condeelis J. Life at the leading edge: the formation of cell protrusions. Annu Rev Cell Biol. 1993;9:411-44.

126. Nobes CD, Hall A. Rho, rac, and cdc42 GTPases regulate the assembly of multimolecular focal complexes associated with actin stress fibers, lamellipodia, and filopodia. Cell. 1995;81(1):53-62.

127. Sells MA, Boyd JT, Chernoff J. p21-activated kinase 1 (Pak1) regulates cell motility in mammalian fibroblasts. J Cell Biol. 1999;145(4):837-49. PMCID: 2133181.

128. Deguchi A, Miyoshi H, Kojima Y, Okawa K, Aoki M, Taketo MM. LKB1 suppresses p21-activated kinase-1 (PAK1) by phosphorylation of Thr109 in the p21-binding domain. J Biol Chem. 2010;285(24):18283-90. PMCID: 2881753.

129. Singh RR, Song C, Yang Z, Kumar R. Nuclear localization and chromatin targets of p21-activated kinase 1. J Biol Chem. 2005;280(18):18130-7.

130. Thiele EA. Managing epilepsy in tuberous sclerosis complex. J Child Neurol. 2004;19(9):680-6.

131. Curatolo P, Seri S, Verdecchia M, Bombardieri R. Infantile spasms in tuberous sclerosis complex. Brain Dev. 2001;23(7):502-7.

132. Bai J, Ramos RL, Ackman JB, Thomas AM, Lee RV, LoTurco JJ. RNAi reveals doublecortin is required for radial migration in rat neocortex. Nat Neurosci. 2003;6(12):1277-83.

133. Ackman JB, Aniksztejn L, Crepel V, Becq H, Pellegrino C, Cardoso C, et al. Abnormal network activity in a targeted genetic model of human double cortex. J Neurosci. 2009;29(2):313-27.

134. Filippi BM, de los Heros P, Mehellou Y, Navratilova I, Gourlay R, Deak M, et al. MO25 is a master regulator of SPAK/OSR1 and MST3/MST4/YSK1 protein kinases. EMBO J. 2011;30(9):1730-41. PMCID: 3101989.

135. Rivera C, Voipio J, Payne JA, Ruusuvuori E, Lahtinen H, Lamsa K, et al. The K+/Cl- co-transporter KCC2 renders GABA hyperpolarizing during neuronal maturation. Nature. 1999;397(6716):251-5.

136. Loscher W, Puskarjov M, Kaila K. Cation-chloride cotransporters NKCC1 and KCC2 as potential targets for novel antiepileptic and antiepileptogenic treatments. Neuropharmacology. 2012.

137. Takahashi K, Tanabe K, Ohnuki M, Narita M, Ichisaka T, Tomoda K, et al. Induction of pluripotent stem cells from adult human fibroblasts by defined factors. Cell. 2007;131(5):861-72.

138. Yu J, Vodyanik MA, Smuga-Otto K, Antosiewicz-Bourget J, Frane JL, Tian S, et al. Induced pluripotent stem cell lines derived from human somatic cells. Science. 2007;318(5858):1917-20.

139. Poduri A, Evrony GD, Cai X, Elhosary PC, Beroukhim R, Lehtinen MK, et al. Somatic activation of AKT3 causes hemispheric developmental brain malformations. Neuron. 2012;74(1):41-8. PMCID: 3460551.

140. Wong M. Mammalian target of rapamycin (mTOR) inhibition as a potential antiepileptogenic therapy: From tuberous sclerosis to common acquired epilepsies. Epilepsia. 2010;51(1):27-36. PMCID: 3022513.

141. Galanopoulou AS, Gorter JA, Cepeda C. Finding a better drug for epilepsy: the mTOR pathway as an antiepileptogenic target. Epilepsia. 2012;53(7):1119-30. PMCID: 3389589.

142. Franz DN, Leonard J, Tudor C, Chuck G, Care M, Sethuraman G, et al. Rapamycin causes regression of astrocytomas in tuberous sclerosis complex. Ann Neurol. 2006;59(3):490-8.

143. Muncy J, Butler IJ, Koenig MK. Rapamycin reduces seizure frequency in tuberous sclerosis complex. J Child Neurol. 2009;24(4):477. PMCID: 3072696.

144. Krueger DA, Care MM, Holland K, Agricola K, Tudor C, Mangeshkar P, et al. Everolimus for subependymal giant-cell astrocytomas in tuberous sclerosis. N Engl J Med. 2010;363(19):1801-11.